IST AUSTRIA
Institute of Science and Technology

From the left to the right

A tale of asymmetries, environments, and hippocampal development

by

Matthew Case

June, 2018

A thesis presented to the
Graduate School
of the
Institute of Science and Technology Austria, Klosterneuburg, Austria
in partial fulfilment of the requirements
for the degree of
Doctor of Philosophy

IST AUSTRIA
Institute of Science and Technology

The dissertation of Matthew Case, titled '*From the left to the right: A tale of asymmetries, environments, and hippocampal development'*, is approved by:

Supervisor: [Name of Supervisor], IST Austria, Klosterneuburg, Austria

Signature: _____

Committee Member: [Name of Committee Member], IST Austria, Klosterneuburg, Austria

Signature: _____

Committee Member: [Name of Committee Member], [Institute], [City], [Country]

Signature: _____

_____

Exam Chair: [Name of Exam Chair], IST Austria, Klosterneuburg, Austria

Signature: _____

I hereby declare that this dissertation is my own work and that it does not contain other people's work without this being so stated; this thesis does not contain my previous work without this being stated, and the bibliography contains all the literature that I used in writing the dissertation.

I declare that this is a true copy of my thesis, including any final revisions, as approved by my thesis committee, and that this thesis has not been submitted for a higher degree to any other university or institution.

I certify that any republication of materials presented in this thesis has been approved by the relevant publishers and co-authors.

Signature: _____

[Matthew J Case]

June 27, 2018

“*Symmetry is what we see at a glance; based on the fact that there is no reason for any difference...*”

— Blaise Pascal, Pensées

Dedication

I'd like to offer a joint dedication for this thesis.

Firstly, to all the mice I used in these experiments. Mice and rats often suffer in our relentless (though arguably necessary) pursuit of knowledge and although they might not appreciate (or even understand) the nod of thanks; I feel that, as scientists, it's important for us not to forget the fact that laboratory animals are not thoughtless robots, which exist only for our benefit.

Secondly, having given a sincere offering of gratitude to the powerless, I'd like to also present an insincere one to the powerful. The second part of my dedication is given to Cthulhu. Like us humble men of science, may you never stop dreaming.

Abstract

Asymmetries have long been known about in the central nervous system. From gross anatomical differences, such as the presence of the parapineal organ in only one hemisphere of the developing zebrafish, to more subtle differences in activity between both hemispheres, as seen in freely roaming animals or human participants under PET and fMRI imaging analysis. The presence of asymmetries has been demonstrated to have huge behavioural implications, with their disruption often leading to the generation of neurological disorders, memory problems, changes in personality, and in an organism's health and well-being.

For my Ph.D. work I aimed to tackle two important avenues of research. The first being the process of input-side dependency in the hippocampus, with the goal of finding a key gene responsible for its development (Gene X). The second project was to do with experience-induced laterality formation in the hippocampus. Specifically, how laterality in the synapse density of the CA1 stratum radiatum (s.r.) could be induced purely through environmental enrichment.

Through unilateral tracer injections into the CA3, I was able to selectively measure the properties of synapses within the CA1 and investigate how they differed based upon which hemisphere the presynaptic neurone originated. Having found the existence of a previously unreported reversed (left-isomerism) *i.v.* mutant, through morpholocal examination of labelled terminals in the CA1 s.r., I aimed to elucidate a key gene responsible for the process of left or right determination of inputs to the CA1 s.r.. This work relates to the previous finding of input-side dependent asymmetry in the wild-type rodent, where the origin of the projecting neurone to the CA1 will determine the morphology of a synapse, to a greater degree than the hemisphere in which the projection terminates. Using left- and right-isomerism *i.v.* mice, in combination with whole genome sequence analysis, I highlight Ena/VASP-like (Evl) as a potential target for Gene X. In relation to this topic, I also highlight my work in the recently published paper of how knockout of PirB can lead to a lack of input-side dependency in the murine hippocampus.

For the second question, I show that the environmental enrichment paradigm will lead to an asymmetry in the synapse densities in the hippocampus of mice. I also highlight that the nature of the enrichment is of less consequence than the process of enrichment itself. I

demonstrate that the CA3 region will dramatically alter its projection targets, in relation to environmental stimulation, with the asymmetry in synaptic density, caused by enrichment, relying heavily on commissural fibres. I also highlight the vital importance of input-side dependent asymmetry, as a necessary component of experience-dependent laterality formation in the CA1 s.r.. However, my results suggest that it isn't the only cause, as there appears to be a CA1 dependent mechanism also at play. Upon further investigation, I highlight the significant, and highly important, finding that the changes seen in the CA1 s.r. were predominantly caused through projections from the left-CA3, with the right-CA3 having less involvement in this mechanism.

Acknowledgements

I'd like to offer particular thanks to the following:

Professor Ryuichi Shigemoto, my supervisor, for providing me with invaluable guidance and support throughout my PhD studies.

Professor Isao Ito, for providing me with different genetic mice lacking input-side dependent asymmetries, such as the original *i.v.* and the PirB ko mouse mutants.

Professor Shuji Shigenobu, for generation of the Illumina sequence libraries and help with whole genome sequence analysis to try and determine Gene X.

David Kleindienst, for design of the AAV virus used in my enriched environment experiments, as well as helping write a script to narrow down SNPs to only those appearing within genes on chromosome 12.

As well as to the rest of the Shigemoto lab, both those from the National Institute of Physiological Sciences (Okazaki, Japan), and those from the Institute of Science and Technology (Austria), for being a great bunch of people to spend a PhD with and supporting as only members of the same lab can.

About the Author

Matthew Case completed a BSc in Biological Sciences at the University of Plymouth and an MSc in Stem Cells and Regenerative Medicine at the University of Bristol, before joining the IST Austria in April. His main research interests focus on the impact of input-side dependent asymmetry formation in the hippocampus, both in its formation and in its effect on hippocampal synapse modulation during experience-dependent learning. During his PhD studies, Matthew has published his results on the regulatory effect of PirB (discussed within this thesis) was in the journal PLoS ONE (Ukai H 2017) and has discussed his work on the effect of environmental enrichment in modulating experience-dependent hippocampal laterality formation in the Japanese Neuroscience Society Symposium (JNSS) in 2017.

List of Publications Appearing in Thesis

1. Ukai, H. *et al.* PirB regulates asymmetries in hippocampal circuitry. *PLoS One* **12,** 1–20 (2017).

Table of Contents

Chapter 2

An investigation into experience-driven modulation of hippocampal laterality formation

Methods

List of Figures

24. Mutations found within Evl gene (2)

25. Both mutations located within promoter region of Evl gene

26. PSD area from PirB ko mice

27. Perforated synapses in PirB ko mice

28. Enrichment and non-enrichment cages

29. Effects of 3 weeks environmental enrichment on CA1 pyramidal-cell density

30. Effect of social isolation on CA1 pyramidal-cell synapse density in non-enriched mice

31. Different enrichment protocols

32. Effects of different environmental enrichment paradigms on CA1 pyramidal-cell synapse density

33. Volumetric analysis of synapse density in NENR and ENR C57BL/6J mice

34. Effect of environmental enrichment on synapse perforation in C57BL/6J mice

35. Effect of environmental enrichment on PSD area size in C57BL/6J mice

36. Synapse density from ipsilateral projections following enrichment and VHCT operation

37. Effects of environmental enrichment on right-isomerism *i.v.* mice

38. Effects of enrichment on left- and right-isomerism *i.v.* mouse lines

39. Effects of visceral organ laterality on CA1 pyramidal-cell synapse density in enriched *i.v.* mice

40. Fluorescence intensity 2 weeks following unilateral injections into either the left or the right CA3 in enriched and non-enriched C57BL/6J mice

41. Ratio of fluorescence intensity from unilateral injections into the CA3 of enriched and non-enriched C57BL/6J mice

42. Effect of environmental enrichment on spine head volume in C57BL/6J mice

43. Formula to estimate ipsilateral and contralateral contributions of CA3 to both hemispheres

44. Estimated synapse density contributions for ipsilateral and contralateral CA3 – CA1 projections from each hemisphere in individual NENR and ENR mice

45. Estimated change in CA1 synapse density for ipsilateral and contralateral projections from each hemisphere

46. Effect of environmental enrichment on synapse perforation from ipsilateral and contralateral CA3-CA1 projections

47. Effect of environmental enrichment on PSD area size from ipsilateral and contralateral CA3-CA1 projections

48. Locomotive activity of NENR mice during NOL

49. Time spent with moved object during training and testing phases for NENR mice

50. Time to complete the training and testing phases for NENR mice

51. % time spent with moved object for NENR mice

52. Locomotive activity of ENR mice during NOL

53. Time spent with moved object during training and testing phases for ENR mice

54. Time to complete the training and testing phases for ENR mice

55. % time spent with the moved object for ENR mice

56. Time to complete the training and testing phases for ENR mice (2)

57. Discrimination index for ENR mice during training and testing phases

58. Discrimination index for NENR and ENR mice during NOL paradigm

59. Changes to CA3 – CA1 projections caused by the environmental enrichment paradigm

List of Symbols/Abbreviations

The following are all abbreviations which I will use throughout this thesis. For the most part, they are common abbreviations. Except for those relating to housing conditions, which will often vary between papers.

B2M	β2 microglobulin
CA[1-3]	Cornu ammonis [1-3]
DG	Dentate gyrus
ENR	Enriched environment
Gene X	Predicted gene responsible for determination of left- or right-input side dependent asymmetry
GluR	Glutamate receptor
ISO	Social isolation, non-enriched environment
i.v.	Inversus viscerum
MHCI	Major histocompatibility complex 1
NENR	Non-enriched environment
NMDA	N-methyl-D-aspartate
NR2B	N-methyl D-aspartate receptor subtype 2B
PirB	Paired-immunoglobulin-like receptor B
SEM	Scanning electron microscope
SI	Situs inversus
s.r.	Stratum radiatum
s.o.	Stratum oriens
s.l.m	Stratum lacnosum moleculare
SS	Situs solitus
TEM	Transmission electron microscope
VHCT	Ventral hippocampal commissure transection
VHCCT	Ventral hippocampal commissure and corpus callosum transection

Chapter 1

Brief summary

Asymmetry, both in morphology and in behaviour, is a very common condition for a biological organism. Although the effects are often obvious, such as in the body axis laterality of a mammal, with the laterality of visceral organs (such as the heart) being established early on, many asymmetries are far more subtle. One example is input-side dependency in the hippocampus (Shinohara 2008). In this phenomenon, the hemispheric origin of the inputs to the CA1 will determine the nature of the terminals, not the specific hemisphere in which the projection does finally terminate. This has been demonstrated in rodents and has been suggested to play a role in memory, a process which has already been found to be highly lateralized (Kawakami 2008, Shinohara 2012, Shipton 2014a). Various mutant mice have been developed to study this process, of note is the inversus viscerum (*i.v.*) mutant. This mouse has randomized laterality in its visceral organs. Interestingly, it has also been found to lack input-side dependency, with all the inputs from the CA3 to the CA1 displaying a morphology similar to those originating from the right-CA3 in wild-type mice (Kawakami 2008). This leads to the classification of this mouse as a 'right-isomerism' mutant.

This chapter demonstrates the existence of a previously unreported left-isomerism mouse mutant, which lacks input-side dependency in hippocampal CA3 to CA1 pyramidal cell connections. Through selectively crossing left- and right-isomerism *i.v.* mutant mice, in combination with whole genome sequence analysis, I aim to highlight a potential gene responsible for left or right determination. Finally, I will discuss the effect of PirB on the generation of input-side dependent asymmetry in the hippocampus.

Asymmetry in nature

Asymmetries can take the form of either morphological (Brueckner 1989), or functional (Arjmand 2017, Piazza 2014), differences between the two halves of the body. Although it appears that asymmetry is a very common condition, its purpose is often disputed. There is strong evidence that the attractiveness of an individual can be determined by how symmetrical it appears (Perett 1999, Rhodes 1998), with this phenomenon being detectable in other primates also (Waitt 2006). One of the prevailing suggestions for this has been that symmetry is often a determinant of the overall good health of an organism (Jones 2001,

Manning 1998). This might lead one to expect that asymmetry is just an undesired consequence of age or health. This is especially true when we consider that evolutionary forces should surely be driving individuals towards greater and greater levels of symmetry. However, contrary to this belief, it is now evident that asymmetry is more than just an interesting phenomenon, but is rather an integral feature of the healthy workings of an organism. This is most evident in the central nervous system, where changes to the underlying asymmetries can lead to the formation of numerous neurological disorders, including schizophrenia, anxiety, and autism spectrum disorder (Dougherty 2016, Francks 2007, Facchin 2015, Hall 2012, Herbert 2005). It appears that symmetry, like beauty, could be considered as being 'only skin deep'.

The laterality of language in the brain (left-hemisphere being responsible) is such a familiar concept that many people might know of its existence, even without the most basic understanding of the morphological or physiological underpinnings. Some of the earliest identifiers of the laterality of language in the brain were the discovery of specialized brain regions, such as Wernicke's and Broca's areas, which have been found to be implicated in the processing and formation of language. Evidence for the existence of these specialized areas came in the 1860s, from autopsies performed on patients suffering with aphasia (Dronkers 2007). Damage to either of these important regions can lead to impairments in both language speech and comprehension, without causing changes to memory, personality, intelligence, or motor function (Bogen 1976, Fridriksson 2015). Asymmetries in hemispheric dominance have been found in other animal species, outside of humans, including in mice, frogs, various songbirds, monkeys, and chimpanzees (Corballis 2014, Oviedo 2016, Poremba 2013, Taglialatela 2009, Yue 2017). There appears to be a link between hand-preference and language laterality. One example being that the degree of asymmetry in the arcuate fasiculus (axonal fibres connecting Broca's and Wernicke's areas) has been found to correspond well with the stability of handedness (Propper 2010).

Limb-preference is another of the more colloquially well-known asymmetries, as it is easy to identify and examine. It is possible for humans to self-diagnose, as it is implicated in the vast majority of manual dexterity tasks which we might perform. Although handedness is a well-known phenomenon in humans, it has also been witnessed in other mammals (Giljov 2015), including in primates (Hopkins 2011) and rodents (Fu 2003, Ribeiro 2011, Sullivan 2012). However, studies into limb-preference have turned up some rather unexpected

implications. For example, left-handedness has been linked with increased risk of depression (Elias 2001, Soyman 2015) and anxiety (Wright 2009). Handedness has also been linked to increased risk of diseases such as cancer (Miller 2018), as well as to various neurological disorders, including schizophrenia (Brandler 2014, Razafimandimby 2011, Somers 2009) and autism (Markou 2017). However, although numerous diseases which have been found to be associated with language lateralization in the brain have also been linked to handedness, it has been found that the genes involved in the development of hand-preference and language-lateralization in the brain are likely wholly unrelated (Schmitz 2017). Outside of purely genetic causes, environmental factors have also been implicated in determining limb-preference (Ribeiro-Carvalho 2010). This demonstrates the apparent complexity of handedness, suggesting there to be both internal as well as external causes.

The generation of functional and morphological asymmetries can be induced through both environmental stimulation (Govind 1992, Ribeiro 2014), genetic stimulation (Bartoloni 2002, Jahanshad 2010, Moskal 2006), or perhaps a combinatorial affect from both (Ocklenburg 2010). Two of the most cited examples of an environmentally- or a genetically-driven asymmetrical development would be the development of the thalamofugal visual pathway in chickens (Rogers 2008) and the epithalmic asymmetry in the zebrafish (Roussigné 2009), respectively.

In the developing chick, the driving force for the formation of visual lateralization is the stimulation of the optic nerves by the sun (Rogers 1999). Due to the head position within the shell, the right-eye is exposed to the light (passing through the thin shell of the egg). The left-eye, however, is pressed against the chick's body, so receives no light stimulation. This leads to an imbalance in the strength of the projections from the thalamus to the hyperstriatum, with more passing contralaterally from the left, than contralaterally from the right. This asymmetry has been found to be involved in the perception of motion (Rugani 2015) and object discrimination (Rogers 2008), using the right eye preferentially for object discrimination and left eye preferentially for detection of motion. Light stimulation during development has also been implicated in a chicken's behaviour in later life, particularly in response to stress (Archer 2014). Light-driven lateralization has also been detected in other avian species, such as the pigeon (Buschmann 2006, Freund 2016, Manns 2014).

The zebrafish, however, develops an asymmetry in its epithalamus purely through

genetic stimulation. In brief, a preferentially left-sided expression of Nodal drives early development of neurones in the left habenula, as well as driving the left-ward migration of parapineal cells, through Fgf8 signalling. This leads to a left-sided parapineal organ, which has been further implicated in the acceleration of neurogenesis in the left habenula, through Wnt and Notch signalling. This early neurogenesis in the left-habenula drives preferential projections towards the dorsal IPN. The later-developing right-habenula will then project predominantly to towards the ventral IPN (for more in-depth reviews on zebrafish development please see: Concha 2009, Roussigné 2011). The asymmetrical positioning of the parapineal organ has been found to be vital to later asymmetrical development, with reversal of parapineal positioning leading to a reversal in the properties of habenular neurones (Dreosti 2014). This asymmetry has been found to have numerous behavioural implications, such as those to do with predator avoidance (Dadda 2010), as well as to different forms of sensory stimulation (Dreosti 2014).

It is possible to divide asymmetries into two separate categories, those being 'class 1' and 'class 2' (Concha 2012). Class 2 asymmetries are often easy to diagnose, as they are structures which are located in only one hemisphere of the body. Class 1 asymmetries, however, consist of similar structures being detectable on both sides of the body, albeit with one side being more developed (Maguire 2000, Saenger 2012), or are preferentially activated/used during specific tasks (Jeong 2016). These are especially common in the central nervous system, and are often much more subtle as they can superficially appear very similar, with evidence for their existence being often only suggested through underlying functional differences between both hemispheres. This tends to make them much more difficult to isolate and examine and as the precision of the techniques open to scientists increases, many more class 1 asymmetries have been found. The prevalence of asymmetry in the brain leads to important questions as to whether the asymmetry drives the function of the system, or whether it is the function itself which generates the asymmetry.

The hippocampus

The hippocampus is one of the most studied areas of the vertebrate brain. The name 'hippocampus' derives from the Greek word 'ἱππόκαμπος' meaning 'sea horse', and is a fitting description of its three-dimensional shape. Of particular interest are its roles in memory formation, processing, and consolidation, as well as its role in spatial navigation (Barker

2011, Bird 2017, Voss 2017, Zemla 2017). Although it is often described as a single structure, the hippocampus is actually constructed of a series of highly specialized and interconnected areas (Figure 1). These include the dentate gyrus (DG) and the Cornu Ammonis (CA) areas, which typically is further subdivided into the CA1, 2, and 3. Historically, a CA4 region was also identified, lying between the CA3 and the DG, however recent findings suggest that this is likely a part of the polymorphic layer of the DG (Andersen 2007). These regions can all be isolated through their functional and morphological differences. Information tends to flow from one region to another, with one of the most important, and studied, pathways being the trisynaptic circuit. In this circuit, information from layer 2 of the entorhinal cortex passes through the DG, to the CA3, and finally onto the CA1, before leaving the hippocampus (Jones 2011, Stepan 2015).

The dentate gyrus is comprised of three distinct regions, these are termed the molecular, the granule, and the polymorphic, cell layers. For a long time it was believed that the only substantial input to the DG was from the endorhinal cortex. However, an inhibitory projection pathway from the CA3 region, contra to the well-established uni-directional flow of information along the trisynaptic circuit, has been identified (Scharfman 2007). Excluding connections within the DG, the main output of the DG granule cells is to pyramidal cells within the CA3 region, through what are known as 'mossy fibers'. Granule cells can be characterized by an extremely sparse firing rate, it has been suggested that this could aid in their efficiency to temporally encode information in the DG (Pernía-Andrade 2014). The DG has been implicated in spatial and associative learning, particularly in pattern separation, as well as in the discrimination of similar contexts (Hunsaker 2008, Lopez-Rojas 2016, Rolls 2017). Rats with lesions to the DG have been found to have impairments to their ability to detect environmental changes (Hunsasker 2008). Interestingly, the granule cell layer of the DG has been identified as a site for adult neurogenesis, using neuroneal progenitor cells from the subgranular zone. This process has been found to be upregulated by the enriched environmental paradigm, and has been implicated in spatial memory processing (Nilsson 1999).

The CA3 region plays a role in the rapid associative encoding and recall, particularly to do with novel spatial and emotional cues (fear conditioning, NOL task, novel environment), of short-term memory information. The CA3 has also been suggested to play an important role in recording environmental layout, in cooperation with the dentate gyrus (Kesner 2007).

Similar to the CA1, the CA3 region has been found to hold place cells. However, unlike the CA1, it has been demonstrated that CA3 place fields will rapidly shift upon exposure of an animal to a novel environment (Lee 2004), further reinforcing the importance of the CA3 in enabling the animal to quickly adapt to environmental novelty. Morphologically, the CA3 can be further subdivided into 3 distinct regions, labelled CA3a, b, and c, with CA3a bordering the CA2 and CA3c the dentate gyrus. It receives the majority of its input from the medial and lateral entorhinal cortex, via the perforant path, from the dentate gyrus granule cell layer, via mossy fibers, as well as from recurrent collaterals from the CA3 itself (Kesner 2013). One of its main outputs is to the CA1 pyramidal cell layer, via the Schaffer collaterals (Kesner 2007). It is these connections, from the CA3 to CA1 pyramidal cell neurones, which are the main topic of this thesis; as it is here where we are able to detect the phenomenon of input-side dependent asymmetry.

One of the key features of the CA1 is the presence of specialized neurones which will fire at precise environmental locations (Mayford 2012). These neurones were classified as 'place cells', as they appeared to encode just one specific place in the environment. When the animal moves to a different environment, these cells have to reorganize in a process called “remapping” (Latuske 2018). Projecting to the subiculum and endorhinal cortex, the CA1 can be seen as the major output from the hippocampus, to the rest of the brain; with its major role being often described as one of retrieval of information to the neocortex (Rolls 2017). The CA1, like the CA3, has been implicated in the processing of temporal and spatial information about contextual information (Dimsdale-Zucker 2018, Rampon 2000). However, whereas the CA3 deals with changes within a single context, the role of the CA1 is to compare and contrast between different unrelated contexts. Following spatial learning, it is possible to detect dynamic remodelling of synapses and increased spine density on CA1 pyramidal neurones, which was different between basal and apical dendrites (Moser 1994, Moser 1997). Pyramidal cell neurones in the CA1 receive input from two different pathways. The 'indirect pathway' to the CA1 s.r., and the 'temperommonic pathway' to the CA1 l.m.. Whilst the 'indirect pathway' consists of the Schaffer collaterals from the CA3, the temperoammonic pathway projects from the entorhinal cortex layer III. Interestingly, a difference in the plasticity of NMDA receptors between synapses in the CA1 s.r. and the CA1 l.m., from the same neurone (Fitzjohn 2016). The CA1 is heavily involved in the formation and recall of many different memory processes including object location, recognition, contextual fear,

spatial, and non-spatial association, with some evidence that learning and memory function might be lateralised within this area (Farovik 2010, Haettig 2013, Ivanova 2009, Maren 2008, Montgomery 2007).

The CA2 is a small region separating the CA1 from the CA3. It is often overlooked due to the apparent difficulty in identifying its borders (Lein 2005), and has been described as potentially more of a transitional barrier between the CA1 and CA3 (Mercer 2007). It can be morphologically identified due to its lack of mossy fiber inputs, as well as being the only region of the Cornu Ammonis to receive input from supramammilary nucleus fibers (Mercer 2007). The CA2 has been shown to be more-easily affected by temporal, social, or emotional events, than contextual or spatial ones (Chevaleyre 2016, Hitti 2014, Mankin 2015). This feature could enable it to play an important role in identifying and remapping memories when they are found to conflict with immediate events (Wintzer 2014).

A simplified schematic of these different fields is provided below. Due to differences in synapse size and area within the CA1 s.r., all analysis in this project was conducted within the inner 1/3rd (marked in red).

Figure 1

Basic schematic of hippocampal fields

Hippocampus proper

Simple schematic to show the basic layout of the hippocampus proper - showing the position of the dentate gyrus (DG) as well as the Cornu Ammonis regions CA1, CA2 and CA3 (CA4 - the hilus - is considered as part of the DG, and is not labelled on this schematic).

CA1 subfields

The right half of the schematic displays the position of the stratum oriens (s.o), stratum radiatum (s.r.), and stratum lacunosum-moleculare (l.m.), subfields of the CA1

All analysis of the CA1 s.r. was performed in the inner 1/3rd - area marked in red

Although they can be found throughout the mammalian central nervous system (Watkins 2001), one area where asymmetries are of particular interest is in the hippocampus. This region is essential in short- and long-term, as well as working memory, formation and consolidation (Zemla 2017). The hippocampus displays many of the characteristics of a class 1 asymmetry, showing strong laterality its activation during various memory tasks. For example, place recall and route planning has been shown to have a strong right-side bias in activation of the hippocampus (Maguire 1997). It has also been shown that there might be a strong right-dominance in spatial memory processing in the right hippocampus, although this effect only appears in the absence of commissural fibres (Shinohara 2012b). However, there is disagreement over how strong this effect is, with hippocampal lesion studies showing less convincing results (Gerlai 2002). Morphologically, the hippocampus has a strong asymmetry in its volume, with the tendency to be significantly larger in the right hemisphere than the left (Pedraza 2004, Shi 2009). Interestingly, it appears that this asymmetry is restricted to the anterior hippocampus, with the degree of asymmetry being a significant correlate for increased cognitive function (Woolard 2012).

Input-side dependent asymmetry

One particularly interesting feature of the rodent hippocampus is the phenomenon of input-side dependent asymmetry (Kawahara 2013, Kawakami 2003, Kawakami 2008). In hippocampal pyramidal cell neurones, in relation to connections terminating in the CA1, the hemisphere where the synapse eventually develops is of far less consequence than the hemispheric origin of the presynaptic input. One of the key features of this asymmetry is a differential expression of the N-methyl-D-aspartate (NMDA) receptor NR2B in projections from either hemisphere.

NMDA receptors are known to be involved in the synaptic plasticity and regulation of memory processing in the hippocampus (Shipton 2014b). Through LTP and LTD activity, based on the differential expression of receptor subunits, they are able to facilitate the insertion and removal of AMPA receptors from the post-synaptic membrane (Malenka 2004). NR2A and NR2B are the most commonly found subunits in the hippocampus, with the ratio of NR2A:NR2B being dynamically altered based upon development, experience, and plasticity (Yashiro 2008). NR2B has been found to be asymmetrically expressed in the hippocampus, based upon the input-origin of the CA3 presynaptic location (Kawakami

2003). Due to the higher capacity for LTP seen in relation to increases in NR2B density, an asymmetry in the plasticity of synapses, based upon input-side, has been suggested.

Differences in NR2B density, between left and right projections, leads to some interesting physiological consequences. For example, it was reported that suppression of the left, but not the right, hippocampus could impact long-term memory retention in mice (Klur 2009, Shipton 2014a). It has also been demonstrated that stimulation of the left CA3 will generate more LTP at the CA1, than stimulation of the right CA3 (Kohl 2011). These findings suggest that the previously reported asymmetries detected in memory function and activity within the hippocampus could be related to differences in input-origin. The morphological consequences of this asymmetry include changes in the PSD area, the spine head volume, as well as the percentage of synapses with a perforated phenotype, all being entirely dependent on the localization of the projecting CA3 (Shinohara 2008). Figure 2 shows a simple schematic representation of input-side dependency in a wild-type mouse. It has also been demonstrated that projections from the right CA3-CA1 tend to be larger, more mature, and have a higher density of GluR1, than those from the left CA3 (Shinohara 2008). Although the absolute expression of NR2B doesn't differ between left or right projections, the density changing as a result of changes in synapse size, the expression of GluR1 appears to increase exponentially along with increases in synaptic area.

Of critical importance to the process of input-side dependent asymmetry formation is the dodecameric serine/threonine protein kinase CaMKII. Through activity-dependent activation, CaMKII has been found to dynamically alter the size of synapses, with activity driving an increase in synaptic size (Pi 2010). NMDA receptors have been implicated as critical binding partners for CaMKII, ensuring that it is strongly expressed in dendritic spines (Hell 2014). The binding of CaMKII to the C-terminal tail of GluN2B has been shown to be critical to its function. Without which, CaMKII might not be able to actively relocate towards the PSD area, in response to the LTP-driven influx of calcium. CaMKII has been implicated in both synapse perforation, as well as transportation of GluR1 to the synapse (Hayashi 2000, Majima 2009). There is a suggestion that, following LTP, synaptic insertion of GluR1 can permit spine enlargement. This is done through the stabilizing of protein complexes that promote spine-growth, and is accompanied by an increase in synaptic strength (Kopec 2007). However, although perforated spines have been discovered to be more stable and longer lasting, than their unperforated conspecifics, perforation has been proposed to be only a

temporary state, in response to synaptic activation via NMDA driven LTP (Neuhoff 1999, Sorra 1998).

Figure 2

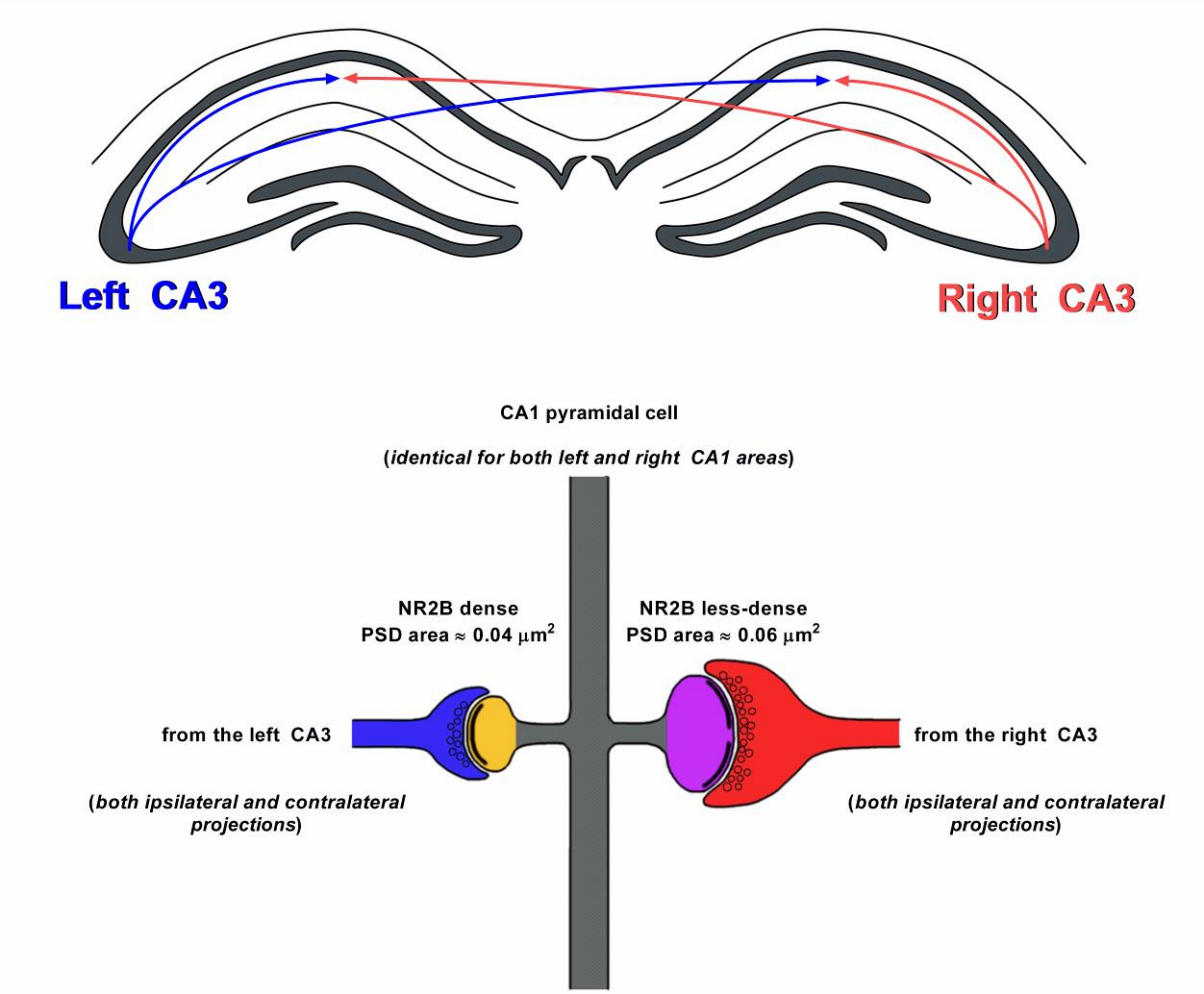

Input-side dependent asymmetry

Simple schematic to display input-side dependent asymmetry in the hippocampus. Above shows a schematic for the projections from the left and right CA3. Below shows a simple schematic of connections from CA3 to CA1 pyramidal cells. Inputs from the left CA3 are in blue, inputs from the right CA3 are in red. Yellow depicts small, thin, NR2B dense spines. Purple depicts larger, mushroom-type, NR2B less-dense spines.

Left-right input-side dependent asymmetry appears to be a fundamental feature of the hippocampus, involved in memory formation as well as the regulation of synaptic plasticity (El-Gaby 2015). This is a critical process, the absence of which could lead to critical deficits in spatial and working memory processing (Goto 2010, Shimbo 2018). However, it's possible that its true implications are yet to be fully realised.

Symmetry breaking

Input-side dependent asymmetry appears to be a fundamental feature of the murine hippocampus. Due to its potential importance, various mutant models have been developed, which lack this phenomenon; one prime example being the inversus viscerum (*i.v.*) mutant. The *i.v.* mouse line was generated through the introduction of a point mutation in the gene encoding Left-right dyenine (Lrd) (Bartoloni 2002, Supp 1997). Lrd is a motor protein, expressed at embryonic day 7.5 in a region called the node. Here, it controls the rotation of cilia, generating a leftward expression of key developmental proteins, including Lefty and Nodal. Through the introduction of a missense mutation, the nodal cilia in the *i.v.* mutant are rendered immobile. This means that the leftward flow of extraembryonic fluid, vital to the localized expression of developmental proteins, is not present, with the morphological consequences of this being a randomized laterality of visceral organs (McGrath 2003). A process of biased chromatid segregation, involving a hypothetical left-right axis development 1 (lra1) gene, rather than the more established Nodal, has been suggested as a possible explanation for visceral organ laterality (Sauer 2012). This model, although unproven, has the benefit of accounting for the huge embryonic lethality found in the *i.v.* mutant . The pups born from *i.v.* parents will fall into two distinct categorizations, based upon their visceral organ laterality; those being, Situs Solitus (where the visceral organs have the conventional positioning) and Situs Inversus (where the positions of the visceral organs are located in a complete mirror image). Figure 3 shows a simplified schematic of these two phenotypes. As the reversal in visceral organ laterality is complete, the condition is not lethal. Interestingly, the *i.v.* mutant has been found to lack the input-side dependent laterality found in CA3 – CA1 pyramidal-cell synapses, with the original *i.v.* mouse line displaying a 'right-isomerism' (Kawakami et al. 2008). This means that irrespective of which hemisphere the projecting CA3 is located within, the resultant connection in the CA1 will have a phenotype similar to the right-CA3 originating projections in the wild-type mouse (see figure 2 – red projection).

Figure 3

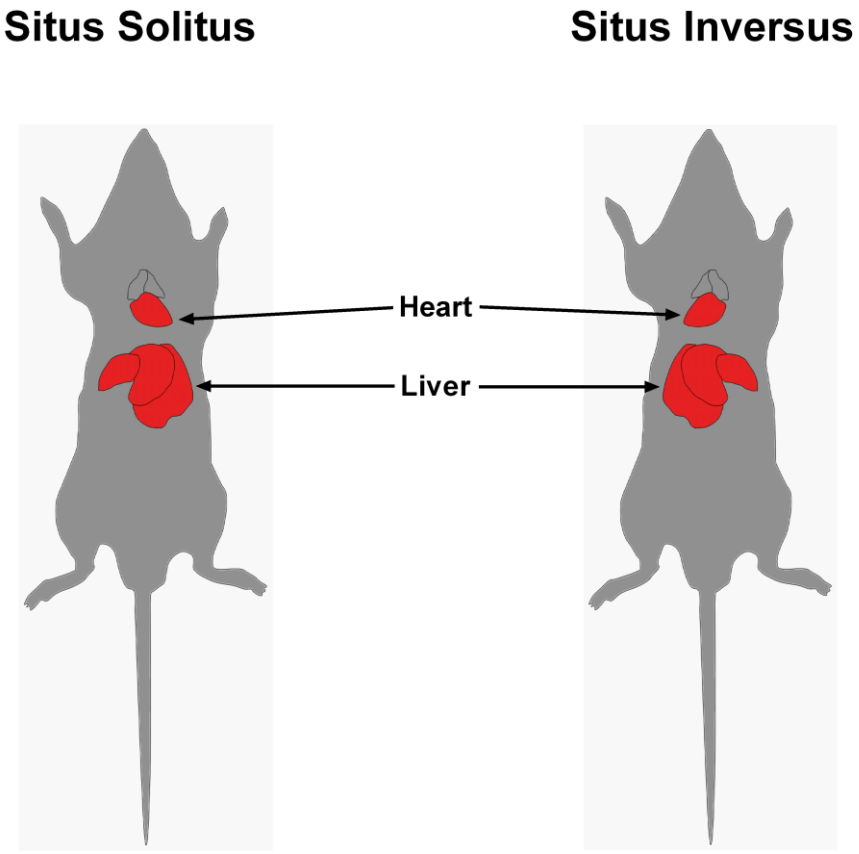

Situs solitus and situs inversus

Simple schematic to display body axis laterality. Situs inversus is a complete inversion of visceral organ laterality (though only the heart and liver are shown in the above diagram) and is therefore not lethal. Situs solitus is the natural wild-type state.

Determining isomerism by morphology alone

1:1

Input-side dependent asymmetry is a phenomenon which causes changes in the synaptic connections of CA3 to CA1 pyramidal cells. This process had already been identified through targetted injections into the CA3 and careful inspection of the terminals in the CA1, through electron microscopy (Shinohara et al. 2008), as well as through electrophysiological examination (Kawakami et al. 2003). As I had no previous training with electrophysiology, I directed my investigations towards electron microscopical analysis of the synapses within the CA1 s.r.. Previously, it had been found that the *i.v.* mouse lacked input-side dependent asymmetry in hippocampal connections (Kawakami et al. 2008), meaning that it wouldn't matter from which hemisphere the projections into the CA1 originated, they would all terminate in connections which were similar to those from the right CA3 in wild-type mice. This was termed as 'right-isomerism'. We had also recently discovered the existence of a left-isomerism *i.v.* mouse line.

The first thing which I aimed to investigate was whether I could demonstrate and characterise the left-isomerism phenotype using only analysis of the synapses within the CA1 s.r. through measuring the PSD area of synapses from TEM images. Although CA3 – CA1 morphological asymmetry had been displayed in the right-isomerism *i.v.* mouse, I decided that it would be important to perform unilateral injections of a tracer into the CA3, then I would only measure and characterise labelled terminals in the CA1 s.r.. The tracer used in this experiment was a biotinylated dextran amine with a molecular weight of 10,000 (BDA 10k). This provided highly detained labelling of both axons and terminals.

Methods and results

Methods used: Unilateral injections into the CA3 (method 1), transcardial perfusion (method 2), preparation of mouse brain for analysis under TEM (method 3), dissector analysis (method 4).

Mice were housed in standard mouse cages (for an image, please see figure 28 NENR), cages were changed once a week, and food and water were supplied ad libitum.

9 – 10 week old *i.v.*4 mice were used in this experiment.

Using unilateral CA3 injections and measuring only labelled terminals (figure 5), I was able to selectively measure the PSD area from the CA3 in each hemisphere (figure 6). Although I did not measure the synapse density, I used the dissector method instead to ensure an unbiased detection of labelled terminals. This meant that I would image a sequential series and only measure the length of newly appearing synapses (figure 4). This helped to minimize size bias, as otherwise larger synapses were more likely to appear in images (as smaller synapses would be present in fewer serial images). I also ensured to only measure intact PSDs, as if the PSD was still visible in the first, or last, image of the series, I could not be sure that my measurements were complete for that synapse.

Measurements of TEM images were conducted using the Reconstruct software (Fiala 2005)

Figure 4

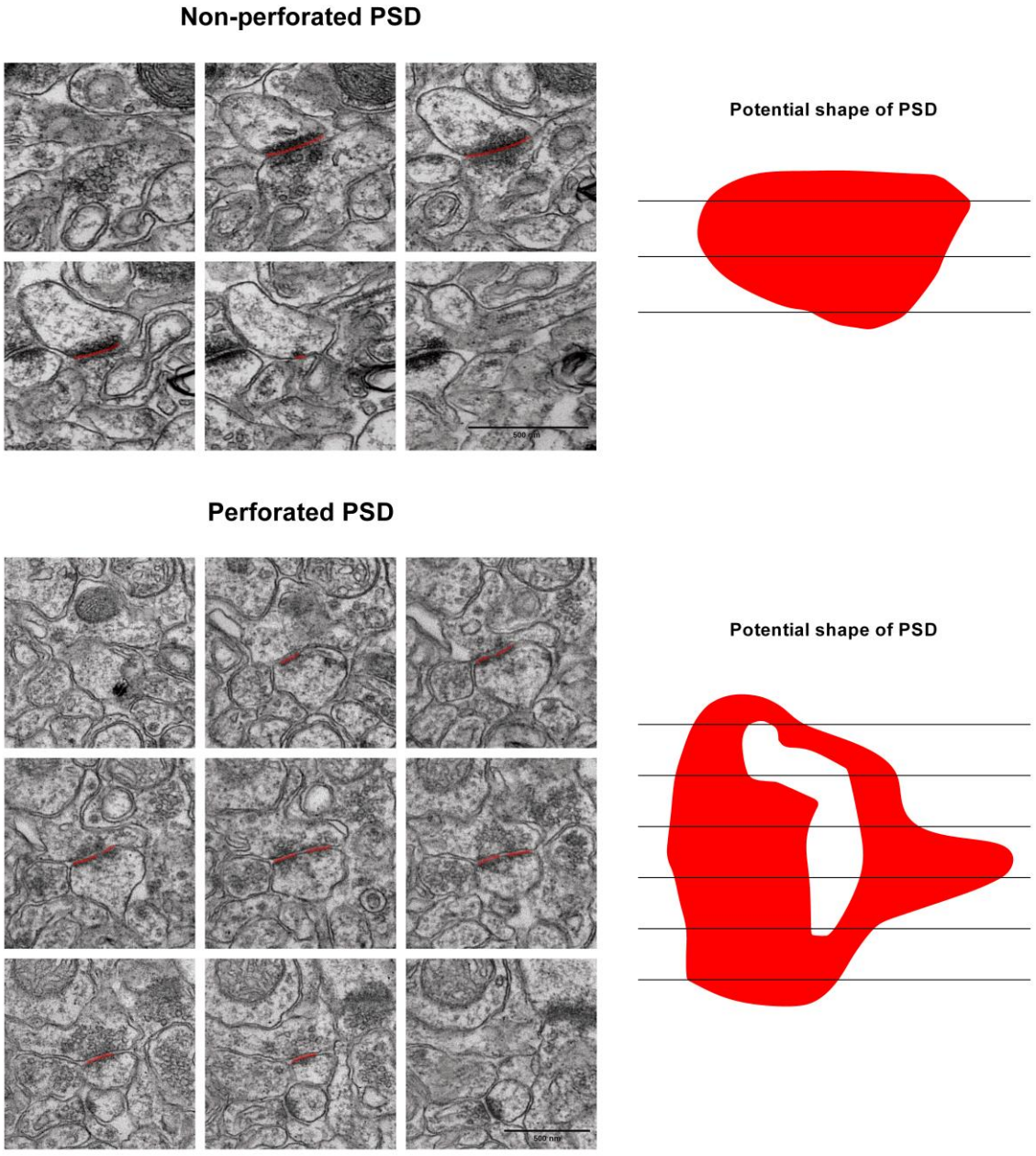

PSD area measurements

Synapses were only measured if the entire length of the PSD could be seen in all images in a series (dissector analysis was used to determine the appearance of a PSD to be measured). Non perforated synapses were categorised via an unbroken PSD in all images. Perforated synapses were categorised by a broken PSD which joined in at least one image of the series. Red lines on TEM images depict measured lengths. Red shape depicts idea of what the PSD may look like if reconstructed from the image series (though this is not to be taken as an entirely accurate depiction). Scalebars measure 500 nm.

Figure 5

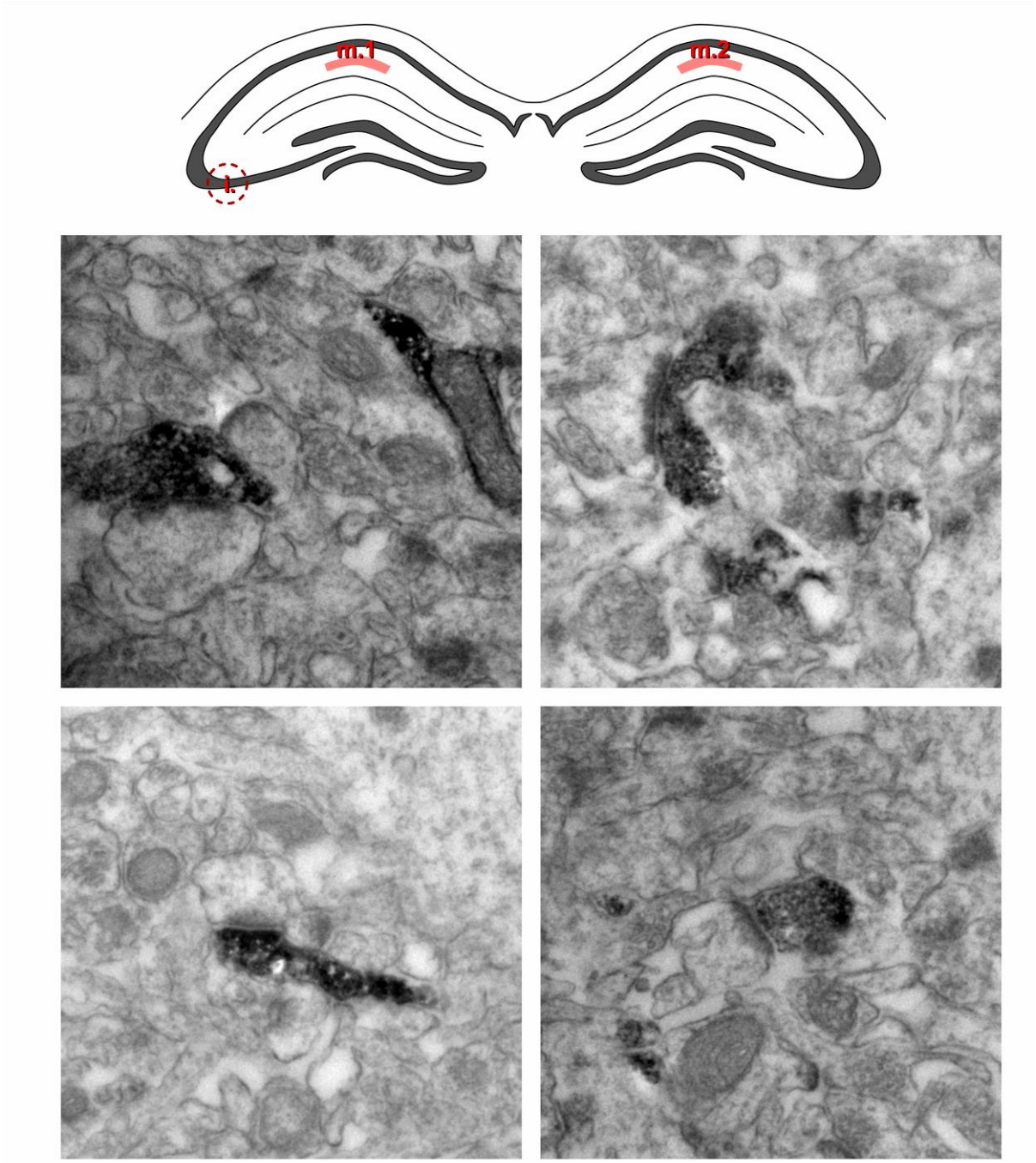

Labelled terminals

Upper schematic shows the hippocampus, with 'i' depicting sight of injection (unilateral injections into CA3 area) and 'm' showing sites of measurement (m.1 and 2 are ipsilateral and contralateral respectively. Only labelled terminals were measured in the CA1 stratum radiatum). Lower images show example EM images of 4 different labelled terminals.

Figure 6

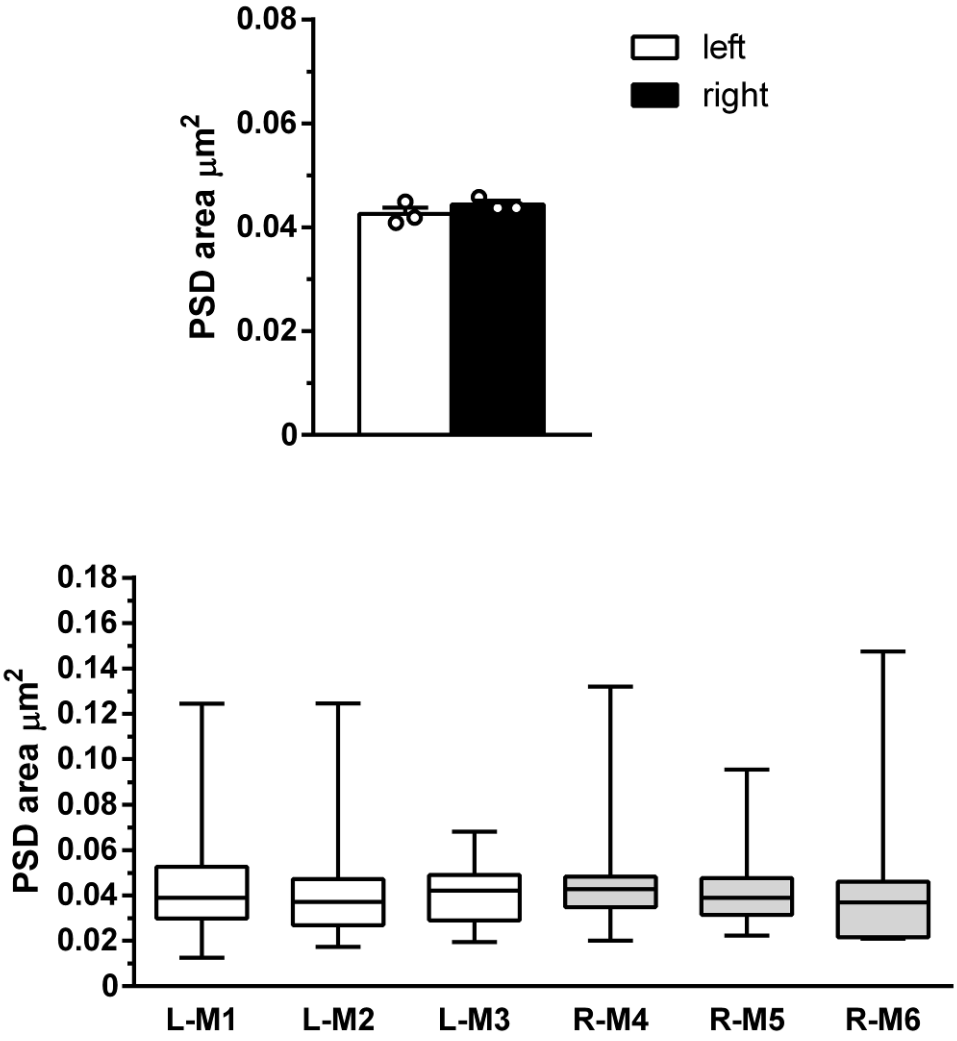

Ipsilateral PSD area from unilaterally injected left-isomerism *i.v.* mice

Upper chart shows average PSD area from labelled terminals in unilaterally injected *i.v.* mice. Left injected n = 3, right injected n = 3. Error bars display SEM and empty circles show average values for individual mice. Lower chart boxplots of PSD are from lebelled terminals for individual mice. The upper chart is an average of the lower values. For both charts, open box denotes density in left CA1, filled box denotes density in right CA1. PSD area was calculated from serial sections. Only synapses with complete PSDs were measured. Synapses were identified using the unbiased dissector analysis technique. Students T-test used for statistical analysis with no significance detectable.

Measuring only intact terminals, I ended up with an average PSD area measurement of around 0.04 μm² from projections originating in both the left- and right-CA1 (figure 6). This is comparable to the area found from left-originating projections in the wild-type mouse (Shinohara et al. 2008). As the hemisphere of injection had no significant effect on PSD area, I can confirm that this mouse line (like the original *i.v.* line) also lacked input-side dependent asymmetry. I therefore term this line as being 'left-isomerism'. Importantly, these results clearly highlight TEM as a viable method for determining left- or right-isomerism.

Finding a right-isomerism *i.v.* mouse line close to the spontaneous right to left-isomerism switch

1:2

The aim of this project was to determine a key gene responsible for input-side dependent asymmetry. One useful route to solving this problem would be through a whole genome sequence analysis study. However, before I proceeded towards that, I determined that it would be important to find a right-isomerism *i.v.* mouse, which was more closely related to the left-isomerism mouse used in experiment 1. If we were able to produce mixed litters (containing pups which were left- and right-isomerism), this would enable us to more-easily detect any key genes responsible for the switch, as there would be fewer differences between the siblings (*i.v.*3 being more-genetically similar to *i.v.*4 than the original *i.v.* line [*i.v.*0]). This meant that any mutations we did find, which are found only in left- or right-isomerism, are more likely to be interesting.

Unfortunately, we are not sure when the right-isomerism *i.v.* mouse line spontaneously switched into left-isomerism, through backcrossing with C57bl/6J. Therefore I chose an *i.v.* line (*i.v.*3) which had been backcrossed 5 times. To compare with the original *i.v.* mouse, I asked our collaborator in Japan (Professor Ito) to send me some fixed *i.v.*0 mouse brains, which I also analysed.

Methods and results

Methods used: Transcardial perfusion (method 2), preparation of mouse brain for analysis under TEM (method 3), dissector analysis (method 4).

As we know that the *i.v.* mouse lacks input-side dependent asymmetry, we felt that the injection of a tracer (as performed in experiment 1) was not necessary. Therefore, steps 2 – 6 of method 3 were omitted in this experiment.

Mice were housed in standard mouse cages (for an image, please see figure 28 NENR), cages were changed once a week, and food and water were supplied ad libitum.

9 – 10 week old *i.v.*3 and *i.v.*0 mice were used in this experiment.

Measurements of TEM images were conducted using the Reconstruct software (Fiala 2005)

Figure 7

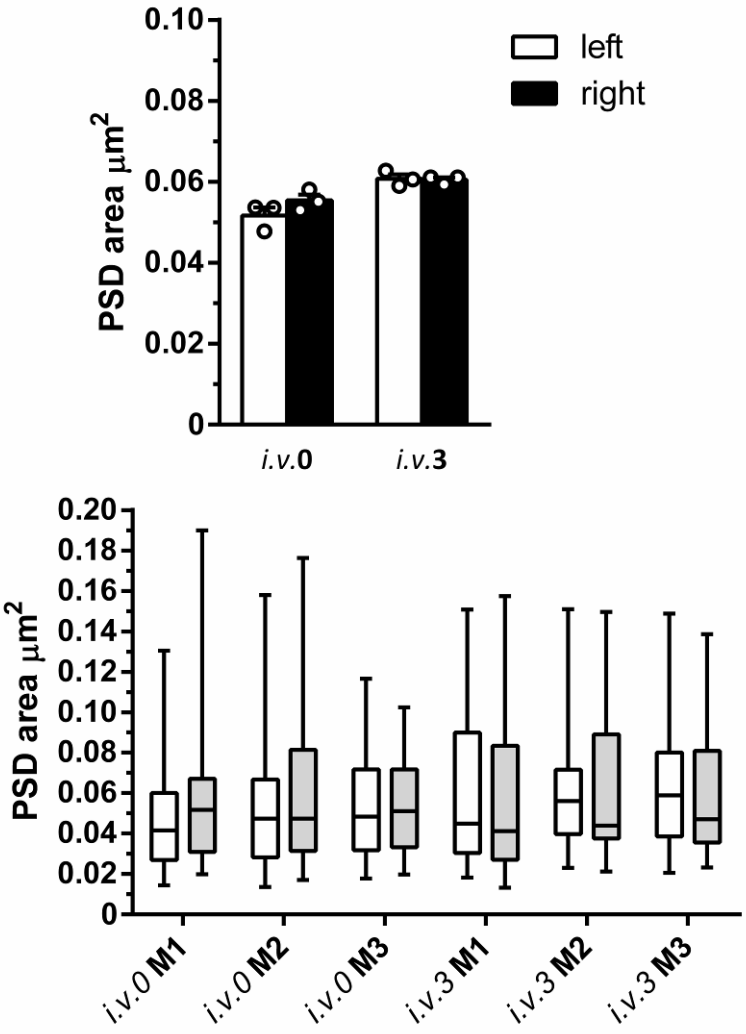

PSD area differences between the original *i.v.* and the *i.v.*3 mouse

Upper chart shows the average PSD area for synapses within the CA1 s.r. from *i.v.*0 and *i.v.3* mice. Error bars display SEM and empty circles show average values for individual mice. Lower boxplot shows PSD area for individual mice. Upper chart is an average of the lower chart's values. For all charts open box denotes density in left CA1 s.r., filled box denotes density in right CA1 s.r.. PSD area was calculated from serial sections. Only synapses with complete PSDs were measured. Synapses were identified using the unbiased dissector analysis technique. Mann Whitney test used for statistical analysis with no significance detectable. If we assume normal distribution and use the Students T-test used $p < 0.05$ between *i.v.*0 and *i.v.*3 for both left and right hemispheres.

Figure 8

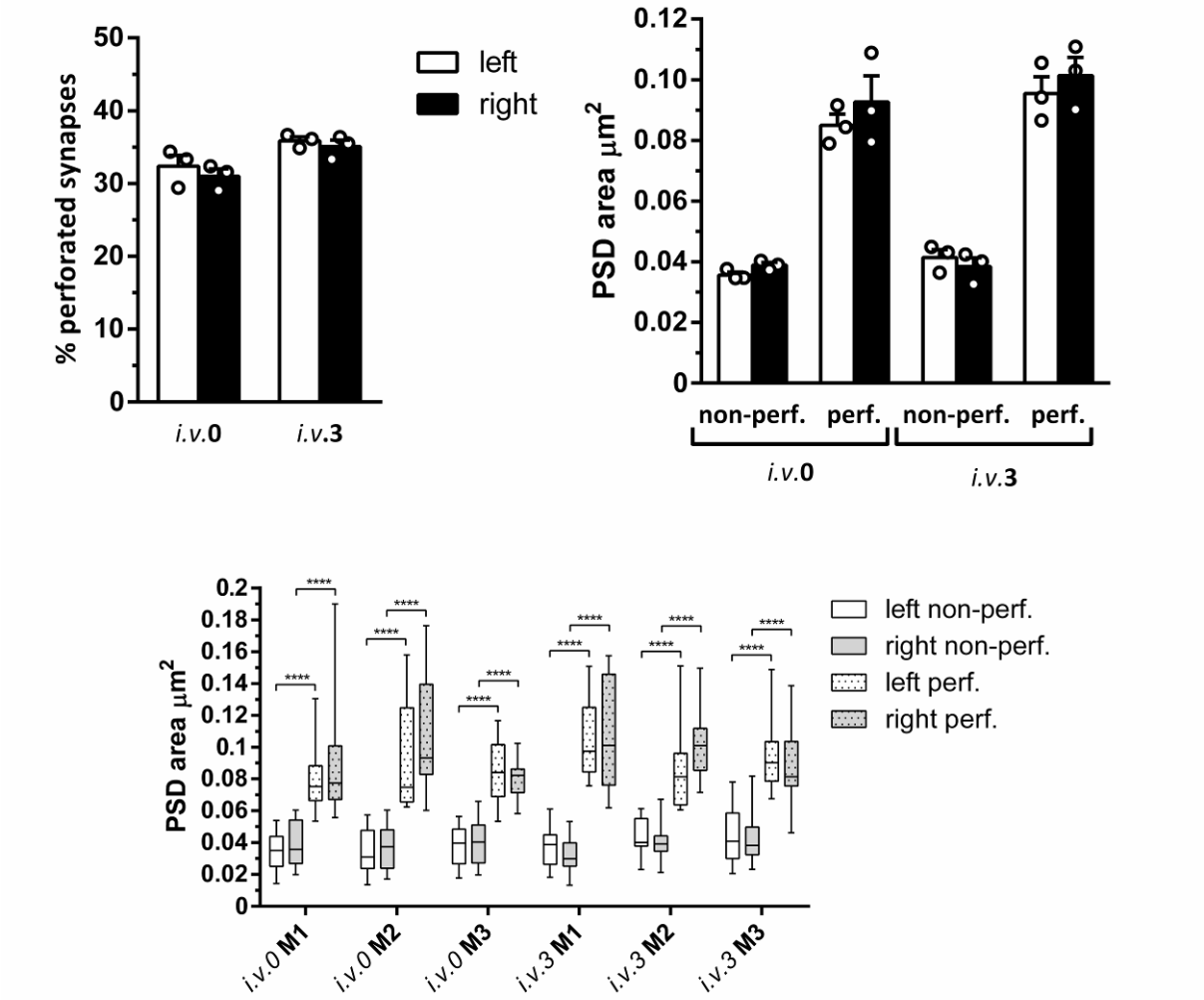

Differences in synapse perforation between the original *i.v.* and the *i.v.*3 mouse

Upper left chart shows the average percentage of synapses within the CA1 s.r., from *i.v.*0 and *i.v.3* mice, that have a perforated PSD. The upper right chart shows the PSD area for *i.v.*0 and *i.v.*3 mice subdivided based upon whether the synapses were perforated (perf.) or non-perforated (non-perf). Error bars display SEM and empty circles show average values for individual mice. Lower boxplot shows PSD area for individual mice, subdivided based upon whether the PSD was perforated or not. For all charts open box denotes density in left CA1 s.r., filled box denotes density in right CA1 s.r.. PSD area was calculated from serial sections. Only synapses with complete PSDs were measured. Synapses were identified using the unbiased dissector analysis technique. For charts displaying averages, Wilcoxon matched-pairs signed rank test used for statistical analysis, with no significance detectable. If normality assumed and Students T-test used $p < 0.05$ between non-perforated synapses in the left and right for both *i.v.*0 and *i.v.*3, as well as between non-perforated and perforated synapses for both the left and right, for both *i.v.*0 and for *i.v.*3. For individuals the Mann Whitney test was used with **** depicting $p < 0.0001$

Measuring only intact terminals in the *i.v.*3 mouse, I ended up with an average PSD area measurement of around 0.06 μm² from both the left- and right-CA1 s.r.. (figure 7). I also found that around 35% of the synapses in either CA1 s.r. were perforated. I found no significance in either PSD area or synapse perforation between either hemisphere. These are comparable to the values found from right-originating projections in the wild-type mouse (Shinohara et al. 2008). When I compared these results to the original *i.v.* mouse, I couldn't detect any significant differences between these two mutants. If I assumed a Gaussian distribution, I could find significant differences in PSD area from both hemispheres, as well a significant difference in synaptic perforation evident in the right hemisphere. As the PSD area of the *i.v.*3 mouse is more similar to the size of right-originating projections previously reported by Shinohara et al. I believe that this difference is more likely a difference in perfusion quality, than in any fundamental difference between either mouse line. Another interesting finding is that I could identify a significant difference in the PSD area size of non-perforated synapses. This has not previously been reported, but as the hemisphere which contains the larger area is different between both *i.v.*0 and *i.v.*3 (larger in the right and left hemispheres respectively), it's possible that it could be an artefact of the small number of mice used in the experiment (three mice used per line). As expected, there's a significant difference in the size of perforated and non-perforated synapses found in both hemispheres, for both lines.

Comparing left- and right-isomerism *i.v.* mice

1:3

As I had not performed injections when determining the phenotype of the *i.v.*3 mouse line, I perfused and stained 3 *i.v.*4 mice, of a similar age as the *i.v.*3 mice previously examined and repeated the experiment 2 on these mice. This enabled me to compare the two lines more reliably than if I had used my previous results from experiment 1.

Methods and results

Methods used: Transcardial perfusion (method 2), preparation of mouse brain for analysis under TEM (method 3), dissector analysis (method 4).

To reliably compare with the results from experiment 2, steps 2 – 6 of method 3 were omitted in this experiment.

Mice were housed in standard mouse cages (for an image, please see figure 28 NENR), cages were changed once a week, and food and water were supplied ad libitum.

9 – 10 week old *i.v.*4 mice were used in this experiment.

Measurements of TEM images were conducted using the Reconstruct software (Fiala 2005)

Figure 9

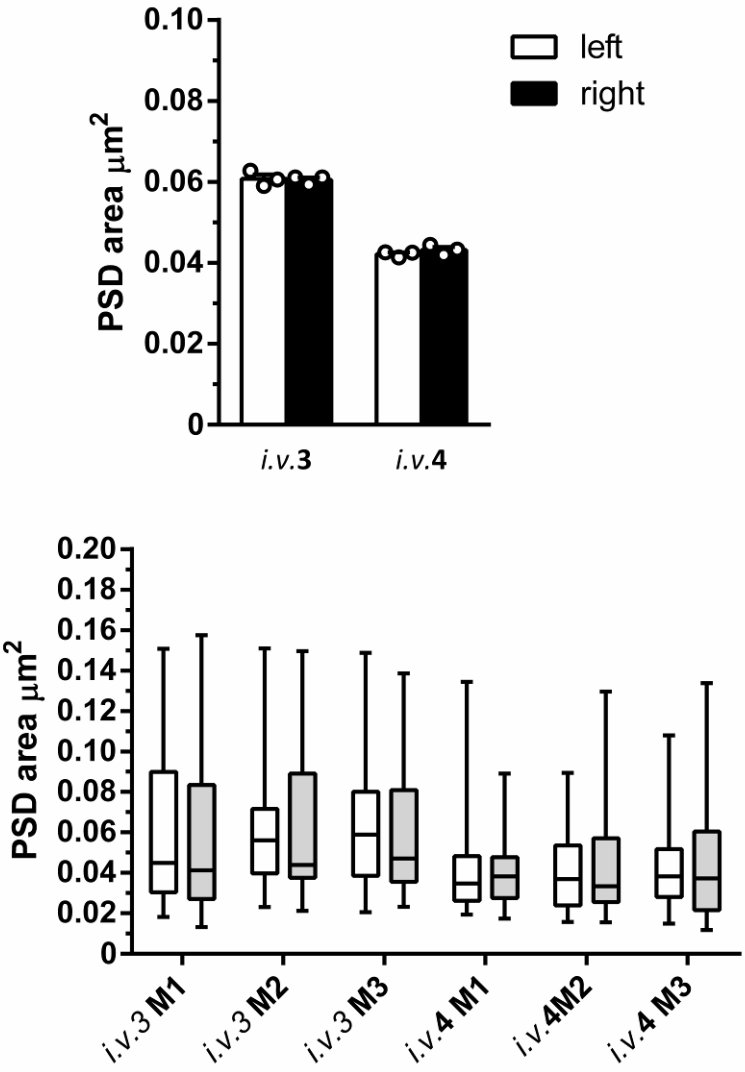

PSD area differences between left- and right-isomerism *i.v.* mouse lines

Upper chart shows the average PSD area for synapses within the CA1 s.r. from *i.v.*3 and *i.v.*4 *i.v.* mice. Error bars display SEM and empty circles show average values for individual mice. Lower boxplot shows PSD area for individual mice. Upper chart is an average of the lower chart's values. For all charts open box denotes density in left CA1 s.r., filled box denotes density in right CA1 s.r.. PSD area was calculated from serial sections. Only synapses with complete PSDs were measured. Synapses were identified using the unbiased dissector analysis technique. Mann Whitney test used for statistical analysis with no significance detectable. If normality assumed and Students T-test used for statistical analysis with $p < 0.0001$ for both left and right hemispheres between *i.v.*3 and *i.v.* 4.

Figure 10

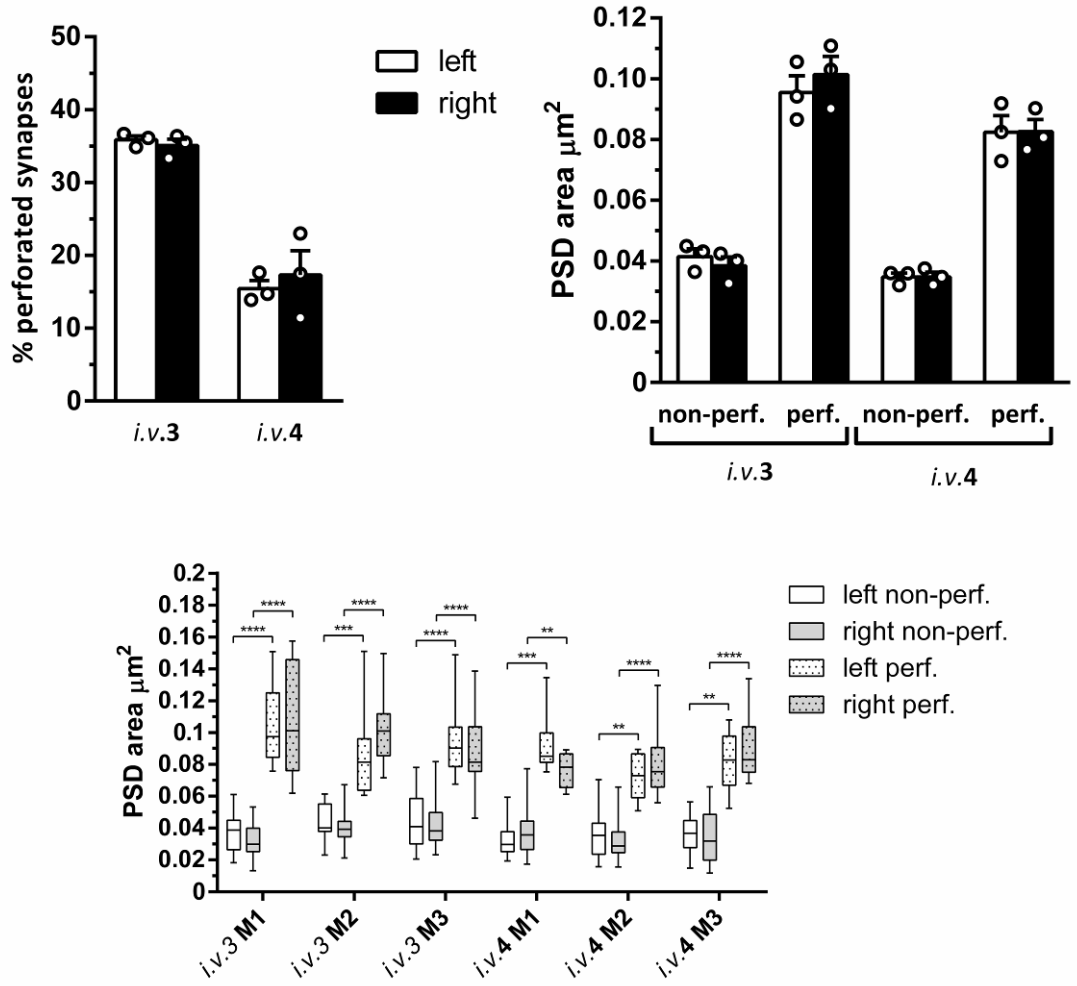

Differences in synapse perforation between left- and right-isomerism *i.v.* mice

Upper left chart shows the average percentage of synapses within the CA1 s.r., from *i.v.*3 and *i.v.*4 mice, that have a perforated PSD. The upper right chart shows the PSD area for *i.v.*3 and *i.v.*4 mice subdivided based upon whether the synapses were perforated (perf.) or non-perforated (non-perf). Error bars display SEM and empty circles show average values for individual mice. Lower boxplot shows PSD area for individual mice, subdivided based upon whether the PSD was perforated or not. For all charts open box denotes density in left CA1 s.r., filled box denotes density in right CA1 s.r.. PSD area was calculated from serial sections. Only synapses with complete PSDs were measured. Synapses were identified using the unbiased dissector analysis technique. For the averages, both the Wilcoxon matched-pairs signed rank and Mann Whitney tests were used for statistical analysis, with no significance detectable. If normality assumed and Students T-test used for statistical analysis, p value < 0.0001 can be detected between *i.v.*3 and *i.v.*4 for the % of perforated synapses in both the left and right. Assuming normality, $p < 0.05$ can be detected between the left and right non-perforated in *i.v.*3, as well as between the non-perforated and perforated for both left and right in *i.v.*3 and the left in *i.v.*4. For the right non-perforated to perforated PSD area in *i.v.*4, the $p < 0.01$. For the individuals, the Mann Whitney test was used, with ** denoting $p < 0.01$, *** denoting $p < 0.001$, and **** denoting $p < 0.0001$.

Figure 11

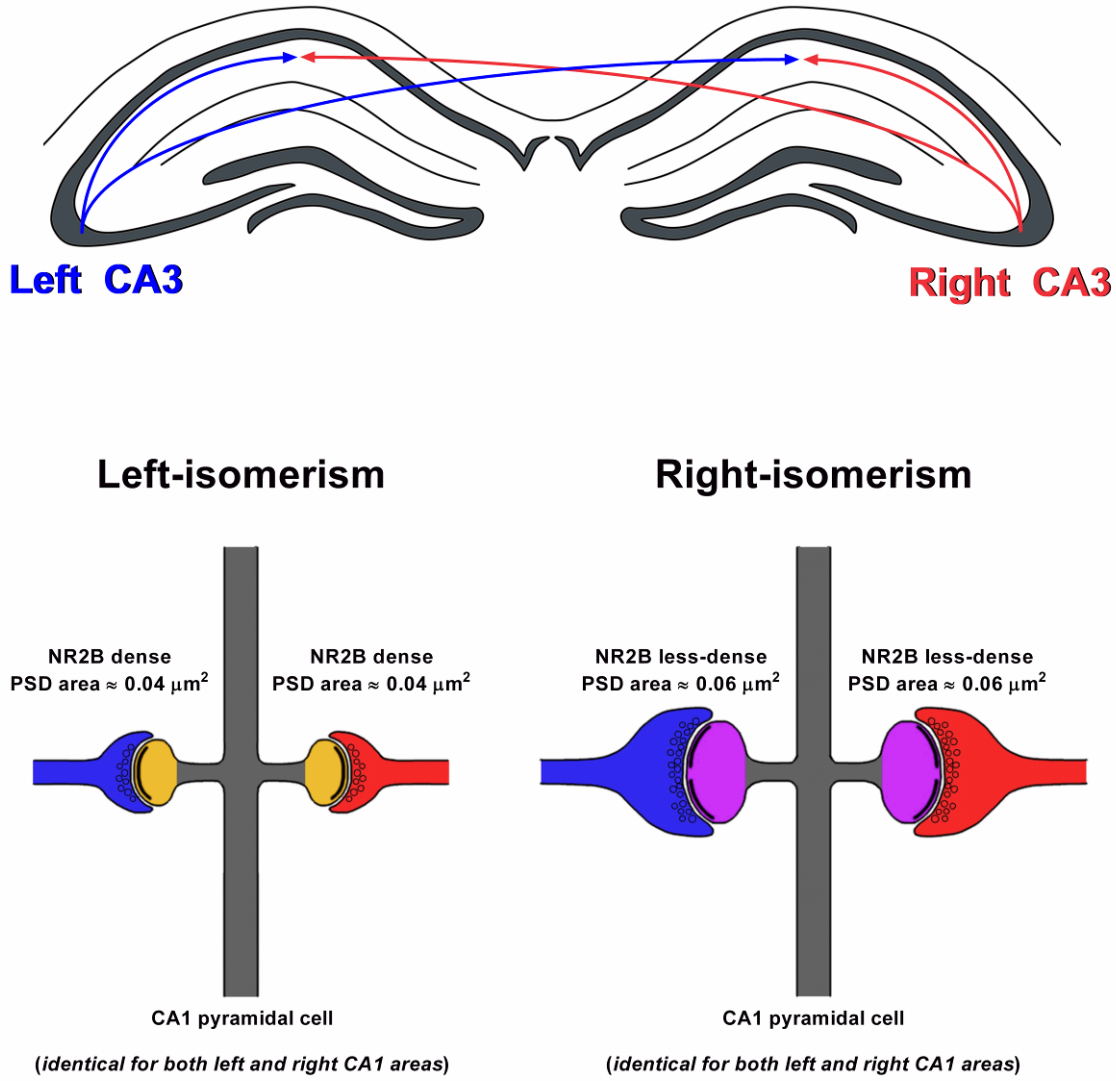

Left- and right-isomerism *i.v.* mutants

Simple schematic to display the lack of input-side dependent asymmetry in the hippocampus in left- and right-isomerism *i.v.* mice. Above shows a schematic for the projections from the left and right CA3. Below shows a simple schematic of connections from CA3 to CA1 pyramidal cells. Inputs from the left CA3 are in blue, inputs from the right CA3 are in red. Yellow depicts small, thin, NR2B dense spines. Purple depicts larger, mushroom-type, NR2B less-dense spines.

Measuring only intact terminals in the *i.v.*4 mouse, I ended up with an average PSD area measurement of around 0.04 μm² from both the left- and right-CA1 s.r.. (figure 9). I also found that around 15-20% of the synapses in either CA1 s.r. were perforated (figure 10). I found no significance in either PSD area or synapse perforation between either hemisphere. These are comparable to the values found from experiment 1. When I compared these results to the results from the *i.v.*3 mouse, I couldn't detect any significance unless I assumed a Gaussian distribution. With this assumption, I could find significant differences in PSD areas, as well as synaptic perforation, from both hemispheres. This is expected and correlates nicely with the findings from Shinohara et al. (2008). Although I did not measure the density of NR2B, if the *i.v.*3 and *i.v.*4 mouse follow the same morphological rules as the wild-type mouse does, then it is likely that I'd detect symmetry in its density in both hemispheres, comparable to those seen from right- or left-originating projections in the wild-type mouse (Kawakami et al. 2003). This is certainly likely in the *i.v.*3 mouse line, as NR2B symmetry has already been demonstrated in the original *i.v.* mouse line (Kawakami et al. 2008). A simple schematic of the difference between left- and right-isomerism is shown as figure 11.

Crossing left- and right-isomerism *i.v.* mice

1:4

Now that I had two closely related *i.v.* lines (separated by around 5 back-crossings) with differing isomerism, the next step was to cross them together and investigate the resulting pups. The aim was to produce a mating pair which would produce mixed litters (containing both left- and right-isomerism offspring), for whole genome sequence analysis. Therefore I crossed a left-isomerism male with a right-isomerism female.

Methods and results

Methods used: Transcardial perfusion (method 2), preparation of mouse brain for analysis under TEM (method 3), dissector analysis (method 4).

As before, steps 2 – 6 of method 3 were omitted in this experiment.

Mice were housed in standard mouse cages (for an image, please see figure 28 NENR), cages were changed once a week, and food and water were supplied ad libitum.

At 9 – 10 weeks old the F1 pups were perfused and their synaptic morphologies investigated.

Measurements of TEM images were conducted using the Reconstruct software (Fiala 2005)

Figure 12

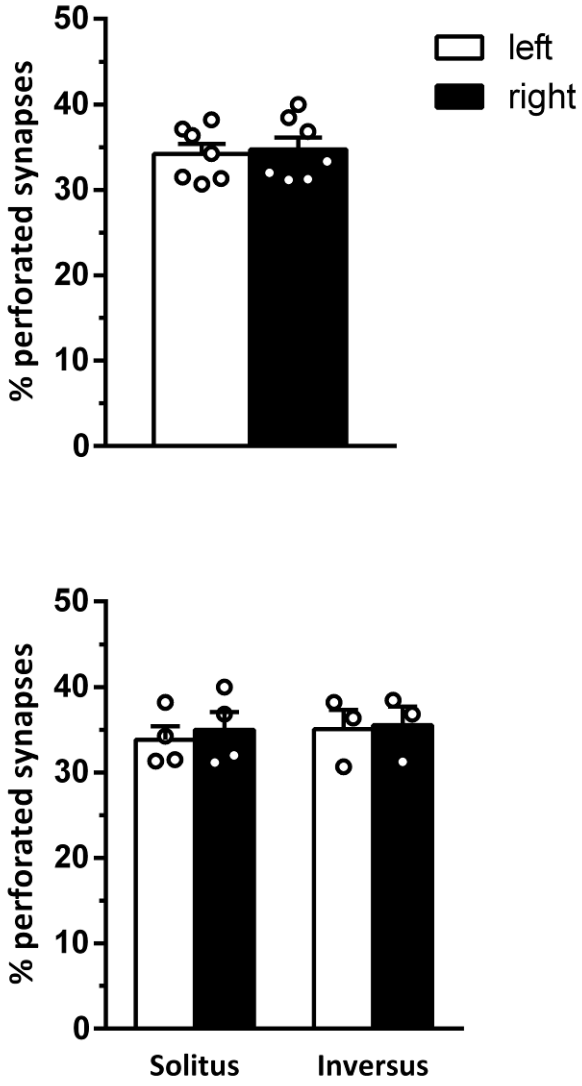

Crossing left- and right-isomerism *i.v.* mice - percentage of perforated synapses in F1

Upper chart shows the percentage of synapses with a perforated PSD within the CA1 s.r. from the F1 generation of a left- and right-isomerism breeding pair (father is left-isomerism). Error bars display SEM and empty circles show average values for individual mice. Lower boxplot shows the same data, subdivided based upon organ laterality. For all charts open box denotes perforation in the left CA1 s.r., filled box denotes perforation in right CA1 s.r.. Perforated synapses were calculated from serial sections. Only synapses with complete PSDs were measured. Synapses were identified using the unbiased dissector analysis technique. Students T-test used for statistical analysis with no significance detectable.

When I examined the percentage of perforated synapses (figure 12) I found that, for all the mice from the F1 litter, greater than 30% of their synapses had a perforated PSD. This is comparable to the right-isomerism phenotype. As expected, I found no significant difference between mice with regular (situs solitus), or inverted (situs inversus), body axis laterality. This suggests that right-isomerism might be dominant phenotype.

Back-crossing the pups from the F1 generation with their father to investigate whether a single gene is responsible for left-right determination

1:5

In generating the left-isomerism *i.v.* mouse line, we back-crossed the original *i.v.* mutant over 10 times with the C57bl/6J wild-type mouse. This meant that the two parents, from the *i.v.*3 and *i.v.*4 lines, were reasonably closely related. If it was a single-gene (Gene X) responsible for the difference between the left- and right-isomerism phenotypes, then it is possible that the right-isomerism mother was homozygous dominant for that gene (XX) and the left-isomerism father was homozygous recessive for that gene (xx). This would make all the pups from the F1 generation heterozygous dominant (Xx).

To investigate this possibility, I back-crossed a female from the F1 generation with her father (figure 13). If my hypothesis was correct, it would mean that, for Gene X, the F2 litter would be a mix of homozygous recessive left- (xx) and heterozygous dominant (Xx) right-isomerism pups.

Methods and results

Methods used: Transcardial perfusion (method 2), preparation of mouse brain for analysis under TEM (method 3), dissector analysis (method 4).

As before, steps 2 – 6 of method 3 were omitted in this experiment.

Mice were housed in standard mouse cages (for an image, please see figure 28 NENR), cages were changed once a week, and food and water were supplied ad libitum.

At 9 – 10 weeks old the F2 pups were perfused and their synaptic morphologies investigated.

Before perfusing, tail biopsies were taken from each mouse. These were stored at -20 °C.

Measurements of TEM images were conducted using the Reconstruct software (Fiala 2005)

Figure 13

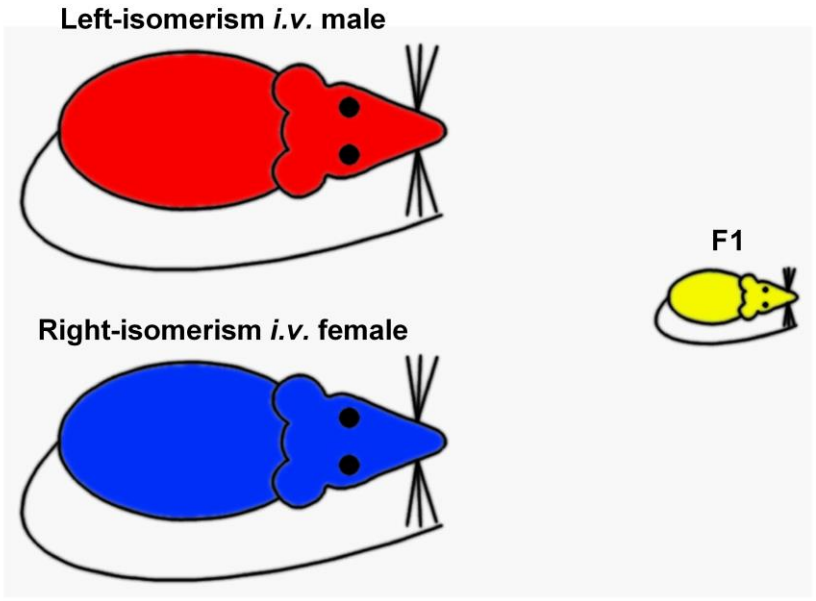

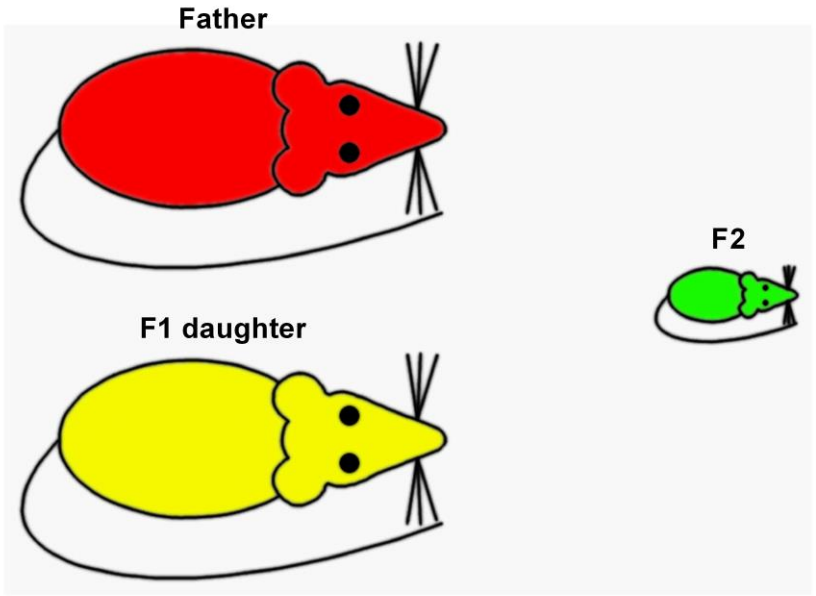

Breeding schemes for F1 and F2

Top scheme shows the breeding plan for the F1 generation. A left-isomerism (*i.v.*4) male (red) and a right-isomerism (*i.v.*3) female (blue) were crossed. All pups in F1 were found to be right-isomerism. Bottom scheme shows the breeding plan for the F2 generation. The father (*i.v.* 4) was crossed with a female from the F1 generation.

Figure 14

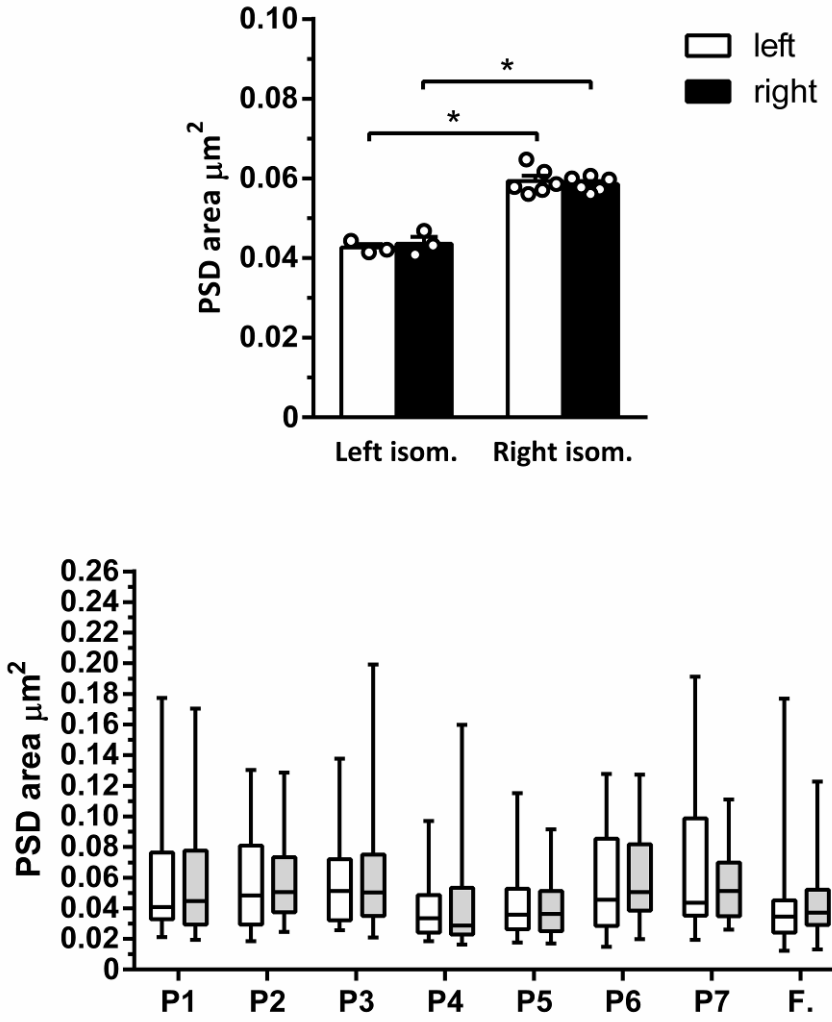

Crossing father with offspring from F1 generation - PSD area in F2

Upper chart shows the average PSD area for synapses within the CA1 s.r. from the F2 generation of a left-isomerism mouse (the father) and its female pups from the F1 generation (F1 produced by crossing father with right-isomerism female *i.v.* mouse). The father and mother are included in the dataset. Mice have been divided into left- or right-isomerism based upon PSD area and the % of perforated synapses in both hemispheres. Error bars display SEM and empty circles show average values for individual mice. Lower boxplot shows the data for individuals. P denotes a pup, F. denotes the father, and M. denotes the mother. For all charts open box denotes PSD area in the left CA1 s.r., filled box denotes PSD area in right CA1 s.r.. PSD measurements were calculated from serial sections. Only synapses with complete PSDs were measured. Synapses were identified using the unbiased dissector analysis technique. Mann Whitney test used for statistical analysis with * denoting $p < 0.05$.

Figure 15

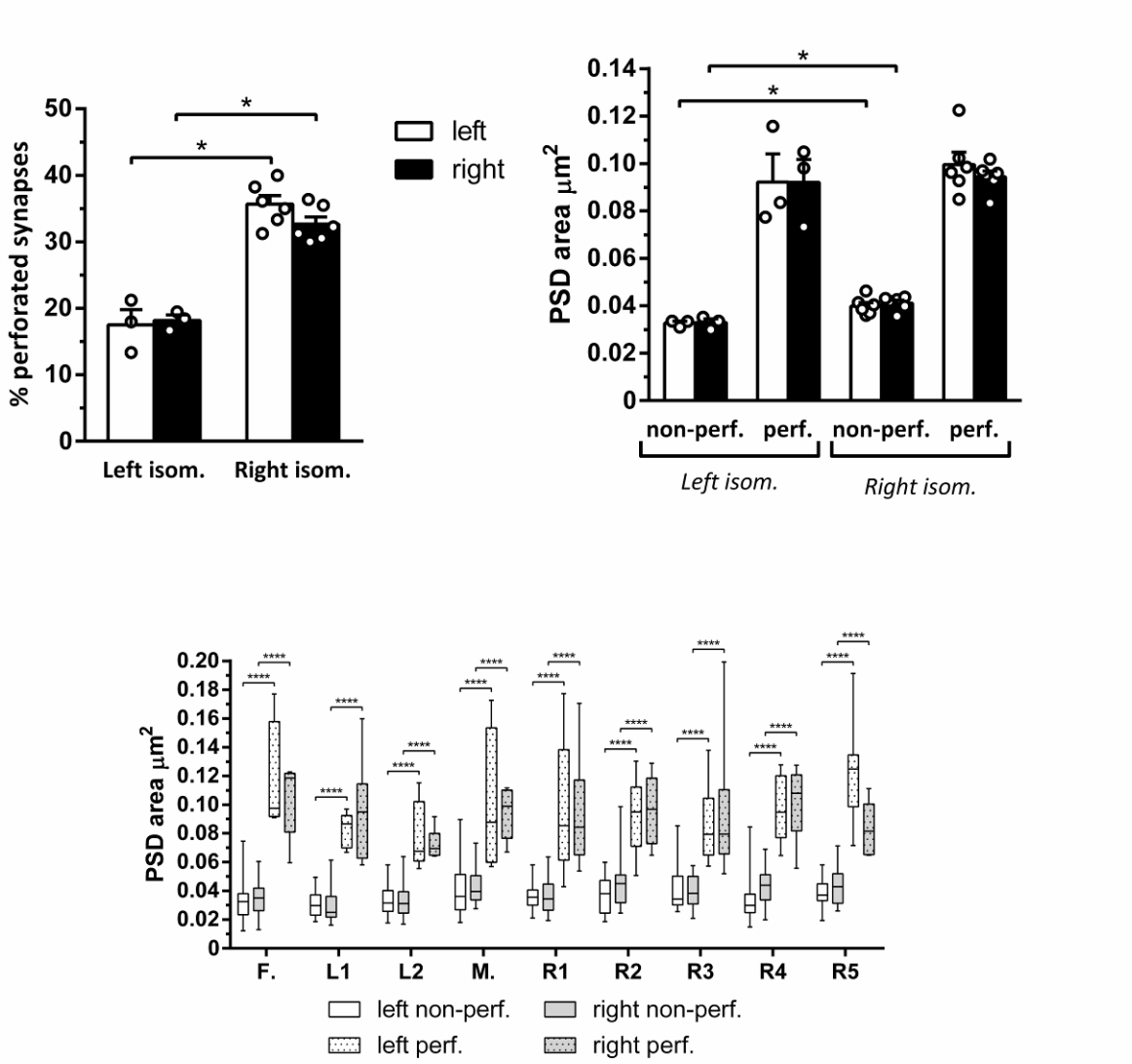

Crossing father with offspring from F1 generation - synapse perforation in F2

Upper left chart shows the average percentage of synapses within the CA1 s.r., from F2 mice and parents, that have a perforated PSD. The upper right chart shows the PSD area for F2 mice and parents, subdivided based upon whether the synapses were perforated (perf.) or non-perforated (non-perf). Error bars display SEM and empty circles show average values for individual mice. Lower boxplot shows PSD area for individual mice, subdivided based upon whether the PSD was perforated or not. F. denotes father, M. denotes mother, L. denotes mouse determined to be left-isomerism, and R. denotes mouse determined to be right-isomerism. For all charts open box denotes density in left CA1 s.r., filled box denotes density in right CA1 s.r.. PSD area was calculated from serial sections. Only synapses with complete PSDs were measured. Synapses were identified using the unbiased dissector analysis technique. Mann Whitney test used for statistical analysis with * denoting $p < 0.05$ and **** denoting $p < 0.0001$.

When I examined the PSD area (figure 14) I found that I could divide the pups into two groups, those with an average PSD area, in either hemisphere, of less than 0.05 μm² and those with an average PSD area, in either hemisphere, of greater than 0.05 μm². When I checked the percentage of perforated synapses between these pups, I found that the mice with an average PSD area of less than 0.05 μm² also had a perforation percentage of less than 22%, whereas all the other mice had perforation percentages of over 30% (figure 15). This gave me confidence to classify the two groups as 'predicted-left' and 'predicted-right'. To ensure that the parents had the phenotypes I expected, I also perfused and analysed them and found that they also fit nicely into their expected PSD and percentage perforated values; therefore I grouped their data into the average graphs shown in figures 14 and 15.

When we compare the average values for the predicted-left (left isom.) and predicted-right (right isom.) groups, we find clear significance between both hemispheres in both PSD area size (figure 14) as well as the percentage of synapses with a perforated PSD (figure 15). Both the PSD area, as well as the perforation percentage, measurements fall neatly into the expected values for left- and right-isomerism *i.v.* mice (as shown in experiments 1 and 2, and summarized in figures 9 and 10). Interestingly, when we subdivide the PSD area measurements into those for non-perforated and perforated synapse types, we find a significant difference between the predicted-left and -right groups in their non-perforated synapses. This finding was not previously detected in the unrelated *i.v.*3 and *i.v.*4 mice (figure 10), however.

These findings give me confidence that a single gene might be responsible for the switch from right- to left-isomerism which was seen in the *i.v.* mouse line. As I was able to produce a mixed litter, containing pups of both phenotypes, I felt confident to move onto whole genome sequence analysis for these mice.

Whole genome sequence analysis of parents and offspring to try and isolate Gene X

1:6

If I were to assume that a single gene (Gene X) was responsible for the determination of left- or right-isomerism in *i.v.* mice, then I could predict that both parents must have differences in this gene. I could also predict that the predicted-left mice should share a similar

genetic sequence as their father, and the predicted-right as their mother. Finally, if my hypothesis about Gene X being homozygous recessive in the left-isomerism and heterozygous dominant in the right-isomerism pups was correct, I should be able to detect this within the individual mouse genomes.

To test this, I decided to perform whole genome sequence analysis of all the pups and both parents.

Methods and results

Methods used: DNA isolation from tail biopsies (using DNeasy blood and tissue kit: Full protocol available here: https://www.qiagen.com/at/resources/resourcedetail?id=6b09dfb8-6319-464d-996c-79e8c7045a50&lang=en).

To isolate high-quality DNA for sequencing I used the DNeasy blood and tissue kit (QIAGEN), then I sent off the DNA to my collaborator, Professor Shuji Shigenobu (NIBB, Okazaki, Japan), for production of the Illumina next-generation sequencing (NGS) libraries.

Following this, I could download the sequences from the NIBB database and perform further processing, before I could view and analyse the sequence to try and isolate Gene X.

Programs used:

For pre-processing reads, I used Cutadapt (Martin 2011)

For mapping the sequences to the mm10 genome, I used Bowtie 2 (Langmead 2012)

For calling up and investigating SNPs, I used SAMtools (Li 2009, Li 2011)

For visualizing the mapping data, I used the Interactive Genomics Viewer (IGV) software (Robinson 2011, Thorvaldsdóttir 2013)

For restricting my search to only SNPs which appeared within genes on chromosome 12, I used a python script which was written for me by my colleague David Kleindienst (figure 16).

For scoring my mutations, I used the following rules, to give a total score (out of 7) for each mutation found:

1. Both parents must not share a similar mutation (if they do, score the mutation as 0)

2. For each predicted-left pup which shares a similar mutation with the left-isomerism parent, score +1
3. For each predicted-right pup which shares a similar mutation with the right-isomerism parent, score +1

For comparing the genomes of different mice, I used Varscan v2.4.2 (Koboldt 2009, Koboldt 2012, URL:http://varscan.sourceforge.net)

Unfortunately, when I checked the depth and mapping ratios of the mice, the coverage was not high enough for my purposes.

Mouse	Mapping ratio
Pup 1	88.8668%
Pup 2	89.8637%
Pup 3	88.7383%
Pup 4	88.2467%
Pup 5	87.2704%
Pup 6	89.8369%
Pup 7	91.5117%
Father	93.8035%
Mother	93.7387%

It was possible that, should a region of a mouse's genome not be sequenced correctly, I might have missed the mutation of interest in Gene X. Therefore, I asked Professor Shigenobu to perform additional runs on the same DNA, to increase the coverage to a more reliable value.

Cutadapt sequences

Cutadapt is a tool designed to remove leftover adapter sequences from the 3' end of the DNA (Martin 2011), which remain from the creation of the Illumina libraries. As these nucleotide sequences are not part of the original genome of the mouse, it is important to remove them before further analysis can be performed. I used the following sequences with the Cutadept script:

UNIV_ADAPTER_COMP = AGATCGGAAGAGCGTCGTGTAGGGAAAGAGTGTAGATCTCGGTGGTCGCCGTATCATT

IDX_CONS = AGATCGGAAGAGCACACGTCTGAACTCCAGTCAC

Figure 16

```
#!/usr/bin/env python2
# -*- coding: utf-8 -*-
"""
Created on Fri Sep  8 13:05:57 2017

@author: David Kleindienst
"""

# File with locations of all genes
genesFile='L:\genes.gtf'
#example line:
#chr1	unknown	exon	3214482	3216968	.	-	.	gene_id "Xkr4"; gene_name "Xkr4"; p_id "P15391"; transcript_id "NM_001011874"; tss_id "TSS27105";

#File containing SNPs of a particular mouse
inputFile='Mouse_SNP_LIST'
#example line:
#chr10	3104323	A	-C	*/-C:13:5:9:64.29%:2.8986E-4	Pass:1:4:6:3:1E0	0	1	0	0	*/-C:13:5:9:64.29%:2.8986E-4

outputFile=inputFile[0:-4]+'_genes.txt'

Genes=dict()
Output=''

#From Gene File: Generate a dictionary with chromosomes as keys,
#values being list of [start, stop, gene name, exon/intron] for each gene
with open(genesFile,'r') as f:
    line=f.readline()
    while line!='':
        line=line.strip('\n')
        l=line.split('\t')
        #Make new key for chromosome or append, if the key already exists
        if l[0] in Genes.keys():
            Genes[l[0]].append([int(l[3]),int(l[4]),l[8].split('"')[1],l[2]])
        else:
            Genes[l[0]]=[[int(l[3]),int(l[4]),l[8].split('"')[1],l[2]]]
        line=f.readline()

with open(inputFile,'r') as f:
    line=f.readline()
    while line!='':
        line=line.strip('\n')
        l=line.split('\t')
        #Search through genes of the corresponding chromosome
        for i in range(len(Genes[l[0]])):
            #If the SNP is within a gene
            if int(l[1])>Genes[l[0]][i][0] and int(l[1])<Genes[l[0]][i][1]:
                Output=Output+l[0]+'\t'+l[1]+'\t'+l[2]+'\t'+l[3]+'\t'+Genes[l[0]][i][2]+'\t'+Genes[l[0]][i][3]+'\n'
                #Add the relevant information about the SNP, the gene-name and information if it's exon or intron to the output
                break

        line=f.readline()

#Write the output to file
with open(outputFile,'w') as f:
    f.write(Output)
```

Restricting search for SNPs to only those found within genes on chromosome 12

To narrow down the search to investigate only mutations found within genes on chromosome 12, my colleague, David Kleindienst, wrote this python script. Red text dictates the SNP list for a mouse, whereas the blue text dictates the genes list (obtained from the IGV software). The position of each mutation on chromosome 12 is compared to the list obtained from the IGV software and, if it falls within the region dictating a gene, it is kept, otherwise it is ignored. The script will then output a file with the positions, mutations, and the genes they are found within.

Figure 17

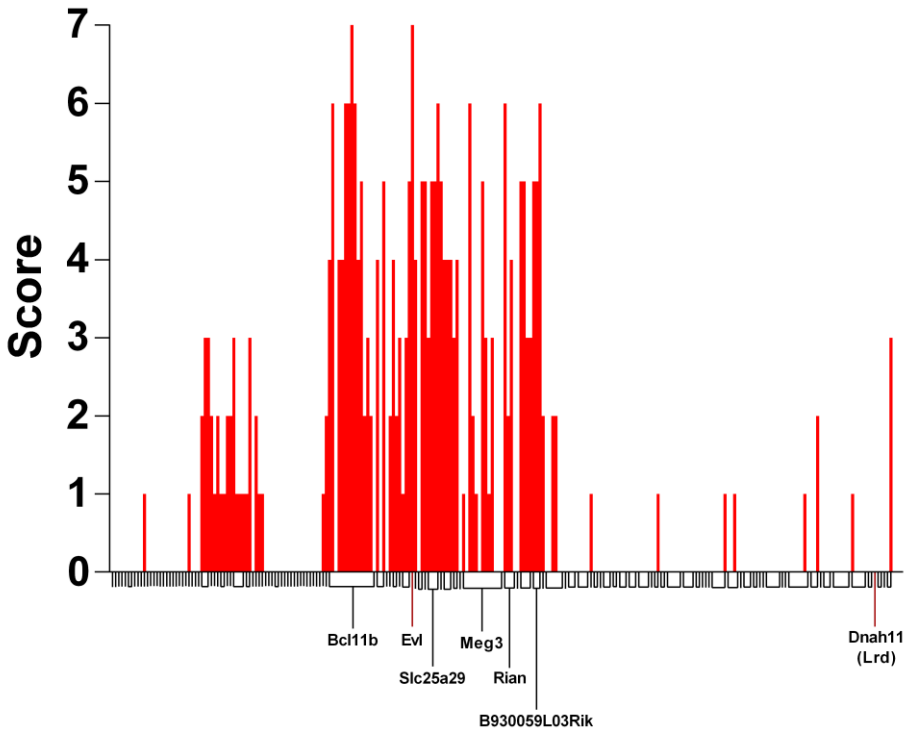

Score for mutations within chromosome 12 in F2 mice

Chart depicting score for mutations found within genes on chromosome 12, in pups from the F2 generation of left- and right-isomerism *i.v.* mouse crossing. Score is determined based upon the following. If both parents share a similar mutation, score = 0. If a right-isomerism pup shares a mutation with the right-isomerism parent (mother), score +1. If a left-isomerism pup shares a mutation with the left-isomerism parent (father), score +1. Max score per mutation = 7 (7 pups). Black marks on the X axis depict different genes found to contain mutations by whole genome sequencing. 6 genes of interest (containing mutations with scores of 6+) are marked, as is the Lrd gene (Dnah11 - responsible for the *i.v.* mutation).

Figure 18

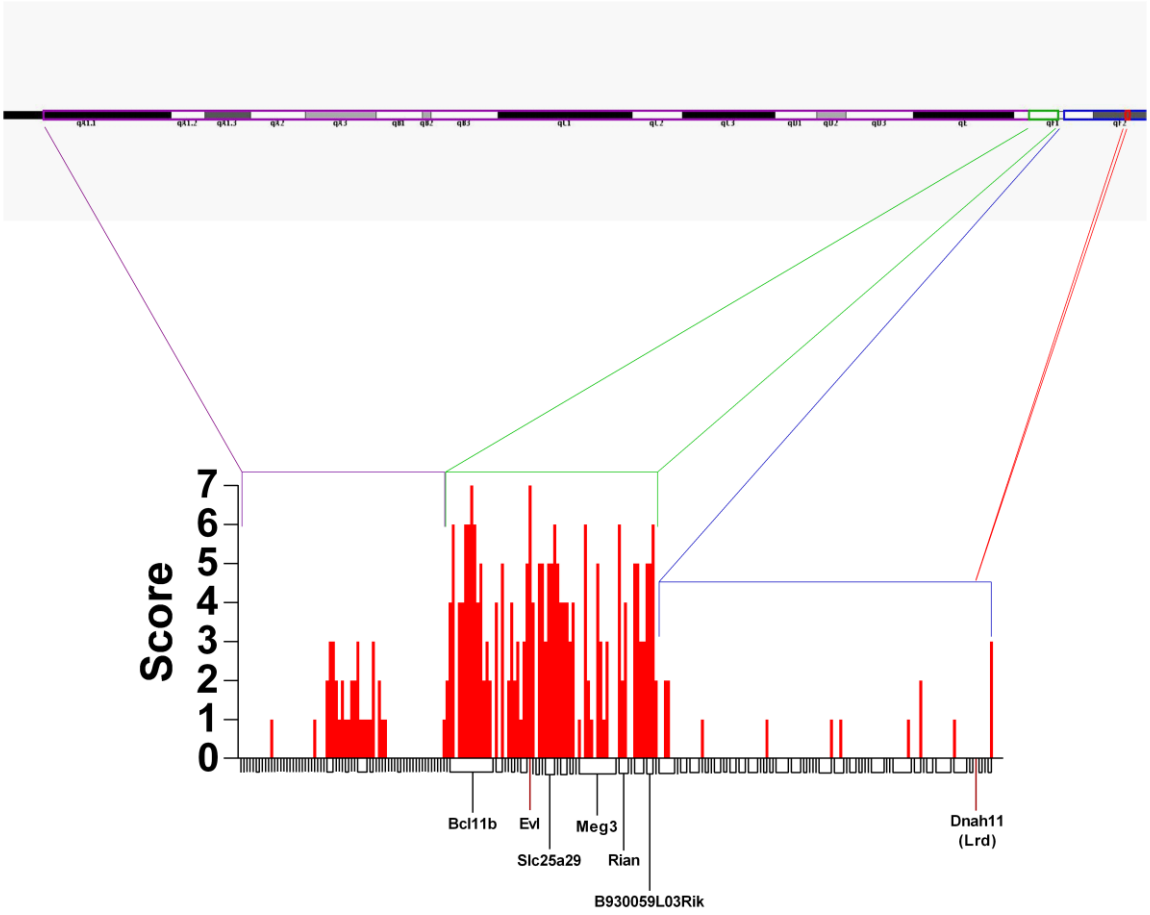

Region of very high mutation

Top figure shows chromosome 12 with regions with high mutations within genes highlighted. Chart depicts score for mutations found within genes on chromosome 12, in pups from the F2 generation of left- and right-isomerism *i.v.* mouse crossing. Purple denotes large area of chromosome 12 with very low score. Green denotes small area with high number of mutations and a high score. Blue denotes region with high mutation, but similarity between both left- and right-isomerism mice. Red denotes Lrd gene.

Having removed any unrelated nucleotides from the sequences, I then had to align them to the mouse genome. I used the Bowtie 2 algorithm for this purpose (Langmead 2012). I decided that it would be best to align the sequences from my individual mice to the mm10 reference genome, as this is currently the most complete genome sequence for the C57bl/6J mouse. Following this, I used SAMtools (Li 2009, Li 2011) to convert and sort the sequences. SAM tools is a software package containing various tools for sorting manipulating DNA sequence alignments. After sorting the sequences, I used the Interactive Genomics Viewer (IGV) software (Robinson 2011, Thorvaldsdóttir 2013) to visualise them.

To narrow down my search, I used three separate methods. Firstly I used the Varscan software (Koboldt 2009, Koboldt 2012) to compare the genomes of different mice. Following the assumption that all left- or all right-isomerism mice should have a similar sequence in Gene X, I created files containing all the mutations which were present in any left- or right-isomerism mouse, as well as files listing all the mutations which were present in every mouse in the left- or right-isomerism groups. I then used Varscan to create files which contained either mutations which all left-isomerism mice had, but no right-isomerism mice, or mutations which all right-isomerism mice had, but no left-isomerism mice. I also tried searching for specifically homozygous mutations which all left-isomerism mice had, which were also heterozygous in all right-isomerism mice. The second approach I used was to restrict my search to include only SNPs which appeared within genes on chromosome 12. To do this I used a python script which was written for me by my colleague David Kleindienst (figure 16). The final method I used was to manually apply a score to each mutation I found (from 0, where either no pups share the mutation with the expected parent, or where both parents share the mutation, to 7, where every pup shares the mutation with the parent which has the similar isomerism). This enabled me to score each mutation, found within genes within chromosome 12 (figure 17), so I could restrict my future searches to only high-scoring regions.

Due to the issue of a particular mutation not being covered in the sequencing, it is possible that I might have missed Gene X through this scoring method. Another possible reason to miss Gene X would be if it was either not located within a gene, or it was located on a chromosome other than 12. However, I decided that, should I include other chromosomes/regions not restricted to within genes, then the number of SNPs would be vastly increased. Therefore, I started my search with this limited search strategy.

By assigning a score of 0 to 7 to each SNP, it was possible to see three distinct regions within chromosome 12 (figure 18). The region close to the Dnah11 gene (the blue region) contained mutations which tended to have a rather low score (0 – 3). This was because the mutations which were found within genes tended to be shared by both parents. The majority of these mutations were also found to be shared with the offspring as well. As *i.v.* mice were always genotyped for a point mutation in the Lrd gene, it is hardly surprising that there would be a bias for similarity in the surrounding region of the chromosome. Next to this is a region which contains many mutations of very high score (the green region). It is possible that this is due to a crossover event between an *I.v.* mouse and the C57bl/6J line and it seems to potentially be an interesting region for Gene X. The final region (the purple region) contains many mutations, but these tend to be of a very low score. This is due to them being mutations limited to individual mice, rather than being shared between all predicted-left or predicted-right mice.

Of the mutations found within the central (the green) region, there are two genes which were found to contain mutations with scores of 7; these genes are the B-Cell CLL/Lymphoma 11B (Blc11b) and the Enah/Vasp-Like (Evl) genes. I also found some mutations of lower scores within the Bcl11b gene.

Confirming the high-scoring mutations within the genes Bcl11b and Evl, using unrelated left- and right-isomerism *i.v.* mice

1:7

Although I had found mutations in both the Bcl11b and Evl genes, within my 9 mice analysed, I wanted to confirm that I could find similar mutations within unrelated *i.v.* mutants. This was because, if either of these 2 genes is Gene X, then that specific mutation, within that gene, must be retained in all left- or right-isomerism *i.v.* mice. To investigate this, I decided that the most simple step to start with would be to design primers around the mutations, then amplify the regions of interest using the polymerase chain reaction (PCR) so that I could sequence the products and confirm if they fit the sequences expected for left- or right-isomerism mice.

The assumption was that all left-isomerism (*i.v.*4) and all right-isomerism (*i.v.*3) *i.v.* mice should have similar mutations to those found in the predicted-left and predicted-right genomes respectively. If I did not find the results that I expected, then it was likely that the mutation I was investigating was not the one I am searching for.

Methods and results

Methods used: DNA isolation from tail biopsies (using DNeasy blood and tissue kit: Full protocol available here: https://www.qiagen.com/at/resources/resourcedetail?id=6b09dfb8-6319-464d-996c-79e8c7045a50&lang=en), PCR and gel electrophoresis examination of interesting mutations (method 5).

Unrelated *i.v.* mice were obtained from our animal storage facility

Mice were housed in standard mouse cages (for an image, please see figure 28 NENR), cages were changed once a week, and food and water were supplied ad libitum.

At 9 – 10 weeks old the tail biopsies were taken and genomic DNA was extracted using the DNeasy blood and tissue kit.

Primers were designed by me and produced by Integrated DNA Technologies (www.idtdna.com)

Sequencing of fragments was performed by LGC genomics (https://shop.lgcgenomics.com/)

Sequence was analysed using the SnapGene software (http://www.snapgene.com/)

Figure 19

Sequence - Bcl11b_3_fw

5'- GCA GCA ATC CCC CTT TAA ACC C -3'

Properties	Amount Of Oligo
Tm (50mM NaCl):* 58.9 °C	4.4 = 21.9 = 0.15
GC Content: 54.5%	OD_{260} nmoles mg
Molecular Weight: 6,584.3	For 100 µM: add 219 µL
nmoles/OD260: 5.0	
ug/OD260: 33.0	
Ext. Coefficient: 199,500 L/(mole·cm)	

Secondary Structure Calculations

Lowest folding free energy (kcal/mole): 2.17 at 25 °C
Strongest Folding Tm: -70.6 °C

Oligo Base Types	Quantity
DNA Bases	22
Modifications and Services	Quantity
Standard Desalting	1

Sequence - Bcl11b_3_rv

5'- AGG TGG GTT AAA CTG TAA GGG AC -3'

Properties	Amount Of Oligo
Tm (50mM NaCl):* 56.5 °C	4.5 = 18.9 = 0.14
GC Content: 47.8%	OD_{260} nmoles mg
Molecular Weight: 7,192.7	For 100 µM: add 189 µL
nmoles/OD260: 4.2	
ug/OD260: 30.2	
Ext. Coefficient: 237,800 L/(mole·cm)	

Secondary Structure Calculations

Lowest folding free energy (kcal/mole): -0.12 at 25 °C
Strongest Folding Tm: 27.1 °C

Oligo Base Types	Quantity
DNA Bases	23
Modifications and Services	Quantity
Standard Desalting	1

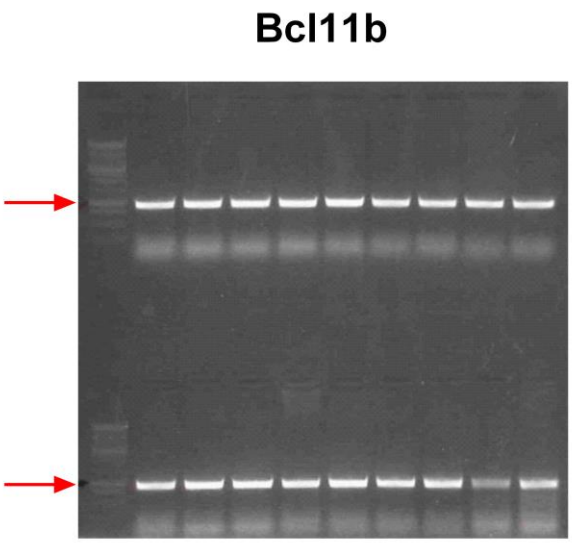

PCR amplification of 7, 6, and 4, score regions in Bcl11b gene, for sequence analysis

Bottom image shows gel electrophoresis for a PCR amplification from primers (top image) designed around the 7, 6, and 4, score regions in the Bcl11b gene. Red arrows show band of interest (extracted for sequence analysis). Primers produced by Integrated DNA Technologies (www.idtdna.com)

Figure 20

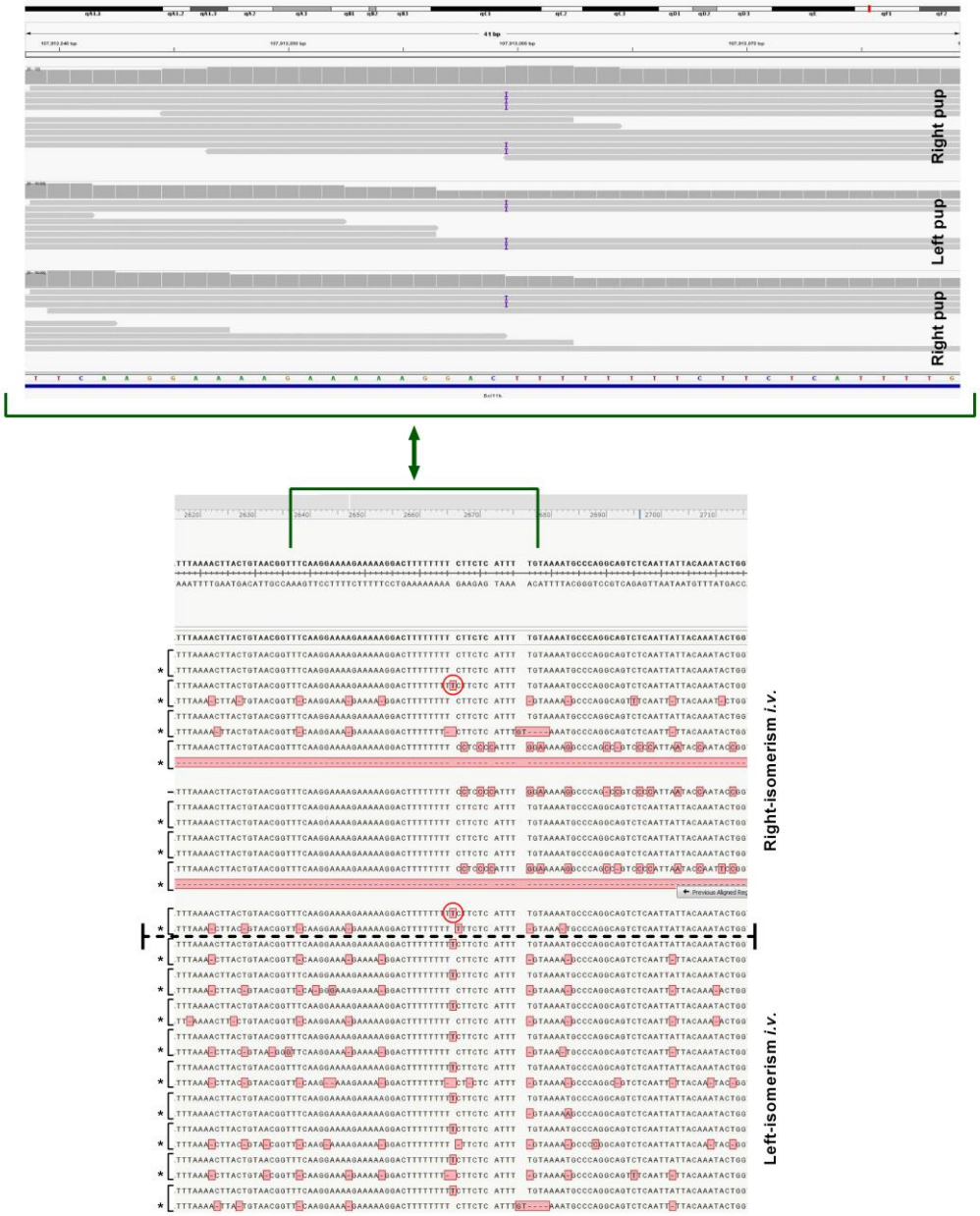

Mutations found within Bcl11b gene - score 7 in pups

Top image shows an insert found within the gene encoding Bcl11b, for three of the F2 pups (two which were determined to have a right-isomerism and one which was determined to have a left-isomerism morphology). Below shows the similar position within 18 unrelated *i.v.* mice (9 right-isomerism [*i.v.*4] and 9 right-isomerism [*i.v.*3]) through sequence analysis of PCR amplified DNA. Red circles represent mutations contrary to predictions. * denotes sequencing with the reverse primer, lack of * represents sequencing with the forward primer. Square brackets (or single line) denote individual mice.

Figure 21

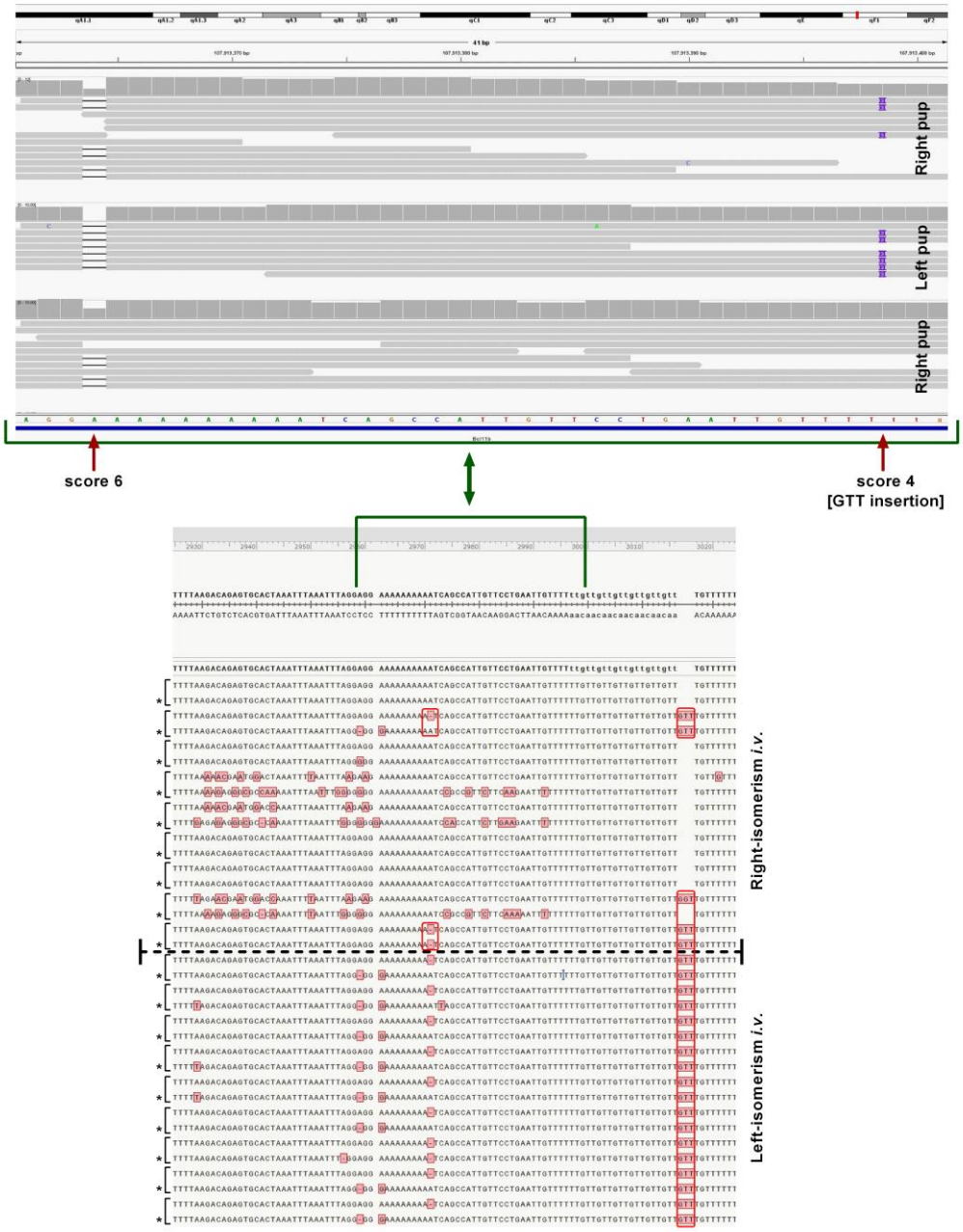

Mutations found within Bcl11b gene - score 6 and 4 in pups

Top image shows an insert found within the gene encoding Bcl11b, for three of the F2 pups (two which were determined to have a right-isomerism and one which was determined to have a left-isomerism morphology). Below shows the similar position within 18 unrelated *i.v.* mice (9 right-isomerism [*i.v.*4] and 9 right-isomerism [*i.v.*3]) through sequence analysis of PCR amplified DNA. Red circles represent mutations contrary to predictions. * denotes sequencing with the reverse primer, lack of * represents sequencing with the forward primer. Square brackets (or single line) denote individual mice. GTT in lower figure not detected in any F2 pups whole genome sequence analysis (top figure)

I designed forward and reverse primer sequence pair which surrounded three of the mutations I had previously found in the Bcl11b gene (figure 19). Importantly, the region to be amplified included the 7 score region, as well as a region including a score of 6. Following gel electrophoresis of the amplified region, I was able to produce clean single bands for sequencing, suggesting that the PCR was a success. Unfortunately, although the mutation with a score of 7 was visible with the F2 pups (top image figure 20) in the previous experiment, through this experiment I found that some of the unrelated right-isomerism mice had a similar mutation to left-isomerism mice (red circles, bottom image figure 20). If my hypothesis was correct, then none of the right-isomerism mice should have a similar mutation as is found in the left-isomerism, so this particular mutation is probably not the one I am looking for. As expected, when I then investigated the regions with lower scores, they also did not follow the expected pattern; with some right-isomerism mice showing the 6 score mutation, and the 4 score mutation being in a completely different place in the sequence (figure 21).

With the highest scoring region of the Bcl11b gene not looking as promising as I had hoped, I then moved on to investigate the 7 score mutations within the Evl gene.

Figure 22

Sequence - Evl_fw

5'- CTA GAT GCC TTT ATC TCT GCC TGT -3'

Properties	Amount Of Oligo
Tm (50mM NaCl):* 56.2 °C	4.9 = 23.3 = 0.17
GC Content: 45.8%	OD_{260} nmoles mg
Molecular Weight: 7,260.7	For 100 µM: add 233 µL
nmoles/OD260: 4.7	
ug/OD260: 34.4	
Ext. Coefficient: 211,100 L/(mole·cm)	

Secondary Structure Calculations

Lowest folding free energy (kcal/mole): -0.62 at 25 °C
Strongest Folding Tm: 31.2 °C

Oligo Base Types	Quantity
DNA Bases	24
Modifications and Services	Quantity
Standard Desalting	1

Sequence - Evl_rv

5'- AGG TAG GTG GTC AAT TCT GAG T -3'

Properties	Amount Of Oligo
Tm (50mM NaCl):* 55.3 °C	3.6 = 16.4 = 0.11
GC Content: 45.5%	OD_{260} nmoles mg
Molecular Weight: 6,845.5	For 100 µM: add 164 µL
nmoles/OD260: 4.5	
ug/OD260: 30.9	
Ext. Coefficient: 221,600 L/(mole·cm)	

Secondary Structure Calculations

Lowest folding free energy (kcal/mole): 0.30 at 25 °C
Strongest Folding Tm: 19.4 °C

Oligo Base Types	Quantity
DNA Bases	22
Modifications and Services	Quantity
Standard Desalting	1

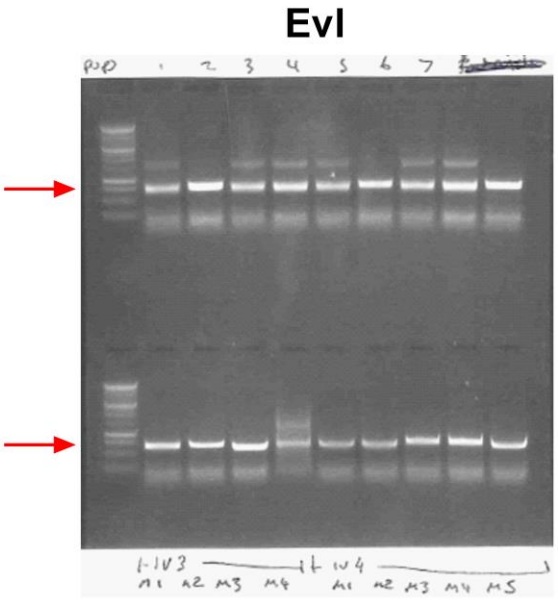

PCR amplification of 7 score region in Evl gene, for sequence analysis

Bottom image shows gel electrophoresis for a PCR amplification from primers (top image) designed around the 7 score region in the Evl gene. Red arrows show band of interest (extracted for sequence analysis). Primers produced by Integrated DNA Technologies (www.idtdna.com)

Figure 23

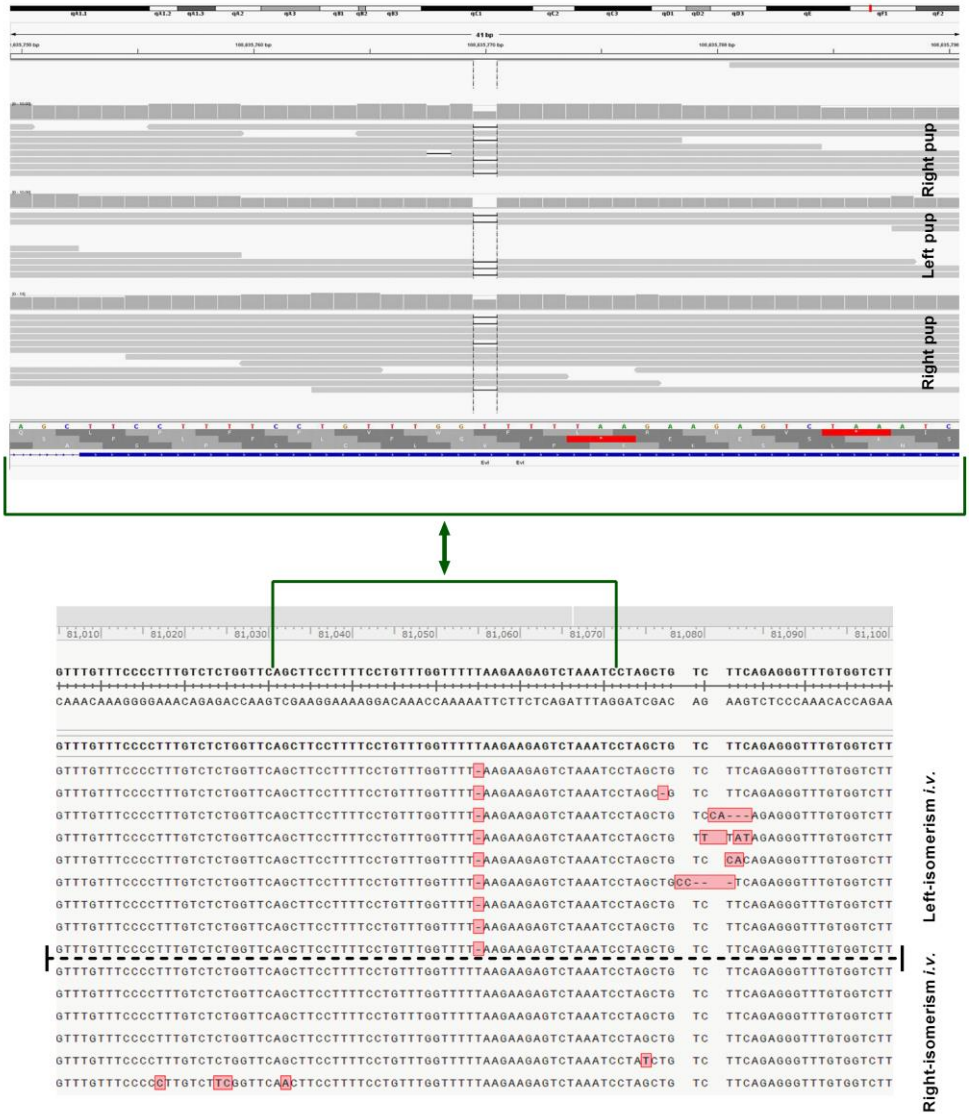

Mutations found within Evl gene

Top image shows an insert found within the gene encoding Evl, for three of the F2 pups (two which were determined to have a right-isomerism and one which was determined to have a left-isomerism morphology). Below shows the similar deletion found within 15 unrelated *i.v.* mice (9 right-isomerism [*i.v.*4] and 6 right-isomerism [*i.v.*3]) through sequence analysis of PCR amplified DNA.

Figure 24

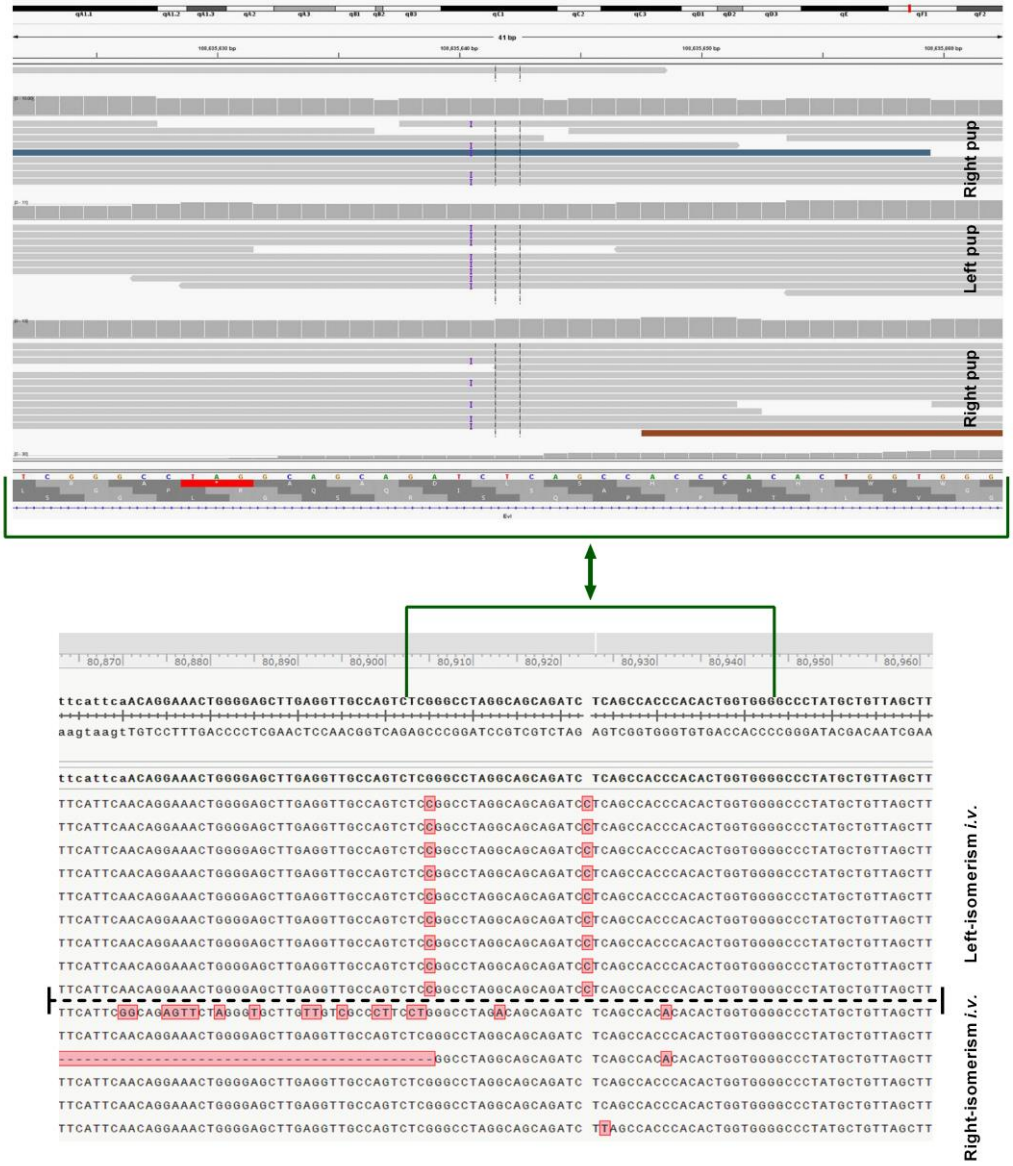

Mutations found within Evl gene (2)

Top image shows an insert found within the gene encoding Evl, for three of the F2 pups (two which were determined to have a right-isomerism and one which was determined to have a left-isomerism morphology). Below shows the similar insertion found within 15 unrelated *i.v.* mice (9 right-isomerism [*i.v.*4] and 6 right-isomerism [*i.v.*3]) through sequence analysis of PCR amplified DNA. The G->C point mutation was not detected in any of the F2 pups, through whole genome sequencing analysis.

Similar to my plan for investigating the mutations within Bcl11b, I designed my primer pair to surround the two 7 score mutations I had found within the Evl gene (figure 22 top image). These primers also appeared to specifically target my region of interest, as seen by the clean single band following gel electrophoresis (figure 22 bottom image). When I analysed the unrelated left- and right-isomerism *i.v.* mice, I found that all the mice analysed contained similar mutations as expected from the mutations found within the F2 generation (figures 23 and 24). Through this second sequencing analysis, we also identified a base pair change (G to C), which appeared to follow the similar pattern, but this was not seen in any of the mice of the F2 generation, analysed using whole genome sequencing (figure 24). I further confirmed this finding by re-running the mice from the previous experiment (the F2 pups and their parents), using the same primers for Evl, and found similar results to the unrelated *i.v.* mice.

Interestingly, when we look at the whole genome sequences for both the F2 pups and their parents, we notice that only half of the reads did in the predicted-right group, with the other half showing the wild-type sequence, whereas every read performed showed the mutations expected in the predicted-left (figures 23 and 24). This fits nicely with the idea that the mutation is homozygous in the left-isomerism mutant, whilst (according to our hypothesis of the F1 mother being heterozygous dominant) the right-isomerism mice would all be heterozygous in this particular experiment.

These findings are highly encouraging and, combined with the fact that we know Evl to be strongly expressed in the hippocampus in in-situ hybridization experiments (as demonstrated in the Allen brain atlas: http://mouse.brain-map.org/experiment/show?id=69838381), and known to have an effect in neuritogenesis (Kwiatkowski 2007) and axonal maintenance in hippocampal neurones (Franco 2010), make Evl to appear a promising candidate for Gene X.

The next step was to find out more about the position of these mutations within the Evl gene, so that we might predict what kind of effect they are having on the gene itself.

Figure 25

Both mutations located within promoter region of Evl gene

Image shows the position of both the insert and deletion found within the gene encoding Evl. Both of these mutations were detectable in all F2 pups, as well as in 14 unrelated *i.v.*4 and 8 unrelated *i.v.*3 mice. Image obtained using the e!Ensemble website (http://www.ensembl.org/index.html)

Using the e!Ensemble website, I could identify that the two mutations which I had previously identified were located within the promoter region of the Evl gene. This suggests that if one, or both, of them is the mutation I am searching for, it is possible that Evl being differentially expressed between left- or right-inputs to the CA1 s.r. could be responsible for the difference in spine morphology which takes the form of input-side dependent asymmetry.

Further analysis to investigate differences in Evl expression, such as QRT PCR, or in situ analysis, should be conducted to investigate this possibility. Following that, the next step would be to generate knock out mice, for these particular mutations, within a right-isomerism *i.v.* mouse mutant, to see if it would be possible to switch the phenotype from right- to left-isomerism purely through introduction of an insertion and/or a deletion into the Evl gene.

Investigation into the effect of PirB knockout on input-side dependent asymmetry

1:8

This work was part of a collaboration and was published in PLoS ONE (Ukai 2017). Although it doesn't directly link with the work I have already presented in this chapter, it is related to the left-right input-side dependent asymmetry process, which I have been investigating.

Through the majority of my studies, I have mainly focussed on how a point mutation in the gene encoding left-right dynein (Lrd), a motor protein involved in the establishment of the internal body axis, could lead to a loss of hippocampal asymmetry formation. Namely a loss of the input-side dependent asymmetry found in the projections from the CA3 to the CA1. However, recently, it was also ascertained that the major histocompatibility complex class 1 (MHC I) molecule might also be involved in the control and formation of input-side dependent asymmetry. This was demonstrated through the use of β2-microglobulin (β2m)-deficient mice (Goto 2017, Kawahara 2013). β2m is necessary for the cell surface expression of the heavy chain of the MHC I protein (the complex consisting of a soluble β2m light chain, a transmembrane heavy chain, and a short peptide antigen) (Bijlmakers 1993). Mice deficient in β2m lack the stable cell surface expression of MHC I seen in wild-type mice, as well as the input-side dependent asymmetry seen in wild-type mice (Kawahara 2013). Interestingly, however, although these mice show symmetry in their hippocampal

connections, these mice have a slightly different phenotype from the *i.v.* mutant. β2m-deficient mice were found to be similar to the left-isomerism *i.v.* mouse in their connections to apical dendrites in the CA1 (forming smaller and NR2B dominant synapses, characteristic of projections from the left CA3 in wild-type mice). However, β2m-deficient mice also were found to form smaller NR2B dominant synapses on their basal dendrites (Kawahara 2013). This phenomenon is similar to that of right-isomerism *i.v.* mice (left-isomerism having larger less-dense synapses in basal dendritic connections). Like *i.v.* mice (Goto 2010), β2m-deficient mice have been found to have impairments to their working memory retention, as demonstrated by their performance on the delayed nonmatching-to-position (DNMTP) task (Goto 2017).

Another molecule which plays a vital role in the function of the MHC I complex is the paired immunoglobulin-like receptor (Pir). There are two different paired immunoglobulin-like receptors which have been identified in mice, PirA and PirB, both allow the binding of various MHC I molecules, including β2m as well as a variable MHC I heavy chain, to their extracellular domains (Nakamura 2004). PirA and PirB have been found to play important roles in the recognition of foreign infections (Takai 2005). Most importantly they enable the initiation of intracellular signalling cascades, something MHCI can not itself do due to the length of its cytoplasmic tail. PirB is found throughout the mammalian central nervous system, including in the visual cortex and hippocampus, where it has been implicated in the regulation of neuroneal plasticity (Bochner 2014, Syken 2006). PirB has being localized to neuroneal somata, axons and dendrites, with a particularly high expression within the CA1 and CA3 pyramidal cell layers of the hippocampus (Starkey 2012). Interestingly, PirB has been found to be involved in the control of spine and excitatory synapse density on pyramidal neurones, with total knockout of PirB resulting in a significant increase in number (Bochner 2014, Djurisic 2013). Although PirB can be detected near synapses, it is unclear whether it is pre- or post-synaptically localised (Raiker 2010).

Methods and results

Methods used: Preparation of mouse brain for analysis under TEM (method 3), dissector analysis (method 4).

Fixed brains were shipped from our collaborators in Japan. Brains had been fixed in 4% PFA containing 0.05% glutaraldehyde solution

Measurements of TEM images were conducted using the Reconstruct software (Fiala 2005)

Figure 26

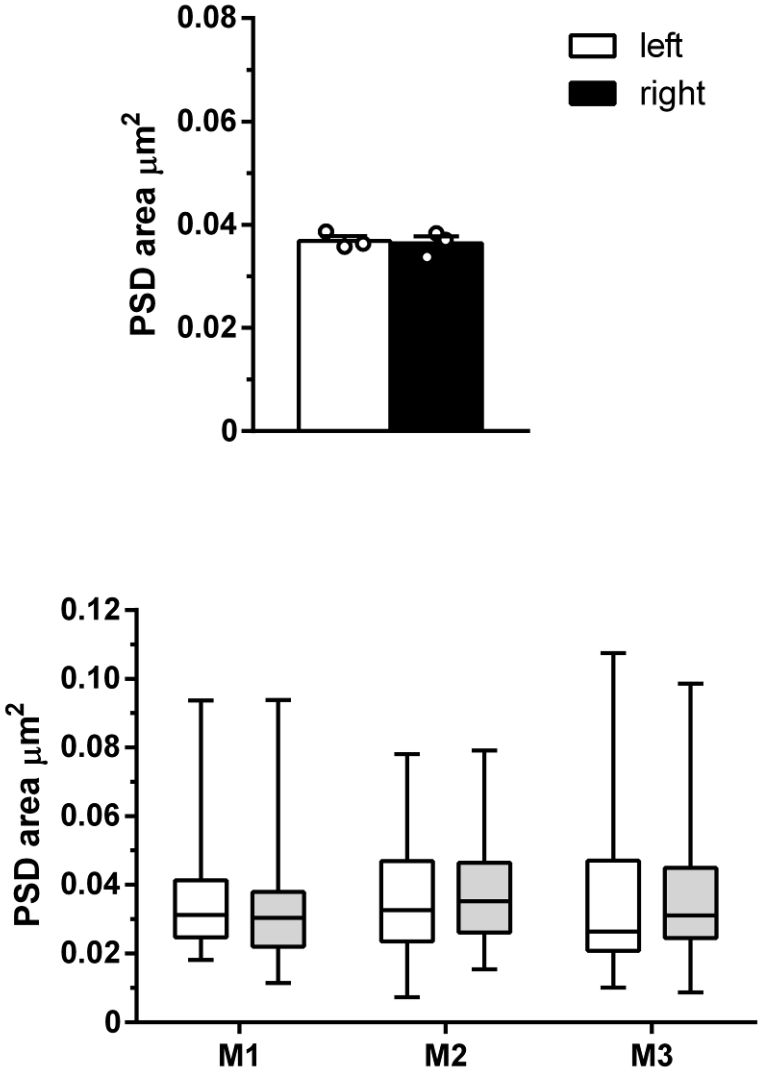

PSD area from PirB ko mice

Upper chart shows average PSD area from PirB ko mice. Error bars display SEM and empty circles show average values for individual mice. Lower chart boxplots of PSD are from individual mice. The upper chart is an average of the lower values. For both charts, open box denotes density in left CA1, filled box denotes density in right CA1. PSD area was calculated from serial sections. Only synapses with complete PSDs were measured. Synapses were identified using the unbiased dissector analysis technique. Students T-test used for statistical analysis with no significance detectable.

Figure 27

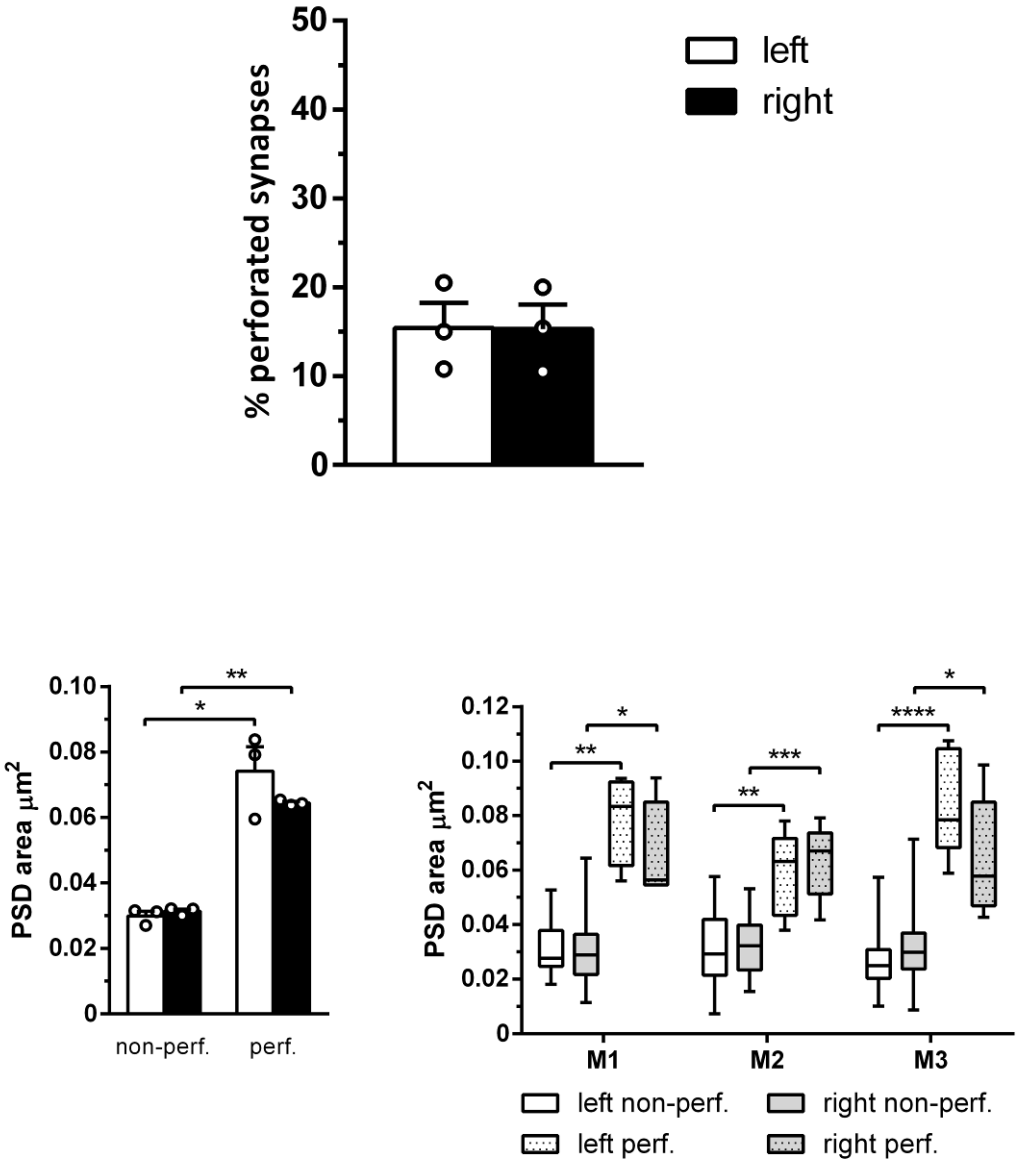

Perforated synapses in PirB ko mice

Upper chart shows average percentage of perforated synapses in PirB ko mice. Lower right chart boxplots for PSD area from perforated and non-perforated synapses from individual mice. The bottom left chart is an average of the bottom right chart's values. For the top and bottom left charts, open box denotes density in left CA1, filled box denotes density in right CA1. Error bars display SEM and empty circles show average values for individual mice. PSD area was calculated from serial sections. Only synapses with complete PSDs were measured. Synapses were identified using the unbiased dissector analysis technique. Students T-test used for statistical analysis with * denoting $p < 0.05$, ** denoting $p < 0.01$, *** denoting $p < 0.001$, and **** denoting $p < 0.0001$.

As part of this collaboration, I was able to demonstrate that the PirB knockout mouse mutant lack input-side dependent asymmetry in the morphology of the synapses formed on the post-synaptic neurone in the CA1 stratum radiatum. This mutant displays a left-isomerism phenotype, having an average PSD area size of around 0.04 μm² with around 15% of the synapses forming a perforated PSD. These anatomical findings were in accordance with the electrophysiological findings of my collaborators on the paper. They found that, through the use of an NR2B-selective blocker, Ro 25–6981, (Fischer 1997) and the VHCT operation (method 6), NMDA EPSC peak amplitude would be reduced to a similar degree in hippocampal slices obtained from either hemisphere. However, when they performed a similar experiment on VHCT operated wild-type mice, they could detect a significant difference between slices obtained from the left or right hemisphere. They also ruled out any effects of the VHCT procedure on detected Ro 25-6981 sensitivity, finding that it was comparable for both Schaffer and commissural fiber synapses. This was similar in both apical and basal synapses, suggesting that the phenotype in the PirB knockout mouse is more similar to that of the β2m-deficient than the *i.v.* mutant. The findings suggest that PirB is critical for transducing the MHCI signalling required for the generation of asymmetrical input-side dependent synapse formation in the hippocampus.

Chapter 1 experimental flowchart

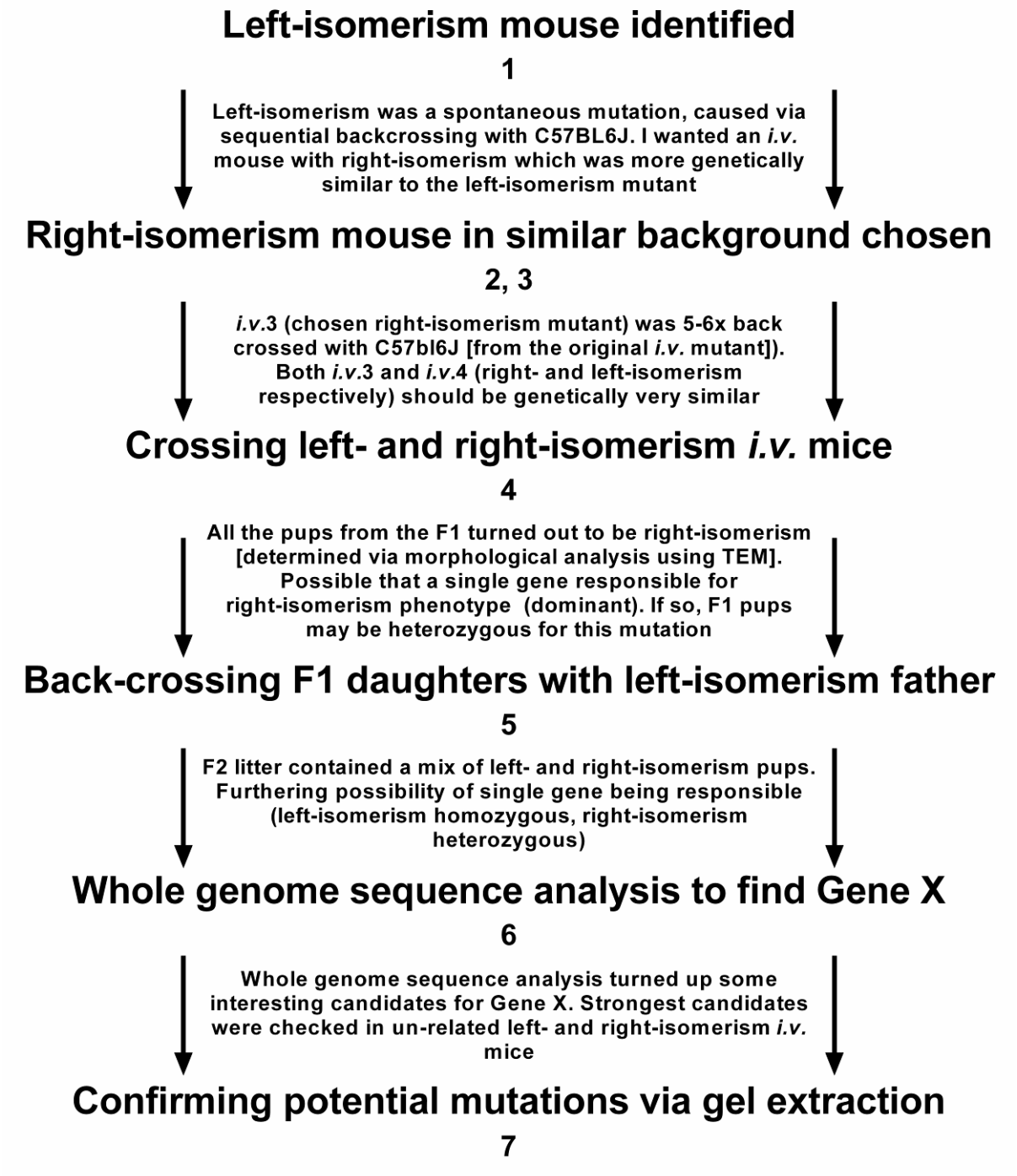

Chapter Summary

This chapter is focussed on the investigation of the process of input-side dependent asymmetry formation in the hippocampus. This appears to be a fundamental feature of the murine hippocampus, leading to an imbalance in the size of synapses, as well as the density of the NR2B receptor, depending on the hemispheric origin (Kawakami 2003, Shinohara 2008, Shinohara 2009). This asymmetry has been shown to lead to an asymmetry in the propensity for LTP between left and right originating projections, with synapses formed from left-CA3 projections potentially being more susceptible to NMDA receptor-dependent synaptic plasticity (Kawakami 2003, Kohl 2011). This phenomenon appears to be vital to hippocampal memory processing and formation, as shown by both the importance of the left-CA3 for long-term memory formation, as well as it being vital to experience-driven laterality formation, a process I will describe in chapter two (Shipton 2014a). The importance of input-side dependency in hippocampal memory formation is further emphasised through the findings that the *i.v.* mouse, a mutant which lacks input-side dependent laterality, has severely compromised spatial learning and working memory (Goto 2010).

The original *i.v.* mouse mutant was characterised as having right-dominancy. This meant that irrespective of the hemispheric origin of the CA3, the projections into the CA1 would terminate in synapses similar to those originating from the right-CA3 in wild-type mice (Kawakami 2008). In this chapter I highlight the novel finding of a left-isomerism *i.v.* mouse mutant. This was a spontaneous mutation, generated through the backcrossing of the original *i.v*. mutant with the C57BL/6J mouse line. Through unilateral viral injections into the CA3, and the measurement of only the labelled terminals, I found that the average PSD area in the CA1 s.r. was around 0.4 μm². Later measurements of unlabelled terminals confirmed this measurement, as well as highlighting that the percentage of synapses with a perforated percentage was below 20%. All of these recordings align nicely with the size and perforation values obtained previously from left-CA3 originating projections in wild-type mice (Shinohara 2008). Having identified a left-isomerism mutant, one important question which could be asked is whether this mutant also suffers from learning and memory deficits, similar to the right-isomerism line. Knowing that there is a difference in NMDAR-related LTP between left and right-CA3 projections to the CA1 (Kohl 2011), and that suppression of the left, but not right, CA3 will cause an impairment in hippocampal memory processing (Shipton 2014a), it is possible that the left-isomerism mutant will not suffer the working-

memory deficits which the right-isomerism mutant does. One additional question which needs to be investigated is the question of the nature of synapses in the CA1 s.o.. Is the left-isomerism *i.v.* mutant a complete inversion of the right-isomerism mutant, with CA1 s.o. terminals in the left-isomerism mutant having a similar morphology to the terminals found from left-CA3-originating projections into the CA1 s.o. of the wild-type mouse? Or is the left-isomerism *i.v.* mutant more similar to the β2m or PirB knockout mutants, where the terminals in the CA1 s.o. mirror those found in the CA1 s.r. (both being small and NR2B-dense)?

Through the selective crossing of two closely related (as determined by their generational distance from the original *i.v.* mutant) left- and right-isomerism *i.v.* mouse lines, it was possible to investigate the dominance of the left and right phenotype. Analysis of all the pups from the F1 generation proved right-dominancy in input-side dependent asymmetrical development. Following back-crossing of F1 female pups with their father, it was possible to generate a mixed population of left- and right-isomerism pups. This demonstrates that the left-isomerism phenotype is recessive. More importantly, in accordance with simple Mendelian inheritance ratios, it suggests the possibility of a single gene (Gene X) being responsible for left or right determination.

Whole genome sequence analysis has proven to be a powerful tool in the investigation of genetic influences in disease and development, as well as in examining genetic inheritance between individuals and within species. Turning these tools towards the examination of Gene X, through whole sequence analysis of the parents and pups from the F2 generation, it was possible to identify some prospective genes which could be responsible for the determination towards a left- or a right-isomerism phenotype in CA3-CA1 synapse morphology. Through further investigation of the candidates, with targetted PCR and gel electrophoresis, I was able to exclude many of these, leaving Ena/Vasp-like (Evl) as a prime candidate for future investigation. Ena/VASP proteins have been attributed to many different processes within the nervous system, including neuritogenesis, axon guidance and maintenance (Drees 2008, Franco 2010, Kwiatkowski 2007). Importantly, Evl has also been found to be a component of the PSD of inhibitory synapses (Uezu 2016) and could therefore be involved in modulating synaptic plasticity. As the mutations in Evl appear to be located in the promoter region, the first question which needs to be asked is whether this mutation has any effect on its expression, and whether the levels of Evl could drive the difference between the phenotypes

of synapses originating from the left and right CA3. This is an important question as the expression levels of ENA/VASP proteins have already been attributed to neuroneal degeneration and axonal maintenance in hippocampal neurones (Franco 2010). Another important avenue for future investigation would be the targetted modification of the Evl gene using the CRISPR/Cas system (Zhang 2014). Both of the promising mutations in Evl were detected in the left-isomerism *i.v.* mouse. Therefore, one question which could be asked would be whether the selective introduction of these mutations into the right-isomerism *i.v.* mutant could cause a switch of phenotype to left-isomerism.

The final part of this chapter deals with the recent publication about the importance of PirB in the formation of input-side dependent asymmetry formation in the hippocampus. PirB, like β2m, is involved in the function of the MHCI complex (Shatz 2009). It turns out that a knockout of PirB will lead to a similar synaptic phenotype to a knockout of β2m (Kawahara 2013). Interestingly, although both of these knockout mice lack input-side dependency in their CA3 – CA1 projections, they appear to have a different phenotype from the *i.v.* mutant. In the wild-type mouse, the projections from the right-CA3 to the CA1 s.o. terminate in small NR2B-dense synapses, whereas the projections to the CA1 s.r. terminate in larger NR2B-less dense synapses. The CA3 – CA1 projections in the right-isomerism *i.v.* mouse mutant followed this pattern, with larger synapses forming in the CA1 s.r. and smaller more NR2B-dense synapses forming in the CA1 s.o.. Both the β2m and PirB knockout mutants, however, appear to have symmetry in their apical and basal dendrites also, with terminals in both the CA1 s.r. and CA1 s.o. terminating in smaller NR2B-dense synapses. This means that it is not so easy to term the β2m or PirB mutants as 'left-isomerism', similar to how we could with the right-isomerism *i.v.* mutant.

Chapter 2

Brief summary

It was recently reported that environmental enrichment alone could induce an asymmetry in the synaptic density of the hippocampus (Shinohara 2013). This effect was highly localized to the CA1 stratum raditum, a region where the synaptic morphology is heavily influenced by pre-existing underlying asymmetries (Kawakami 2003, Shinohara 2008). It has been found that asymmetries in hippocampal activity can be detectable in relation to environmental stimulation, therefore it is possible that the changes in synaptic density, seen by Shinohara and his colleagues, could play a part in enabling the organism to deal with changes to its environment.

As with all animal experiments, one has to be careful in generalizing results between different organisms, strains, or sub-strains. This leads to the question of whether the asymmetrical changes in synapse density seen in rat CA1 pyramidal cells, induced through environmental enrichment, could be generated in other rodent species. Through the use of C57BL/6J mice, as well as the *i.v.* mouse mutant, this chapter aims to tackle that question, as well as trying to further elucidate the specific causes for this localised change. One key question asked is whether the underlying input-side dependent asymmetry in the hippocampus, may be responsible for this change, or whether there are other underlying mechanisms in play during experience driven formation of laterality in the rodent hippocampus.

The environmental enrichment paradigm

Environmental enrichment is a loose term which encompasses modifying the housing environment of an organism, to make it more novel, stimulating or complex than conventional housing conditions. It has been shown to have a marked effect on the general well-being of animals (Hüttenrauch 2016, National Research Council (US) Committee on Recognition and Alleviation of Distress in Laboratory Animals 2008). Unfortunately, there is no consensus on what defines 'enrichment'. Enrichment doesn't just have to be a change in cage layout, the term also encompasses inducing enrichment through social, auditory, olfactory, visual, dietary, exercise, and tactile, stimulations (Hutchinson 2005). Each of these

can potentially lead to different effects on an organism, giving the enrichment paradigm great flexibility in how it can be specifically tailored towards a particular condition or organism. However, this flexibility in the paradigm comes with some important drawbacks. Most notably, the degree of variation in what constitutes an 'enriched environment, can often make interpreting and comparing results from different groups difficult. For example, nowadays many animal facilities will include cardboard tubes/shelter in mouse cages, giving them places to hide, but not all laboratories will do this. This could lead to differences in the control mice, with one laboratory's 'controls' potentially being more 'enriched' than another laboratory's. It has also been demonstrated that the enrichment paradigm might induce greater differences to between different mouse strains (Heinla 2014). This could be explained by the unnatural state of conventional laboratory housing, with the enriched environment being a more 'natural' setting. Another huge potential drawback is that it becomes incredibly important to control every tiny detail about the environment during an enrichment paradigm as, due to the length for which animals are often subjected to enrichment, it is easy for undesired external/uncontrolled influences to potentially lead to dramatic changes in the behaviour, health, or neurological condition, of an organism (Bayne 2005).

The social component of environmental enrichment

Rodents, in particular, tend to benefit from social interactions, therefore a lot of effort has been put into investigating the effects of social influences upon their development, behaviour, and emotional well-being. Housing conditions have been found to induce changes in the social behaviour of rodents, particularly in their increased sociability and willingness to interact with novel individuals (Arakawa 2018, Aujnarain 2018). Interestingly, it has been possible to detect changes in neurogenesis in the olfactory bulb and BDNF expression relating to whether adult mice were kept in group housing or not, with this effect being irrespective of whether the environment was an enriched or standard mouse cage (Monteiro 2013).

Recent evidence suggests that enrichment paradigms targetted specifically towards social enrichment, rather than environmental, have been found to only aid in the reversal of social, but not object, recognition deficits (Prado Lima 2018). This is supported by the comparison of ultrasonic vocalizations of rats in different enrichment paradigms. In paradigms designed to promote social interactions, it was found that rats would increase their

vocalizations, however in paradigms designed to promote purely environmental enrichment (and suppress social interactions), this increase was not detectable. In fact, the rats showed a reduction in their vocalizations in response to auditory stimuli, suggesting the onset of social behaviour deficits (Brenes 2016). However, although the environmentally enriched rats displayed an increase in hippocampal neurogenesis, this was not evident in the rats exposed to a purely social enrichment paradigm. This furthers the notion that enrichment isn't a single process, but rather a multitude of different stimulations which lead to the beneficial effects detectable in an organism's health and wellbeing.

Counter to social enrichment is social isolation. Social isolation can induce a huge stress upon an organism, especially in rodents, leading to an increase in depression, anxiety, changes in brain state and morphology, as well as changes to the cardiovascular activity and general health of an organism (Gaudier-Diaz 2017, Huang 2017, Normann 2018). When trying to use environmental enrichment to counter these effects, the results are highly variable. For example, it was found that environmental enrichment could reduce the recovery time for prairie voles subjected to isolation, even if the animals in question remained in isolation (Normann 2018). However, it has also been demonstrated that isolation can prevent the beneficial effects of enrichment on neurogenesis in the ventral hippocampus (Kozareva 2018). It is likely that a combination of social and environmental enrichment paradigms would be most effective in treating socially-isolated rodents.

Exercise as a form of enrichment

The inclusion of objects such as tunnels, boxes, and tubes, has often been used as a form of enrichment for rodents. This is because, as far as enrichment paradigms go, this kind of inclusion is easy and cheap, as well as being highly controllable (as the 'toys' can be rapidly removed and reintroduced, when needed). An increase in exercise has been found to induce a powerful effect on the central nervous system, increasing neurogenesis, synaptic plasticity, cell survival, and memory performance, as well as an individual's performance on a multitude of behavioural paradigms (Fabel 2009, van Praag 1999, van Praag 2005). This is particularly evident in aged individuals (Goes 2015, van Praag 2005), where exercise has been suggested as a powerful method for treating/protecting against the development of age-related neurological disorders such as dementia (Fratiglioni 2004), as well as against other neurological disorders, such as multiple sclerosis (Prakash 2010). Its possible therapeutic

effects have been demonstrated in laboratory animals also (Bettio 2017, Pang 2013, Skillings 2014).

The effect of an increase in exercise, which these objects bring to an organism, is often not considered in the evaluation of the benefit of environmental enrichment. When it is, however, it's possible to isolate differences in the specific effect of both exercise and environmental stimulation. By specifically tailoring the enrichment protocol away from one which might encourage exercise, it has been found possible to still cause a striking behavioural effect, including a reduction in anxiety-like behaviour and an increase in spatial learning and memory (Hendershott 2016). Removing the exercise component of enrichment also has been found to not effect the increases seen in hippocampal synaptogenesis, with the length of enrichment being the most important determinant of the increase (Birch 2013). It was found that longer periods of enrichment would induce a significant improvement in spatial and working memory performance, as well as an increase in the early (but not long term) cell survival in the dentate gyrus. It has also been identified that there can be a vast difference in hippocampal neurogenesis, induced through treadmill exercise, between many commonly used mouse strains (Kim 2017). This could prove to be yet another potentially confounding variable when comparing different enrichment studies, especially where disease model mice are used.

It is likely that, like with social enrichment, the greatest effects come from the combination of multiple different forms of enrichment, rather than just simple changes to the environment/housing of an organism. For example, in mice where the neural progenitors had been selectively ablated, the negative impacts of this procedure on recognition and contextual fear memory formation could be greatly diminished through a combination of exercise and environmental enrichment. Moreover, the reductions in neurogenesis, detectable in these mice, could be reversed (Sakalem 2017). It has also been demonstrated that combining voluntary physical exercise with environmental enrichment, through the inclusion of a running-wheel in the enrichment paradigm, it it possible to induce a 30% greater increase in adult neurogenesis than is possible with stimulation through either physical exercise or enrichment alone (Fabel 2009).

Neurological changes following enrichment

The beneficial effects of environmental enrichment are quite widespread. Of particular interest are the changes caused to an organism's nervous system, which can be induced through environmental stimulation alone, include increases in neurogenesis and synaptogenesis (Clemenson 2015, Kempermann 1997, Leggio 2005, van Praag 2005). These changes have been shown to lead to improvements in both learning and memory formation (Cortese 2018, Hullinger 2015), reduction in the spread or adverse effects of neurological disorders (Restivo 2005), and the changes to the emotional condition of the organism (Hüttenrauch 2016, Rojas 2013). What makes enrichment such a useful tool for the treatment of neurological disorders is that it is completely non-invasive in nature. The fact that many symptoms of disease can be alleviated purely through a change in the housing conditions of an organism has made environmental enrichment to be one of the most frequently used tools for the investigation of various animal models of neurological disorders and disabilities (Bhagya 2017, Restivo 2005). Unfortunately, environmental enrichment has more often been used as a tool to test specific mutant models of neurological diseases and/or disorders, than as a tool to investigate more fundamental questions about neurological development.

In this chapter I direct my focus towards the development and formation of asymmetries in the hippocampus. It has been reported that environmental enrichment can induce a significant change in gene expression, including in many genes responsible for neuroneal signalling, growth, and formation (Rampon 2000). Of particular interest are changes to the expression levels of genes like PSD-95, which are associated with NMDA receptor functioning, as well as various molecules downstream of the NMDA receptor, such as calmodulin. It is well established that an asymmetry exists in the NR2B density between synapses originating from either hemisphere in the hippocampus (Shinohara 2008). As NR2B has been associated with neuroneal plasticity (Loftis 2003, Yashiro 2008), it is possible that changes in hippocampal density, induced through enrichment, could be related to changes in NMDA receptor function at the synaptic level.

Exercise and general fitness have been correlated with an increase in the volume of the hippocampus, combined with an increase in performance on relational memory tasks (Chaddock 2010). This corresponds well with evidence that the rate of hippocampal neurogenesis, as well as the successful integration of granule cells into the dentate gyrus, are

positively correlated with increased exercise (Bouchard-Cannon 2018). As enrichment environments often result in an increase in locomotive activity in their occupants, it is no wonder that the hippocampus would be strongly affected by enrichment. However, like all enrichment procedures, the degree of benefit of the procedure has been shown to vary dramatically between reports. This could well be attributable to variations in the enrichment protocols, species, strains and sub-strains, used.

One of the best observed effects of environmental enrichment on the hippocampus is an increase in neurogenesis and neuroneal survival. Enrichment has been shown to be able to have a dramatic effect on neurogenesis dentate gyrus in both young as well as adult mice (Fabel 2009, Kempermann 1997, Kempermann 1998a, Kempermann 1998b). It has been demonstrated that enrichment in later life can aid in increasing hippocampal plasticity in aged rats, resulting in better spatial learning performance (Neidl 2016). This can be especially beneficial, as hippocampal neurogenesis and cognitive flexibility have been found to dramatically decrease with age (Bettio 2017, Kuhn 1996, Sakalem 2017). Environmental enrichment alone has been found to dramatically increase the density of dendritic spines on CA1 neurones (Rampon 2000). Behaviourally, enrichment has been found to lead to improvements in memory formation and function, including many hippocampal-dependent processes (Harburger 2007, Hullinger 2015, Leggio 2005, Mesa-Gresa 2013, Pham 1999). However, the beneficial effects of enrichment on memory performance are controversial, with some enrichment paradigms failing to show any improvements from enrichment (Zeleznikow-Johnston 2017).

Recently, it was reported that a right-dominant increase in the number of hippocampal pyramidal cell synapses could be generated in rats, with the use of environmental enrichment alone (Shinohara 2013). This effect was localized specifically to the CA1 stratum radiatum, with little changes seen in any other hippocampal subregions. Many questions still remain, however, including questions relating to specifically how this right-side specific increase occurs and what the significance of it is. Importantly, it is also unclear whether this phenomenon is only prevalent in rats, or if it is a more fundamental feature of hippocampal experience-dependent memory formation. This chapter will aim to tackle these important questions, to try and further our overall knowledge about this fascinating discovery.

Confirming experience dependent asymmetry formation in mice

2:1

Environmental enrichment is known to cause an asymmetry in the synaptic density of the CA1 stratum radiatum (s.r.) in rats (**Shinohara 2013**), through a significant increase in the synaptic density in the right-hemisphere. However, it isn't known if this is a phenomenon restricted only to rats, or whether it is a more common feature of experience-driven hippocampal laterality formation.

To investigate this I decided to examine whether experience alone would be enough to generate an asymmetry in synapse density in the mouse hippocampus. As there is a wide definition of what constitutes an 'enriched environment', I decided that the most simple starting approach would be to repeat the same enrichment protocol used in Shinohara's paper on mice. This meant that, immediately after weaning, I would move mice into an environment full of interesting items and toys, and change the location and constitution of these toys twice a week. Should the effect of experience-driven laterality be a more fundamental feature of the mammalian hippocampus, then we could imagine that a similar asymmetry might form following the enriched environment protocol.

Methods and results

Methods used: Transcardial perfusion (method 2), preparation of mouse brain for analysis under TEM (method 3), 2D analysis (method 4).

Mice were housed in groups of 3, in either standard mouse cages (figure 28, NENR), or in enriched cages (figure 28, ENR), for 3 weeks (contrary to the 6 weeks shown in the protocols for each condition). Cages were changed once a week, and food and water were supplied ad libitum.

3 week old C57bl/6J mice were used in this experiment.

As this was a preliminary experiment, to investigate if experience-dependent changes in synapse density were even present in mice to begin with, I used the 2D analysis method (a much faster method than serial electron microscopical investigation by dissector analysis). This choice was supported by the huge increase in density seen in rats. Such a marked difference should be easily visible using this choice of method.

Measurements of TEM images were conducted using the Reconstruct software (Fiala 2005)

Figure 28

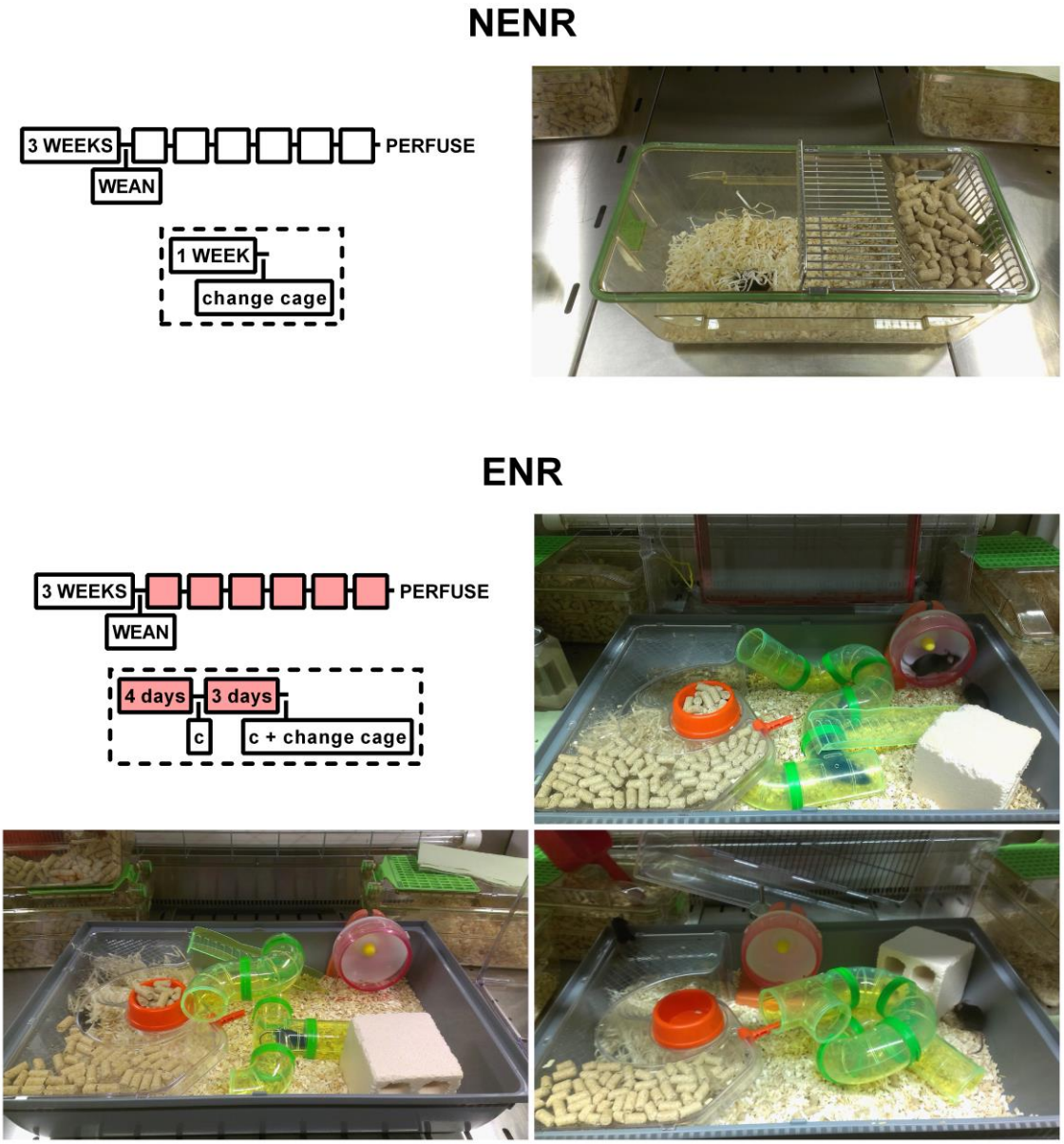

Enrichment and non-enrichment cages

NENR left shows the protocol for 6 weeks of the non-enriched condition. White boxes show one week of NENR. With the time for changing cage represented within the dotted box. NENR right: cage example of NENR cage - dimensions 32.5 x 16.5 x 13 cm
ENR upper left shows the protocol for 6 weeks of the environmentally enriched condition. Red boxes show one week of ENR. With the timeline for single week of enrichment represented within the dotted box. 'c' represents changing the toys and/or their position within the cage. Remaining 3 images show examples of ENR cages - dimensions 54 x 34 x 24 cm

Figure 29

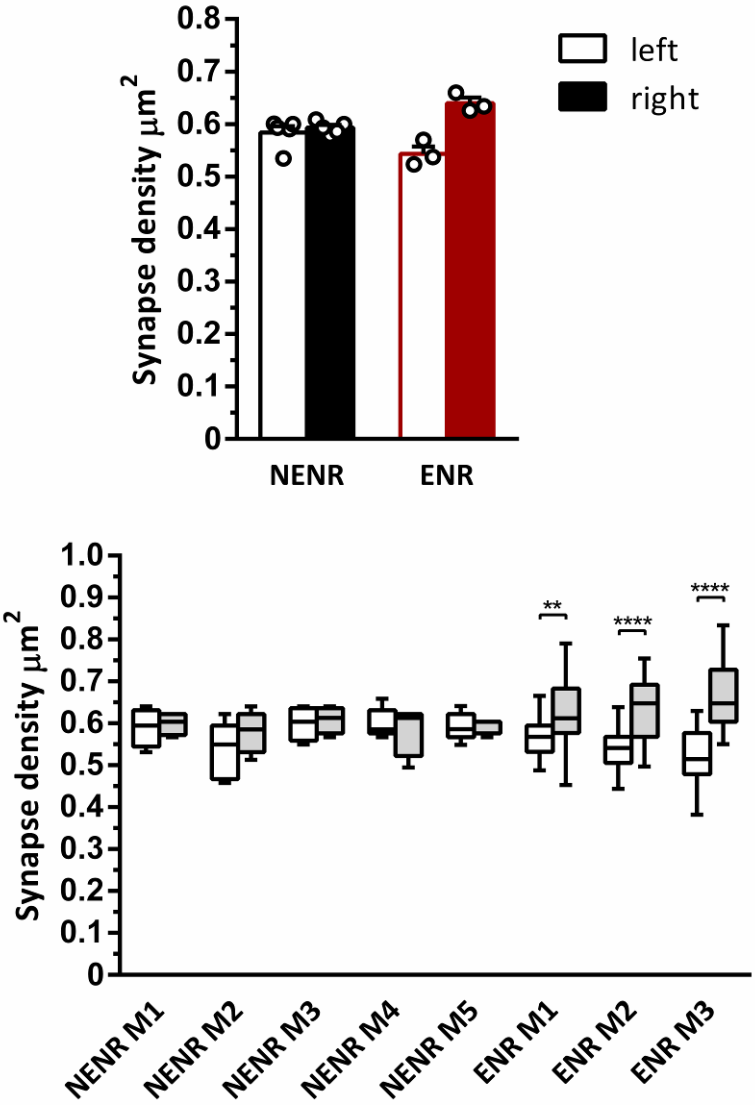

Effects of 3 weeks environmental enrichment on CA1 pyramidal-cell synapse density

Upper chart shows average synapse density in NENR and ENR C57bl6J mice. NENR n = 5, ENR n = 3. Error bars display SEM and empty circles show average values for individual mice. Lower chart boxplots of density values for individual mice. The upper chart is an average of the lower values. For both charts, open box denotes density in left CA1, filled box denotes density in right CA1. Black denotes NENR and red denotes ENR. Density values were calculated using the 2-dimensional analysis technique. Mann-Whitney test used for statistical analysis with ** for p values < 0.01, and **** for p values < 0.0001.

In this preliminary experiment, I could detect a difference in the synaptic density in the CA1 s.r. between the two hemispheres in the enriched mice. This difference was not detectable in any of the non-enriched group. Similar to the findings presented in the Shinohara paper, I was able to identify significance only in the right hemisphere. However, the change we observed in this experiment was far from the two-fold difference seen in rats (the change in mice was only around an 18% difference between both hemispheres, or an increase in only 8% from the NENR condition). One difference between these results and those presented by Shinohara et al. is in the control animals used. Here, I use a group of animals, in a standard housing. However, in the experiments on rats, the experimenters compared the densities in the hippocampus between enriched and isolated animals.

Does social isolation have an effect on synaptic density in the CA1 stratum radiatum?

2:2

To see if social isolation was responsible for the degree of change I observed in mice, I performed an additional experiment using isolated mice. This was important to determine if the small change observed in mice could be explained solely through the difference in the control animals.

Methods and results

Methods used: Transcardial perfusion (method 2), preparation of mouse brain for analysis under TEM (method 3), 2D analysis (method 4).

Mice were housed individually standard mouse cages (figure 28, NENR) for 3 weeks (contrary to the 6 weeks shown in the protocols for NENR). Cages were changed once a week, and food and water were supplied ad libitum.

3 week old C57bl/6J mice were used in this experiment.

To directly compare with the data from experiment 1, I used the 2D analysis method for examining the synapse density values in the CA1 s.r.

Measurements of TEM images were conducted using the Reconstruct software (Fiala 2005)

Figure 30

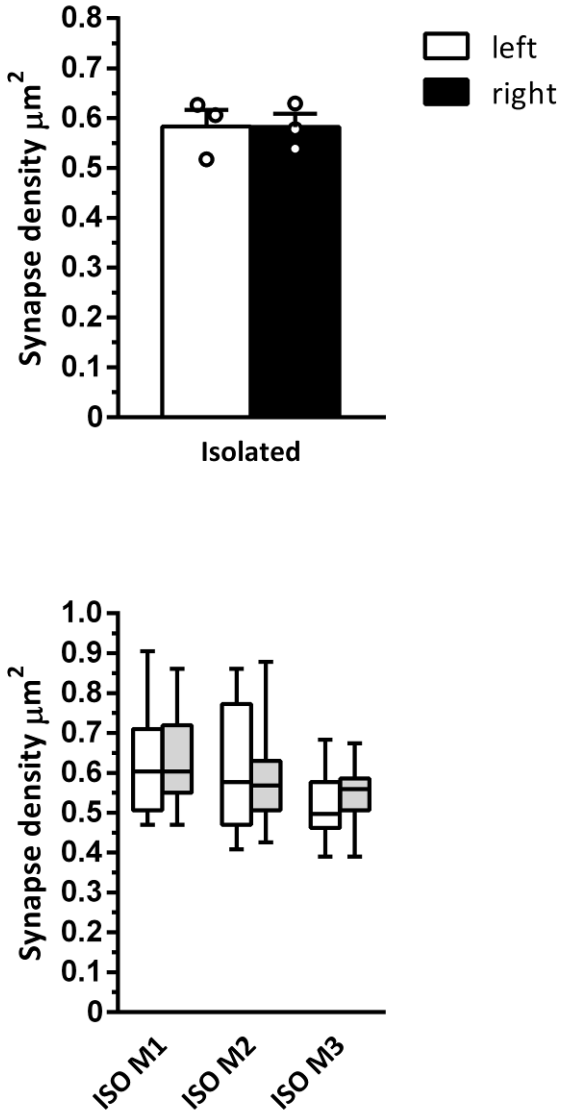

Effect of social isolation on CA1 pyramidal-cell synapse density in non-enriched mice

Upper chart shows average synapse density in socially-isolated C57bl6J mice, n = 3. Error bars display SEM and empty circles show average values for individual mice. Lower chart boxplots of density values for individual mice. The upper chart is an average of the lower values. For both charts, open box denotes density in left CA1, filled box denotes density in right CA1. Density values were calculated using the 2-dimensional analysis technique.

Similar to 6 week-old NENR mice, mice which have undergone 3 weeks of social isolation (ISO) do not display a difference in synapse density in their CA1 s.r. between hemispheres. The density observed, around 0.6 synapses per μm², is comparable between both ISO and NENR mice. This leads me to question whether the slight change observed in mice, contrary to the much larger difference seen in rats, isn't rather due to the effect of enrichment itself. The two most simple explanations would be that: either the enrichment protocol wasn't stimulating enough for the mice, or that there is a more fundamental difference between mice and rats, in how experience drives selective hemispheric changes to synapse density in the CA1.

The effect of different enrichment conditions on synapse density changes in the CA1

2:3

The first thing which I wanted to do was to examine changes to the enrichment protocol itself. It is well known that exercise can influence synaptic plasticity (Dong 2018, van Praag 1999, Fabel 2009), therefore it is possible a change in the activity of the mice during enrichment, rather than novelty of the condition, might be what was responsible for the changes in synapse density observed. To investigate this, I prepared differing housing environments, one which would increase physical exercise (exENR), with the inclusion of wheels, hanging chains and tubes, and one with only static objects (stENR), with the inclusion of lego bricks and wooden blocks (figure 31).

The hypothesis being that should an increase in locomotive activity between ENR and NENR mice explain the change in synapse density seen in the right hemisphere, then it should also distinguishable between two differing enrichment protocols.

Methods and results

Methods used: Transcardial perfusion (method 2), preparation of mouse brain for analysis under TEM (method 3), 2D analysis (method 4).

Mice were housed in groups of 3 in enriched mouse cages (figure 31, stENR and exENR) for 6 weeks (see timeline [top image] in figure 31). Cages were changed once a week, and food and water were supplied ad libitum.

The stENR condition did not contain any wheels or tubes. It only included objects which could be climbed over, or investigated. It was designed only to provide stimulation through the novelty of the items, rather than specific interaction with them.

The exENR condition contained wheels, tubes, and multiple levels. It was designed to provide an environment which would encourage exercise.

3 week old C57bl/6J mice were used in this experiment.

To directly compare with the data from experiment 1, I used the 2D analysis method for examining the synapse density values in the CA1 s.r.

Measurements of TEM images were conducted using the Reconstruct software (Fiala 2005)

Figure 31

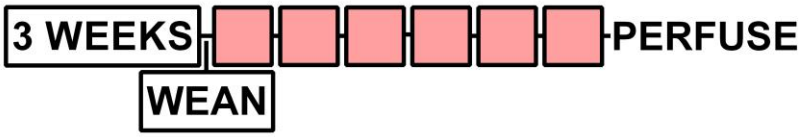

stENR

exENR

Different enrichment protocols

Top scheme represents timeline of experiment. Red boxes display 1 week of ENR condition. stENR shows 2 examples of cage layout for cages which are not designed to encourage exercise. These cages contained no tunnels or wheels, but only toys which could be climbed over and explored. exENR shows 2 examples of cage layout for cages which are designed to encourage exercise. These cages contained wheels, multiple layers, tubes and toys which could be climbed through and around.

Figure 32

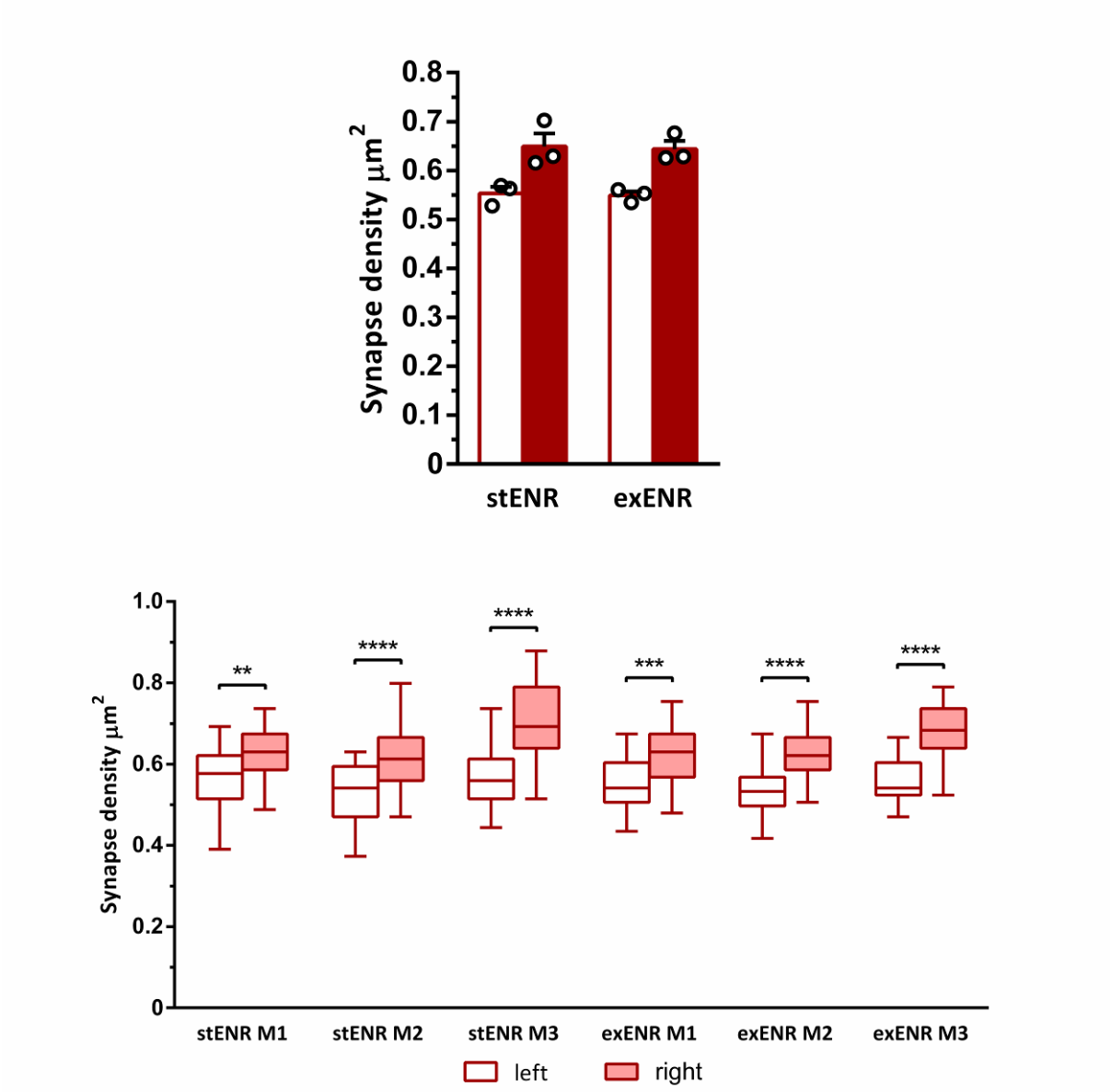

Effects of different environmental enrichment paradigms on CA1 pyramidal-cell synapse density

Upper chart shows average synapse density in ENR C57bl6J mice for enrichment protocols designed to encourage exercise (exENR), or those which just containing interesting items (stENR). stENR n = 3, exENR n = 3. Error bars display SEM and empty circles show average values for individual mice. Lower chart boxplots of density values for individual mice. The upper chart is an average of the lower values. For both charts, open box denotes density in left CA1, filled box denotes density in right CA1. Density values were calculated using the 2-dimensional analysis technique. For upper chart, both Wilcoxon matched-pairs signed rank and Mann Whitney tests used for statistical analysis, with no significance detectable. If normality assumed and students T-test used for statistical analysis, $p < 0.05$ between left and right CA1 for both stENR and exENR. For lower chart, Mann Whitney test used with ** denoting $p < 0.01$, *** denoting $p < 0.001$, and **** denoting $p < 0.0001$

Following 6 weeks of enrichment (figure 32), I found that the synapse density value in the right hemisphere was slightly higher than the results from 3 weeks enrichment (figure 29). This works out to an increase in density in the right hemisphere of around 9% in both of these 6 week conditions, compared to wild-type. However, although suggestive of a possible trend between enrichment time and synapse density, the difference between either the stENR or exENR and the 3 weeks ENR condition is not significant. Interestingly, when normality was assumed amongst groups, it was now possible to detect significance between both hemispheres, in the enriched mice following 6 weeks of enrichment. Contrary to my expectations, there were no differences in synaptic density detectable between either group. This suggests that it is the process of enrichment itself, rather than the specific form of exercise, which has a greater effect on synapse density in the CA1.

Experience-driven changes to synapse morphology in the CA1

2:4

Having demonstrated that the enrichment paradigm was enough to introduce an asymmetry in the density of synapses in the CA1 s.r. of wild-type mice, I could now focus more on identifying whether there were any specific changes to the morphology of individual synapses themselves. The hippocampus is highly asymmetrical in its activation during various memory tasks. For example, place recall and route planning has been shown to have a strong right-side bias in activation of the hippocampus (Maguire 1997). It has also been suggested that increased activity can lead to an increase in the size, as well as the perforation, of synapses in the hippocampus (Neuhoff 1999). Therefore, it is possible that there might be a change in the size and perforation of synapses following environmental enrichment.

Methods and results

Methods used: Transcardial perfusion (method 2), preparation of mouse brain for analysis under TEM (method 3), dissector analysis (method 4).

Mice were housed in groups of 5 in either enriched, or non-enriched mouse cages (figure 28) for 6 weeks (see timelines next to NENR and ENR). Cages were changed once a week, and food and water were supplied ad libitum.

3 week old C57bl/6J mice were used in this experiment.

To account for the possibility of changes in synaptic area affecting density values, I used the unbiased dissector method to determine synaptic density values. This was because, if there had been an increase in synaptic area, following enrichment, then these larger synapses would be more likely to appear in electron microscopy images and so they might bias the results.

When calculating PSD area, or the percentage of synapses with a perforated PSD, I used the dissector analysis method to find synapses for analysis. This was again to remove any potential bias towards the detection of larger synapses, which would appear in more images in a stack.

I also made sure to only measure synapses for which I could see the complete PSD area. If a synapse was still visible in either the first, or last, image of a series, I ignored it. This was because, otherwise, I couldn't be 100% sure that the synapse had ended in that last image, so I would, again, introduce a potential bias to my measurements.

Measurements of TEM images were conducted using the Reconstruct software (Fiala 2005)

Figure 33

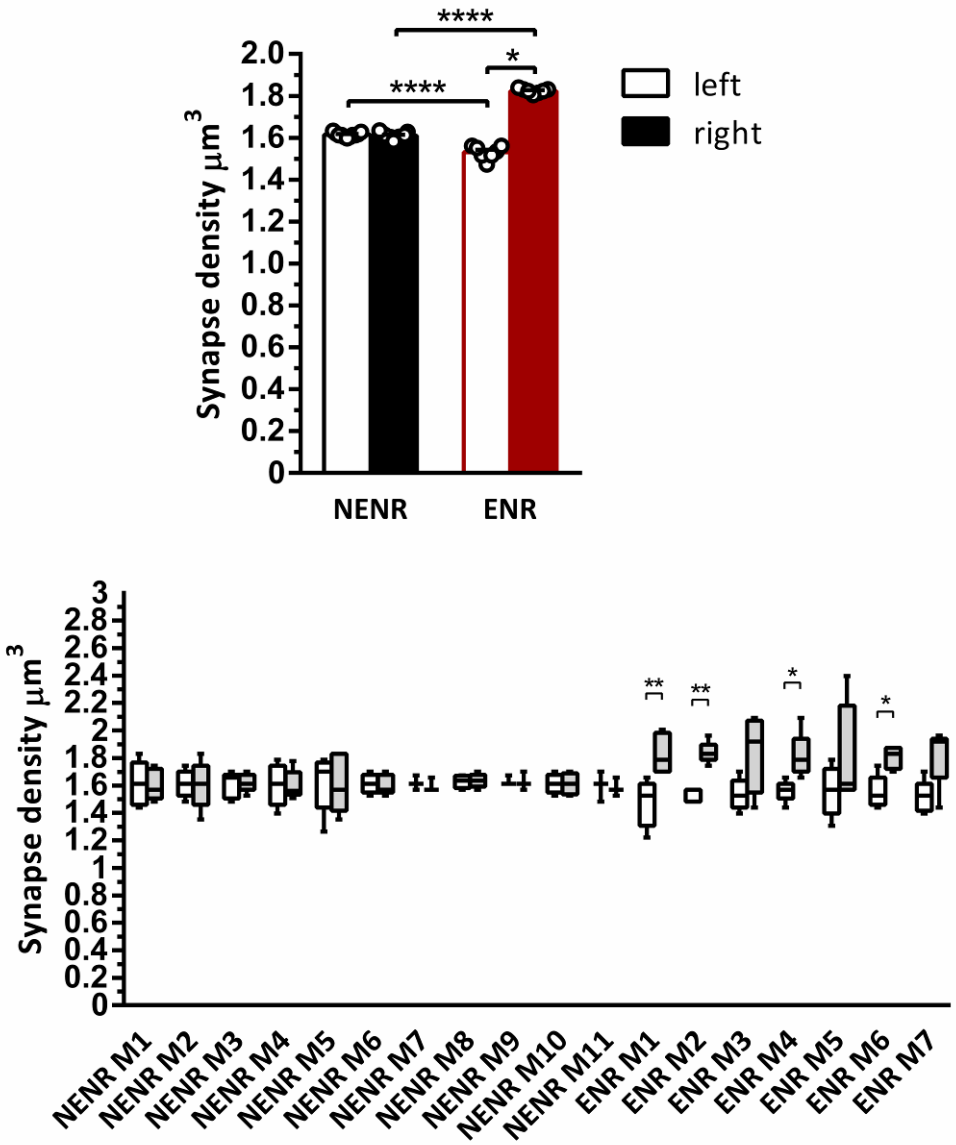

volumetric analysis of synapse density in NENR and ENR C57bl6J mice

Upper chart shows average synapse density in enriched (ENR) and non-enriched (NENR) C57bl6J mice. NENR n = 11, ENR n = 7. Error bars display SEM and empty circles show average values for individual mice. Lower chart boxplots of density values for individual mice. The upper chart is an average of the lower values. For both charts, open box denotes density in left CA1, filled box denotes density in right CA1. Black denotes NENR and red denoted ENR. Density values were calculated using the unbiased dissector analysis technique. Paired Wilcoxon matched-pairs signed rank test used for statistical analysis between average synaptic density in left and right CA1 of NENR and ENR groups. For comparrisons betwen groups, or individuals, Mann-Whitney test was used. * for p values < 0.05, ** for p values < 0.01, and **** for p values < 0.0001.

Figure 34

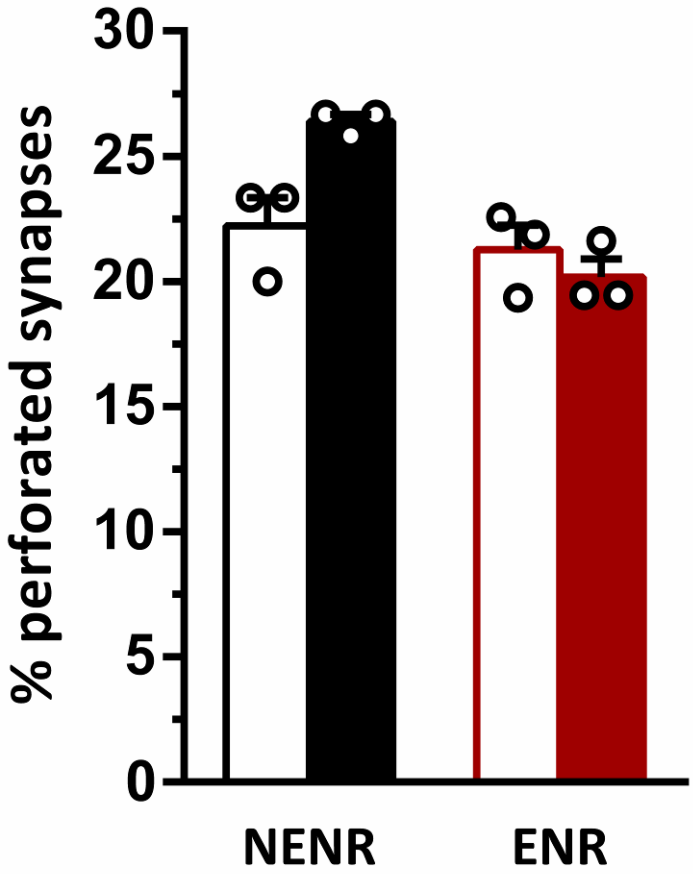

Effect of environmental enrichment on synapse perforation in C57bl6J mice

Percentage of synapses with perforated PSDs in the CA1 s.r. from C57bl6J mice. NENR n = 3, ENR n = 3. Error bars display SEM and empty circles show average values for individual mice. Only synapses where the total PSD area could be visualised were measured. Open box denotes density in left CA1, filled box denotes density in right CA1. Black denotes NENR and red denotes ENR. Both Wilcoxon matched-pairs signed rank and Mann Whitney tests used for statistical analysis, with no significance detectable. If normality assumed and Students T-test used for statistical analysis $p < 0.01$.

Figure 35

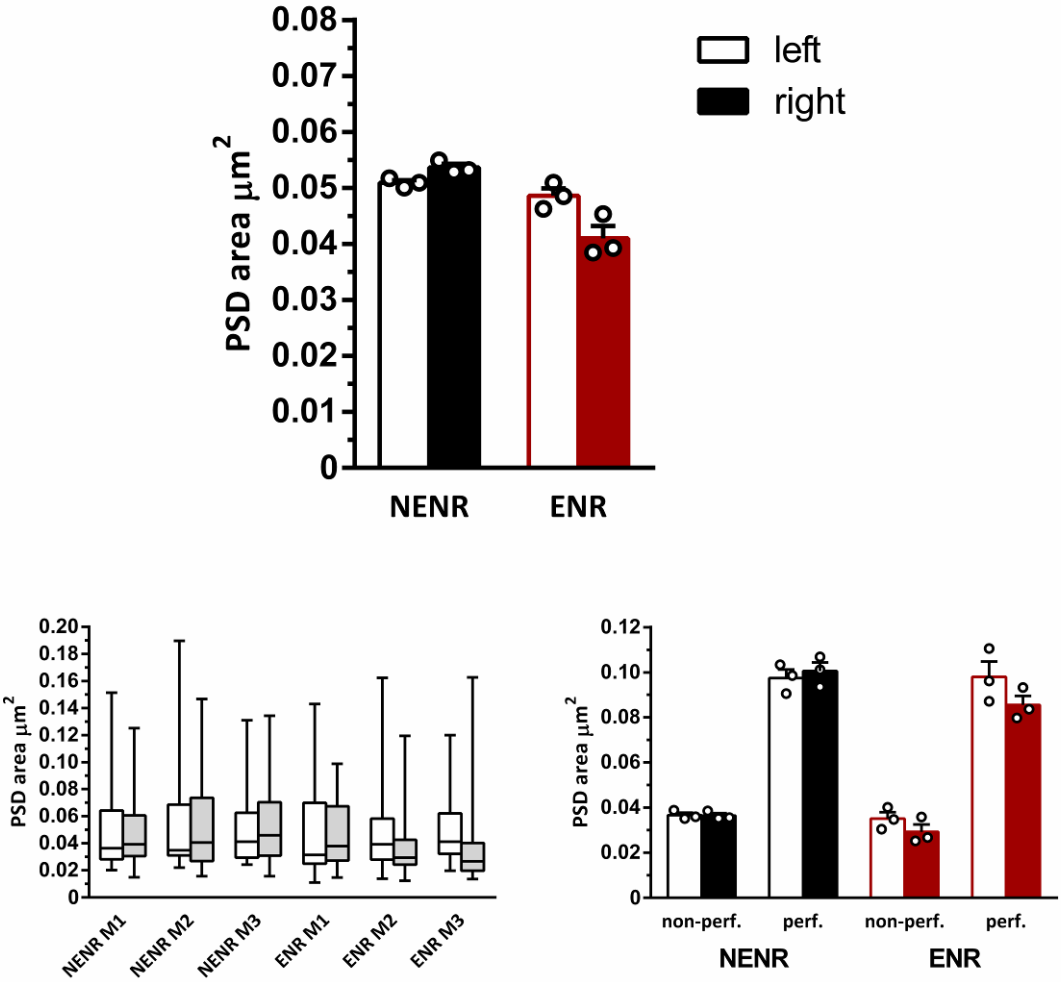

Effect of environmental enrichment on PSD area size in C57bl6J mice

Upper chart shows average PSD area from spine synapses in CA1 s.r. from C57bl6J mice. NENR n = 3, ENR n = 3. Error bars display SEM and empty circles show average values for individual mice. Lower left chart shows boxplots of density values for individual mice. The upper chart is an average of the lower left values. Lower right chart shows average PSD area from perforated (non-perf.) and perforated (perf.) synapses in NENR and ENR mice. Only synapses where the total PSD area could be visualised were measured. Error bars display SEM and empty circles show average values for individual mice. For all charts, open box denotes density in left CA1, filled box denotes density in right CA1. Black denotes NENR and red denotes ENR. Wilcoxon matched-pairs signed rank and Mann-Whitney tests used for statistical analysis with no significance detectable. If normality assumed and T test used, $p < 0.01$ detectable between right CA1 PSD areas of NENR and ENR (top graph).

In concordance with my previous findings, I could detect a significant increase in the right CA1 s.r. following environmental enrichment, as well as a significant difference between both hemispheres in the enriched mice. I could also detect a significant decrease in the left-hemisphere, following enrichment. I did not previously detect this, so it could be related to the change from the 2D analysis, to the unbiased dissector analysis, method. Interestingly, this significant decrease in the left-hemisphere had not been previously reported.

Using serial electron microscopy, we could detect a decrease in the number of perforated synapses [figure 34] as well as the average PSD area [figure 35] in the right CA1 s.r., following enrichment. There was no significant change in the left CA1 s.r.. This goes against my idea that the enriched protocol might lead to an increase in perforation. However, as smaller synapses in the CA1 tend to be more NR2B-dense and more prone to LTP (Sobczyk 2005, Wu 2005), it is possible that this change could reflect an increase in overall synaptic plasticity in the right-CA1. No changes in PSD area or perforation were previously reported in rats, following environmental enrichment.

Changes in the ipsilateral projections from the CA3 during enrichment

2:5

Having found a significant decrease in PSD area and perforation in the right CA1, I decided that it would be worth investigating the projections from the CA3 in each hemisphere. Input-side dependent asymmetry is a fundamental feature of the rodent hippocampus (Kawakami 2003, Shinohara 2008), where the characteristics of a synapse will be determined based upon the hemisphere where the projection originated, rather than the hemisphere where the projection terminates. Previous literature has demonstrated that each CA3 will send the majority (60%) of their projections to the ipsilateral side (Shinohara 2012a, Wu 2005), therefore it is possible that the right-sided increase in synapse density, induced through enrichment, relies on an increase in projections from the right CA3.

To investigate this, I decided to perform a similar 6 week enrichment paradigm on wild-type mice, then follow this up with the total transection of the hippocampal commissure. This

would damage the contralateral projections, causing them to degenerate, and would enable the specific investigation of the ipsilateral projections to each CA1 s.r..

Methods and results

Methods used: Transcardial perfusion (method 2), preparation of mouse brain for analysis under TEM (method 3), dissector analysis (method 4), Ventral Hippocampal Commissure Transection [VHCT] (method 6).

Mice were housed in groups of 5 in the enriched (figure 28) condition for 6 weeks (see timelines on method 6). Cages were changed once a week, and food and water were supplied ad libitum.

3 week old C57bl/6J mice were used in this experiment.

I only measured synapses for which I could see the complete PSD area. If a synapse was still visible in either the first, or last, image of a series, I ignored it. This was because, otherwise, I couldn't be 100% sure that the synapse had ended in that last image, introducing a potential bias to my measurements.

Only synapses on intact spines were measured. Synapses on degenerating projections were ignored, as these originated from the contralateral side.

Measurements of TEM images were conducted using the Reconstruct software (Fiala 2005)

Figure 36

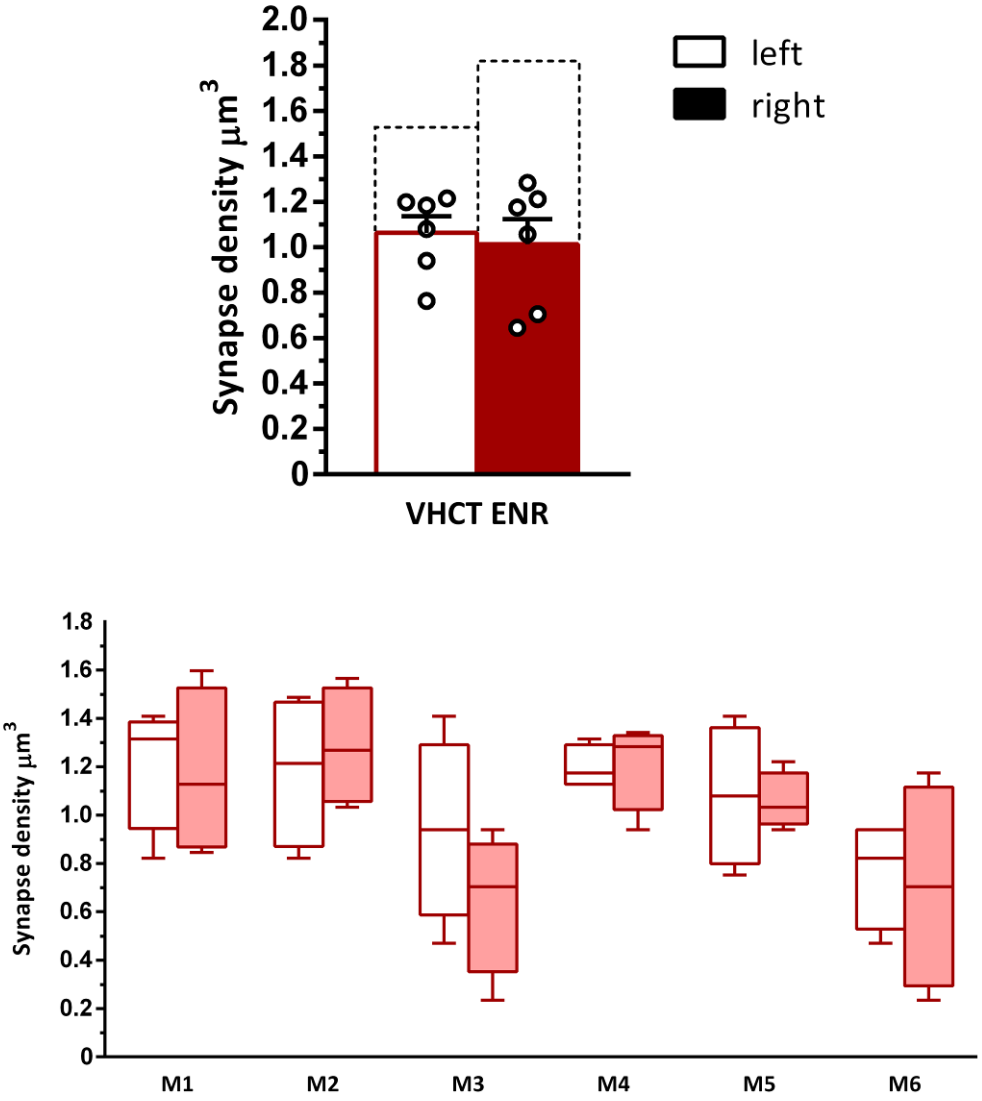

Synaptic density from ipsilateral projections following enrichment and VHCT operation

Upper chart shows average synapse density in 6 weeks enriched (ENR) C57bl6J mice following VHCT operation. n = 6. Error bars display SEM and empty circles show average values for individual mice. Dotted line displays average synapse density of non-VHCT ENR mice. Lower chart boxplots of density values for individual mice. The upper chart is an average of the lower values. For both charts, open box denotes density in left CA1, filled box denotes density in right CA1. Density values were calculated using the dissector analysis technique. Students T-test used for statistical analysis with no significance seen.

Following total transection of the ventral hippocampal commissure (VHCT operation), I no longer could detect an asymmetry in the synaptic density values between the CA1 in either hemisphere (figure 36). The synaptic densities were around 1 synapse per μm³, which is comparable to the density previously reported in non-enriched wild-type mice (Wu 2005). This is around 44% lower in the left hemisphere and around 80% lower in the right-hemisphere, compared to non-VHCT enriched animals (dotted lines). This suggests that the increase in density, following enrichment, relied heavily on these connections. It has been shown that the commissural fibres can mask asymmetries in hippocampal dominance during spatial learning paradigms, with the right-hemispheric dominance only becoming evident through the destruction of the commissural fibres (Corballis 2002, Shinohara 2012b). However, the asymmetry described here appears to rely on a completely unrelated mechanism, as it is only in the presence of the connections, rather than their absence, where this phenotype can be examined.

Judging from the ratios of ipsilateral and contralateral projections into the CA1, one might expect that the right-side specific increase in experience-driven synapse density would rely heavily on the right CA3, but it appears that this isn't the case. It is known that CA3 and CA1 gamma oscillation synchrony within and between hemispheres is associated with accurate reactivation of stored hippocampal memories (Carr 2012). Therefore, these results could highlight the importance of interhemispheric coordination experience-driven memory formation.

The effect of environmental enrichment on mice which lack input-side dependent hippocampal asymmetry

2:6

Having determined that hippocampal commissural fibres are likely to be important in the experience-driven laterality changes which I had detected in the hippocampus, the next question was whether the input-side dependent mechanism was really involved or not. To do this, I decided to use a mouse mutant which lacked input-side dependent asymmetry in its hippocampal projections. The mutant I used was the right-isomerism *i.v.* mouse (see chapter 1). Should input-side dependent asymmetry be truly responsible experience-driven laterality

formation, one could expect that there would be no change to the synaptic density values in *i.v.* mice.

My hypothesis was that, as the mouse lacks input-side dependent asymmetry, there would be no discernible difference in synaptic density between either hemisphere in enriched *i.v.* mice.

Methods and results

Methods used: Transcardial perfusion (method 2), preparation of mouse brain for analysis under TEM (method 3), dissector analysis (method 4).

Mice were housed in groups of 5 in either enriched, or non-enriched mouse cages (figure 28) for 6 weeks (see timelines next to NENR and ENR). Cages were changed once a week, and food and water were supplied ad libitum.

3 week old right-isomerism *i.v.* mice were used in this experiment.

I only measured synapses for which I could see the complete PSD area. If a synapse was still visible in either the first, or last, image of a series, I ignored it. This was because, otherwise, I couldn't be 100% sure that the synapse had ended in that last image, introducing a potential bias to my measurements.

Measurements of TEM images were conducted using the Reconstruct software (Fiala 2005)

Figure 37

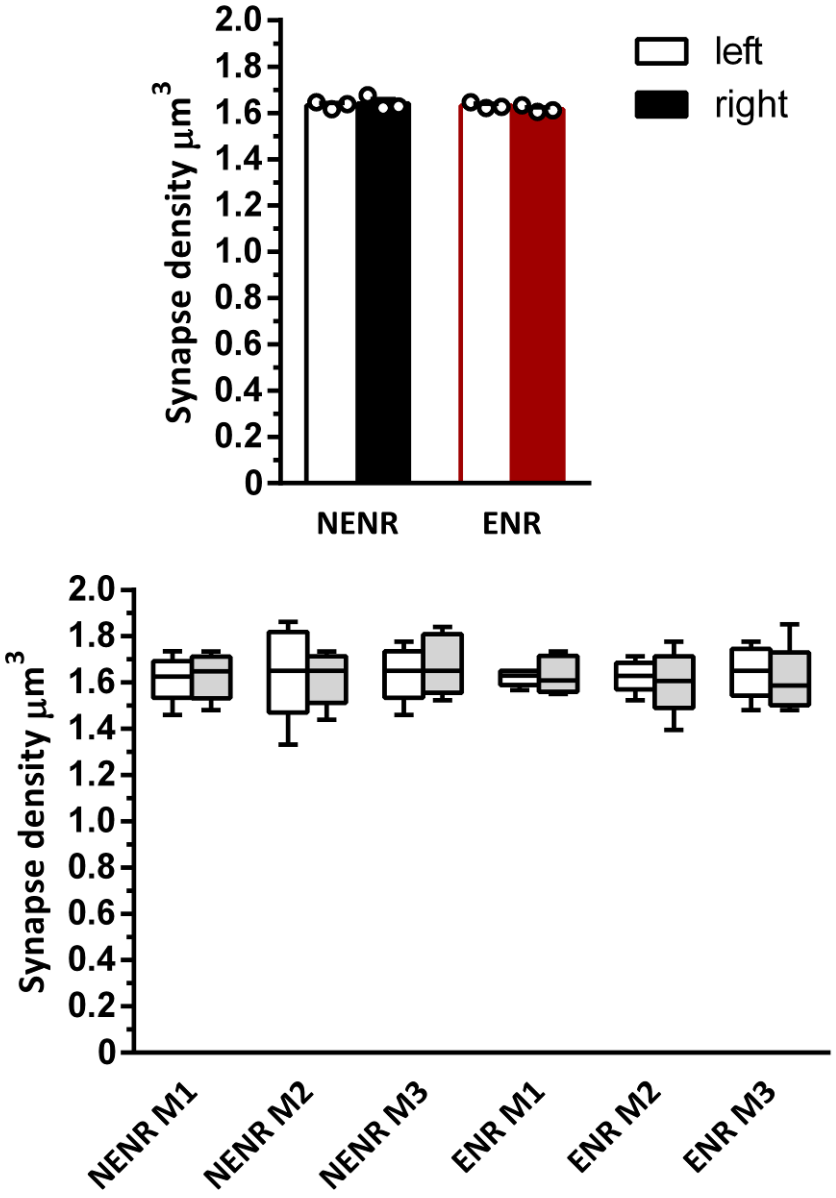

Effects of environmental enrichment on right-isomerism *i.v.* mice

Upper chart shows average synapse density in non-enriched (NENR) and 6 weeks enriched (ENR) right-isomerism *i.v.* mice. NENR n = 3, ENR n = 3. Error bars display SEM and empty circles show average values for individual mice. Lower chart boxplots of density values for individual mice. The upper chart is an average of the lower values. For both charts, open box denotes density in left CA1, filled box denotes density in right CA1. Density values were calculated using the dissector analysis technique. Students T-test used for statistical analysis with no significance seen.

Using the right-isomerism *i.v.* mouse mutant, I could not detect a difference in the synapse densities between hemispheres following enrichment. Interestingly, there was no discernable difference between non-enriched and enriched mice. This supports my hypothesis that the environmentally-driven induction of an asymmetry in synaptic density, seen in wild-type mice, relies on the a difference in the CA3 inputs to the s.r.. However, this can not be the entire story as, if this were true, otherwise it is likely that I should have been able to detect a difference following VHCT. In fact, should the presence of input-side dependent asymmetry be the only relevant factor, the VHCT operation should have led to an increased difference between the hemispheres. This is because it would mean that the right CA3 would project solely to the right CA1, and vica versa in the left hemisphere.

Comparing the effect of environmental enrichment between left- and right-isomerism *i.v.* mice

2:7

As the results from the previous experiment suggested that input-side dependent asymmetry could be a vital mechanism in experience-driven laterality changes to the CA1 s.r., I decided to further investigate this using a left-isomerism *i.v.* mouse mutant. As with the right-isomerism mutant, this mouse lacks input-side dependent asymmetry formation. However, in this mutant, all the inputs to the CA1 from the CA3 form synapses similar to left-originating (rather than right-originating) synapses seen in wild-type mice (see chapter 1 for more information). As with the right-isomerism *i.v.* mouse, I believed it likely that these mice would also lack the ability to generate an asymmetry in synaptic density following enrichment. However, as the increase seen in the wild-type occurs in the right CA1, which receives 60% of its input from the ipsilateral hemisphere, I imagined that I might be able to detect a difference in synaptic density between the left- and right-isomerism *i.v.* mutant.

Methods and results

Methods used: Transcardial perfusion (method 2), preparation of mouse brain for analysis under TEM (method 3), 2D analysis (method 4).

Mice were housed in groups of 5 in either enriched, or non-enriched mouse cages (figure 28) for 6 weeks (see timelines next to NENR and ENR). Cages were changed once a week, and food and water were supplied ad libitum.

3 week old *i.v.* mice were used in this experiment.

I used the 2D analysis method for examining the synapse density values in the CA1 s.r.

Measurements of TEM images were conducted using the Reconstruct software (Fiala 2005)

Figure 38

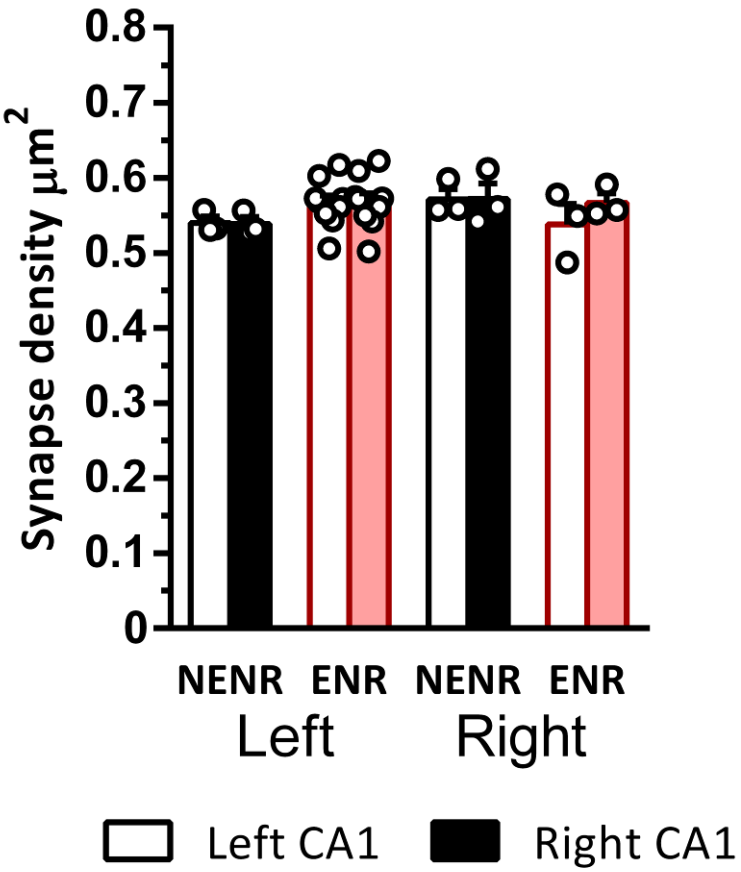

Effects of enrichment on left- and right-isomerism *i.v.* mouse lines

Upper chart shows average synapse density in left and right isomerism *i.v.* mice, under NENR and ENR conditions. Left NENR n = 3, ENR n = 9, Right NENR n = 3, ENR = 3. Error bars display SEM and empty circles show average values for individual mice.Open box denotes density in left CA1, filled box denotes density in right CA1. Black denotes NENR and red denotes ENR. Density values were calculated using the 2-dimensional analysis technique. Students T-test used for statistical analysis with no significance detected.

Figure 39

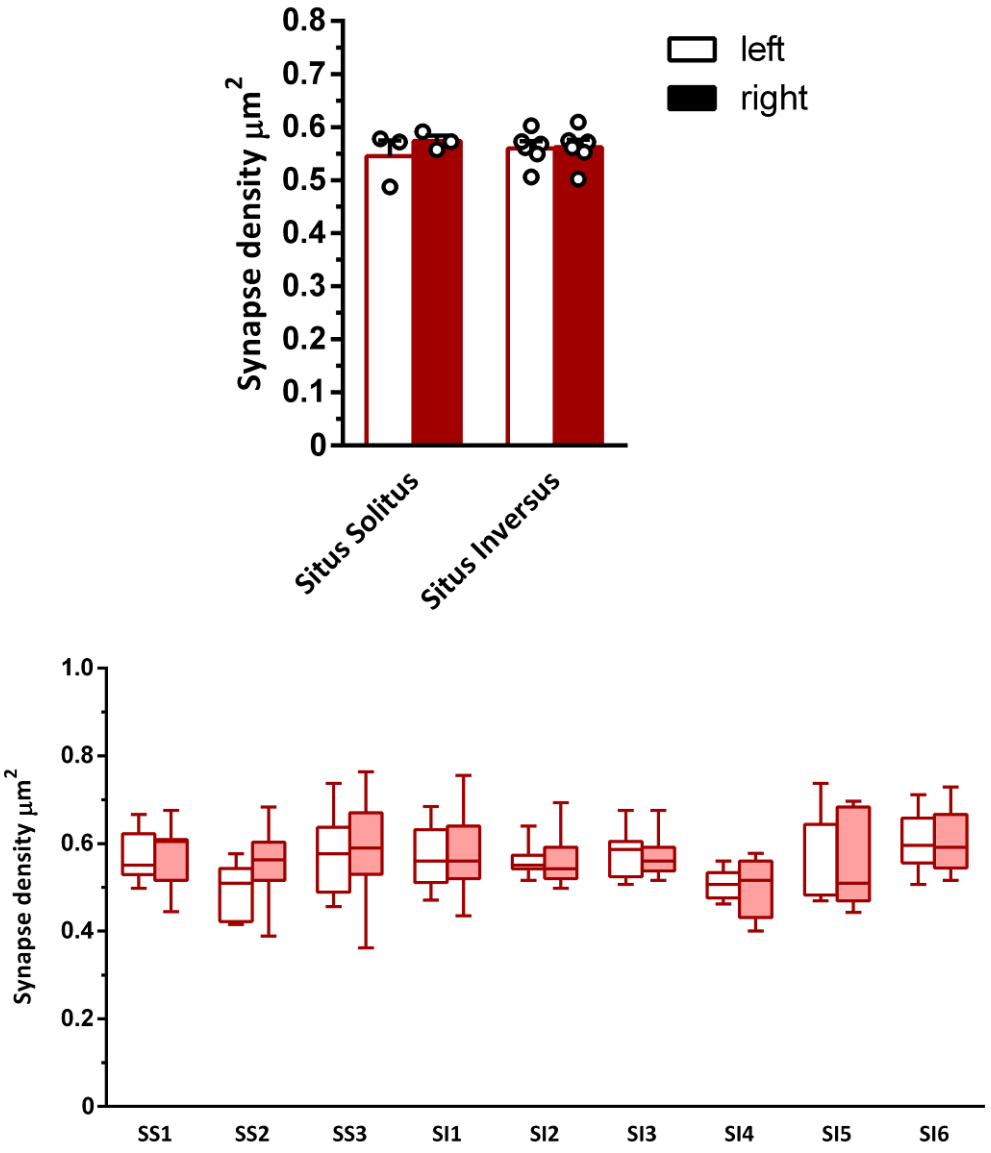

Effects of visceral organ laterality on CA1 pyramidal-cell synapse density in enriched *i.v.* mice

Upper chart shows average synapse density in enriched situs solitus and situs inversus *i.v.* mice. Situs solitus n = 3, situs inversus n = 6. Error bars display SEM and empty circles show average values for individual mice. Lower chart boxplots of density values for individual mice. The upper chart is an average of the lower values. For both charts, open box denotes density in left CA1, filled box denotes density in right CA1. Density values were calculated using the 2-dimensional analysis technique. Students T-test used for statistical analysis with no significance seen.

Similar to the right-isomerism line, left-isomerism *i.v.* mice do not develop an asymmetry in the synaptic densities of the CA1 s.r. between either hemisphere, further confirming my hypothesis that input-side dependency is critical to this process. However, interestingly, there was no significant differences between left- or right-isomerism *i.v.* mice. This fits with my previous findings with the VHCT operated wild-type mice (experiment 4), as should input-side dependency be the only determining factor, then an asymmetry in synaptic density should have been evident (or amplified) in the VHCT model. It also confirms that the changes seen in synapse density were not an artefact of the surgery. This suggests a specific importance of contralateral projections, working in combination with the input-side dependent mechanism, to achieve the density changes in experience-driven laterality formation.

As expected, I could detect no significant difference in the effect of enrichment on synaptic density, between *i.v.* mice, based on the laterality of their visceral organs. There was no expectation of any effect, due to the previous literature and my findings in chapter 1. However, due to the fact that input-side dependency appears important, but not the sole cause of change, in experience-driven laterality formation, I determined it to be worth investigating, just in case.

Changes in the ratio of ipsilateral and contralateral projections caused through environmental enrichment

2:8

Having determined the possibility of two separate mechanisms being involved in the process of experience-driven laterality formation in the CA1 s.r., it was important to examine how the CA3 in each hemisphere changes its projection dynamics in relation to an ever-changing environment. To investigate this, I decided to perform unilateral injections of an adeno-associated virus (AAV) expressing fluorescent Venus-VAMP2 (AAV1-CaMKIIa-Venus-VAMP2) into the CA3, then measure fluorescence intensity values in the inner 1/3rd of the CA1 s.r.. As there could be a localized effect, based on which region of the CA3 the injections were performed altering the target site (Li 1994), I targetted the injections towards the distal CA3b subregion.

Methods and results

Methods used: Unilateral injections into the CA3 (method 1), transcardial perfusion (method 2), measurement of fluorescence intensity using Fiji image software (Schindelin 2012), preparation of mouse brain for analysis under TEM (method 3), dissector analysis (method 4).

Mice were housed in groups of 5 in either enriched, or non-enriched mouse cages (figure 28) for 6 weeks (see timelines next to NENR and ENR). Cages were changed once a week, and food and water were supplied ad libitum.

3 week old C57bl/6J mice were used in this experiment.

Fixed brains were sectioned into 50 μm-thick sections using a vibrotome (Leica VT1000S), mounted on gelatine-coated glass slides, then imaged using a fluorescence microscope (Keyense model?!).

Using the Fiji imaging software, fluorescence intensity values were taken from the inner 1/3rd of the CA1 s.r. from both the ipsilateral and contralateral hemisphere, in relation to hemisphere of injection.

A ratio of fluorescence was determined by taking the fluorescence intensity value in each hemisphere and dividing it by the sum of fluorescence intensity from both hemispheres (figure 40). This gave me an estimation of the ratio of ipsilateral and contralateral projections from each CA3.

Measurements of TEM images were conducted using the Reconstruct software (Fiala 2005)

Figure 40

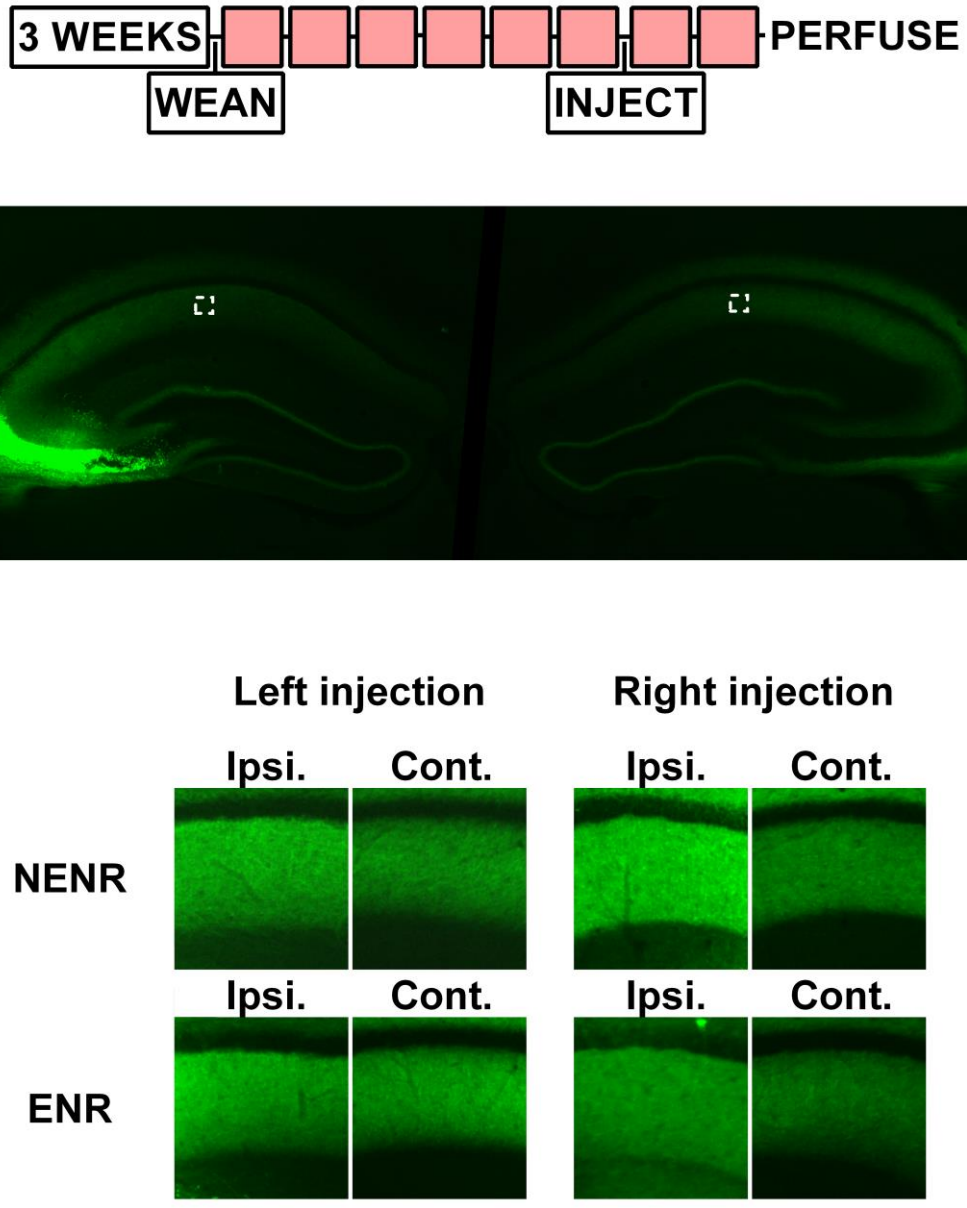

Fluorescence intensity 2 weeks following unilateral injections into either the left or right CA3 in enriched and non-enriched C57bl6J mice

Top scheme represents timeline of experiment. Red boxes represent 1 week of ENR. Middle image shows an example of a unilateral CA3 injection using an adeno-associated virus expressing fluorescent Venus-VAMP2 (AAV1-CaMKIIa-Venus-VAMP2). Fluorescence measurements taken from inner 1/3rd of s.r. (white box). Examples below for fluorescence intensities in the ipsilateral (ipsi.) and contralateral (cont.) CA1 s.r. from left and right injections into non-enriched (NENR) and enriched (ENR) C57bl6J mice.

Figure 41

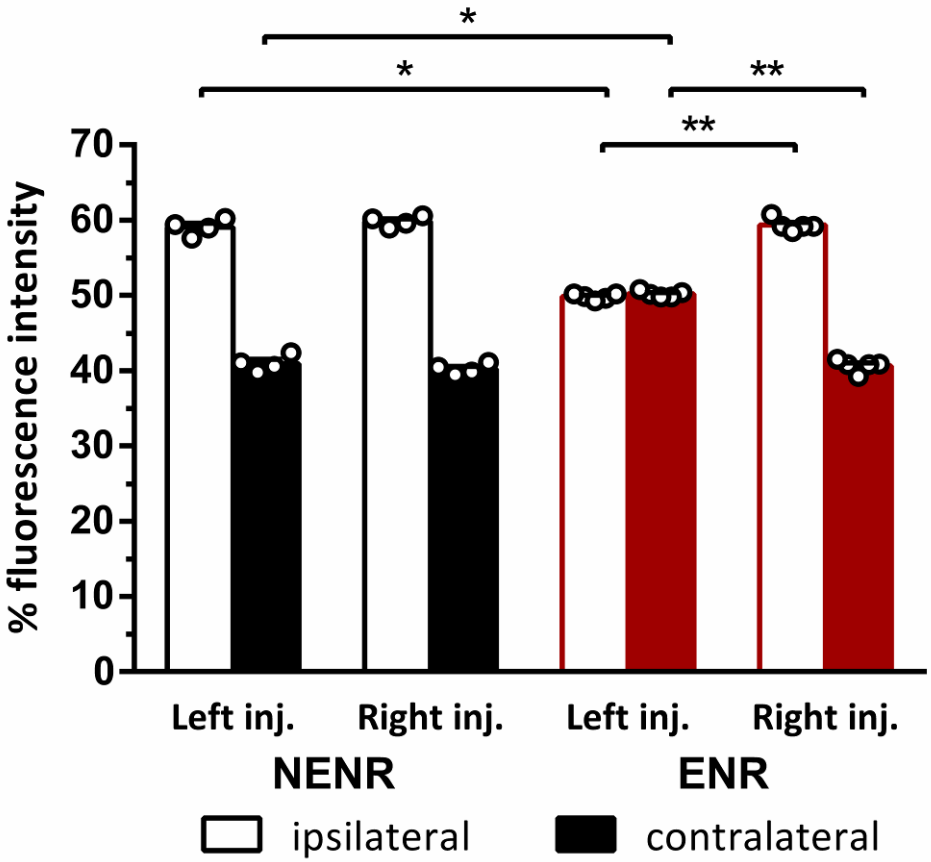

Ratio of fluorescence intensity from unilateral injections into the CA3 of enriched and non-enriched C57bl6J mice

Ratio of fluorescence intensity was taken 2 weeks following unilateral CA3 injection. NENR left injected n = 4, NENR right injected n = 4, ENR left injected n = 5, ENR right injected n = 5. Error bars display SEM and empty circles show average values for individual mice. Open box denotes fluorescence intensity from ipsilateral CA1 s.r., filled box denotes fluorescence intensity from contralateral CA1 s.r.. Fluorescence intensity ratio was determined by dividing the fluorescence intensity value in the hemisphere of interest by the total fluorescence intensity value from both hemispheres. Only the inner 1/3rd of the CA1 s.r. was analysed. Mann Whitney test used for statistical analysis with * denoting p value < 0.05 and ** denoting a p value < 0.01.

Figure 42

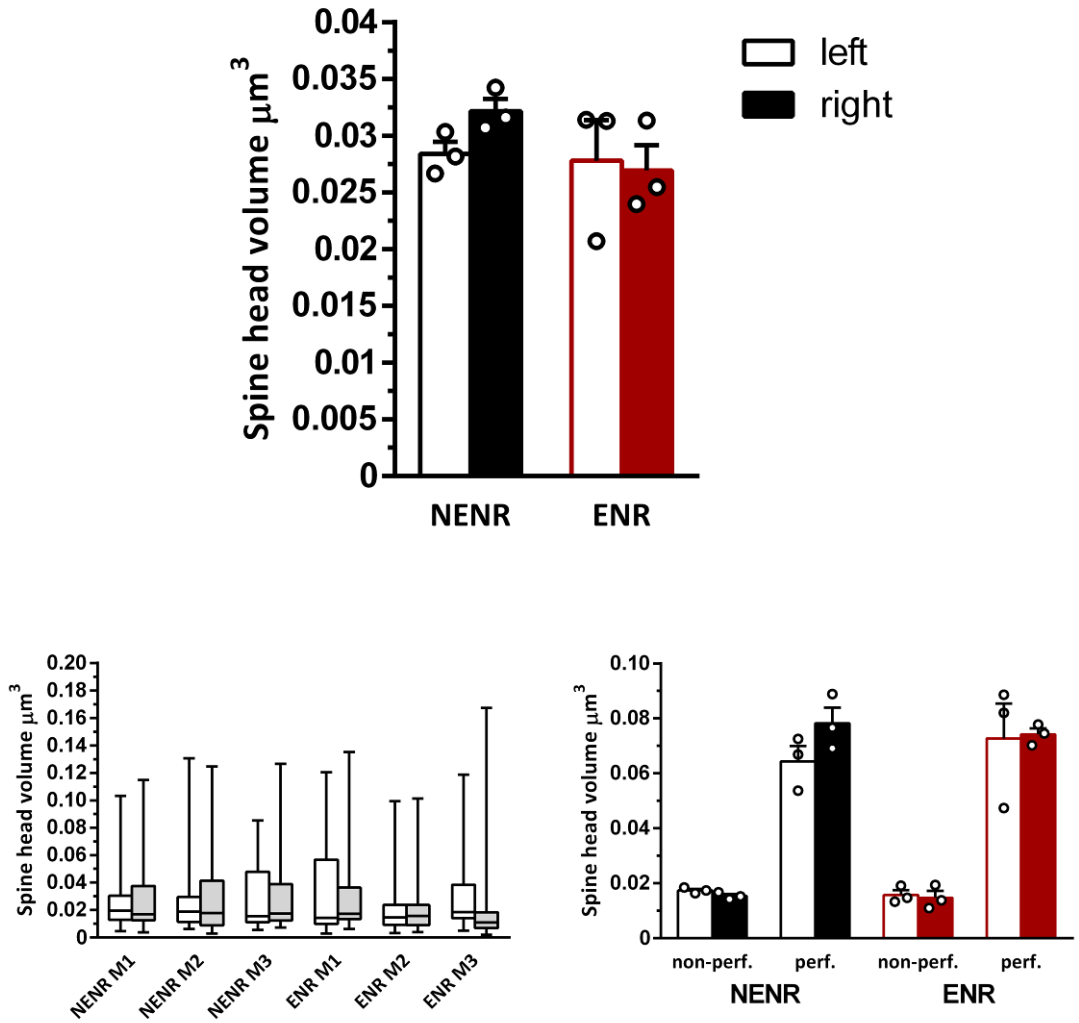

Effect of environmental enrichment on spine head volume in C57bl6J mice

Upper chart shows average spine head volume from spine synapses in CA1 s.r. from C57bl6J mice. NENR n = 3, ENR n = 3. Error bars display SEM and empty circles show average values for individual mice. Lower left chart shows boxplots of spine head volume values for individual mice. The upper chart is an average of the lower left values. Lower right chart shows average spine head volume from perforated (non-perf.) and perforated (perf.) synapses in NENR and ENR mice. Only synapses where the total area could be visualised were measured. Error bars display SEM and empty circles show average values for individual mice. For all charts, open box denotes volume in left CA1, filled box denotes volume in right CA1. Black denotes NENR and red denotes ENR. Students T-test used for statistical analysis with no significance seen.

Using unilateral injections into the CA3 (figure 40), I found that the ratio of ipsilateral to contralateral projections from either the left- or right-CA3 was around 60% ipsilateral to 40% contralateral, in non-enriched wild-type mice. This fits with the previously reported values for CA3 projections into the CA1 s.r. (Shinohara 2012a, Wu 2005), thus validating this method as a viable approach to determine the CA3 projection dynamics in the hippocampus. Although I could detect no changes in the ratio of ipsilateral to contralateral projections from the right-CA3, following environmental enrichment, a significant change could be found in projections from the left-CA3 (figure 41). There are a few possible explanations for this marked ratio change, including an increase in the contralateral projections, a decrease in the ipsilateral projections, or a change in both the ipsilateral and contralateral projections.

As changes in spine head volume could be responsible for changes in fluorescence intensity, due to larger terminals potentially having stronger fluorescence, I also investigated the spine head volume for non-enriched and enriched mice. I found no significant difference in spine head volume between non-enriched and enriched mice, in either hemisphere (figure 42). This helps to validate my assumptions about enrichment leading to a change in the projection dynamics of the left, but not right, CA3.

Specific contribution of individual CA3 projections to synaptic density in the CA1 stratum radiatum

2:9

Having determined that only the left-, but not the right-, CA3 will change the ratio in its ipsilateral to contralateral projections, I decided that it was important to further investigate this phenomenon. As I have stated in experiment 7, although I could isolate a change in ratio, the previous experiment didn't give any clues as to exactly what was happening to the ipsilateral and contralateral projections. Therefore, I decided to perform an additional series of unilateral injections of the fluorescent AAV construct and then combine these samples with TEM imaging of the same samples. This would enable me to combine both the fluorescence and electron microscopical imaging methods to specifically examine the projection dynamics of the left-CA3, so that I could determine if it was an increase or a decrease in the contralateral or ipsilateral projections specifically, which accounted for this ratio change.

Methods and results

Methods used: Unilateral injections into the CA3 (method 1), transcardial perfusion (method 2), measurement of fluorescence intensity using Fiji image software (Schindelin 2012), preparation of mouse brain for analysis under TEM (method 3), dissector analysis (method 4).

Mice were housed in groups of 5 in either enriched, or non-enriched mouse cages (figure 28) for 6 weeks (see timelines next to NENR and ENR). Cages were changed once a week, and food and water were supplied ad libitum.

3 week old C57bl/6J mice were used in this experiment.

Fixed brains were sectioned into 50 μm-thick sections using a vibrotome (model), mounted on gelatine-coated glass slides, then imaged using a fluorescence microscope (Keyence BZ-9000).

Similar to the previous experiment, fluorescence intensity values were taken from the inner 1/3rd of the CA1 s.r. from both the ipsilateral and contralateral hemisphere, in relation to hemisphere of injection, using the Fiji imaging software.

A ratio of fluorescence was determined by taking the fluorescence intensity value in each hemisphere and dividing it by the sum of fluorescence intensity from both hemispheres (figure 40). This gave me an estimation of the ratio of ipsilateral and contralateral projections from each CA3. Following this, the sections were gently removed from the glass slides and were prepared for TEM imaging (method 3).

The dissector method was used ensure an unbiased detection of synapse density. This meant that I would image a sequential series and only count newly appearing synapses. This was done for each mouse, so I could combine the ratio of ipsilateral to contralateral fluorescence intensity directly with the synapse density values in each hemisphere, for individuals.

Measurements of TEM images were conducted using the Reconstruct software (Fiala 2005)

Figure 43

$$\left(\frac{\text{Synapse density Left CA1}}{\text{Ratio L} + \text{Avg. ratio L}} \right) \times \text{Ratio L}$$

$$\left(\frac{\text{Synapse density Right CA1}}{\text{Ratio R} + \text{Avg. ratio R}} \right) \times \text{Ratio R}$$

Worked example for left-injected mouse

$$\left(\frac{\text{Synapse density Right CA1}\ 1.82\ \text{synapses per } \mu m^3}{\underset{\text{Ratio R}}{50.76} + \underset{\text{Ratio R}}{59.35}} \right) \times \underset{\text{Ratio R}}{50.76}$$

= 0.84 contralateral synapses (left to right)

$$\left(\frac{\text{Synapse density Right CA1}\ 1.82\ \text{synapses per } \mu m^3}{\underset{\text{Ratio R}}{50.76} + \underset{\text{Ratio R}}{59.35}} \right) \times \underset{\text{Ratio R}}{59.35}$$

= 0.98 ipsilateral synapses (right to right)

Formula to estimate ipsilateral and contralateral contributions of CA3 to both hemispheres

Red values are obtained from the mouse that is being investigated. Black values are obtained from the average ratios from mice which had CA3 injections in the opposite hemisphere. Ratios are calculated by taking the fluorescence intensity values from the s.r. of the hemisphere in question and dividing it by the total fluorescence intensity values from the s.r. of both hemispheres. The third formula (blue text) shows a worked example for the right CA1 in a left-injected mouse.

Figure 44

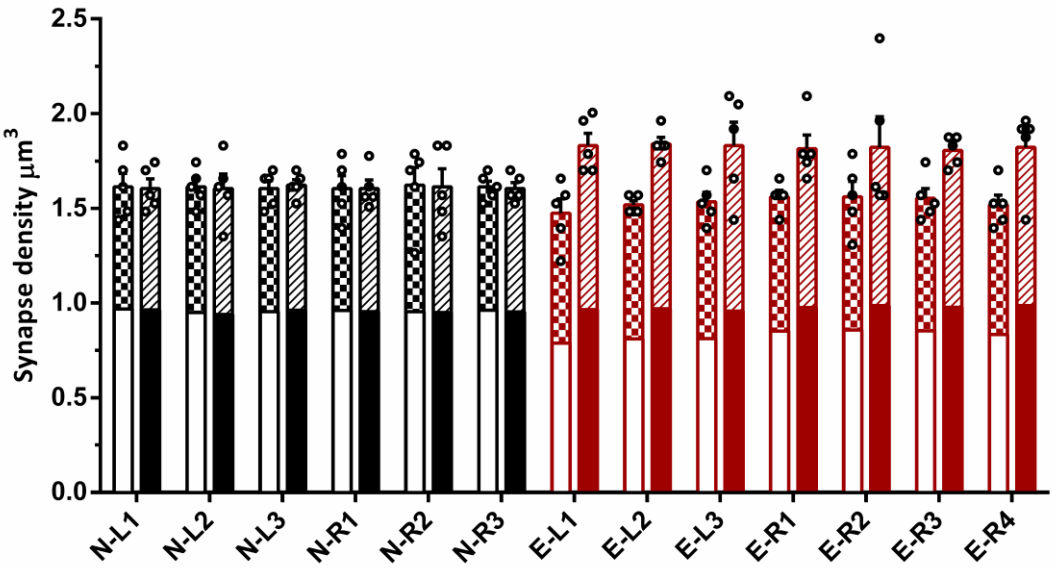

Estimated synapse density contributions for ipsilateral and contralateral CA3 - CA1 projections from each hemisphere in individual NENR and ENR mice

N-L# = non-enriched left-injected mouse, N-R# = non-enriched right-injected mouse, E-L# = enriched left-injected mouse, E-R# = enriched right-injected mouse. L/L (empty bars) = ipsilateral projections from left CA3, L/R (striped bars) = contralateral projections from left CA3, R/R (filled bars) = ipsilateral projections from right CA3, R/L (chequered bars) = contralateral projections from right CA3. Black denotes NENR and red denotes ENR. Height of the bar denotes the absolute synaptic density as determined by dissector analysis, with empty circles show average values for one dissector series and error bars showing SEM.

Figure 45

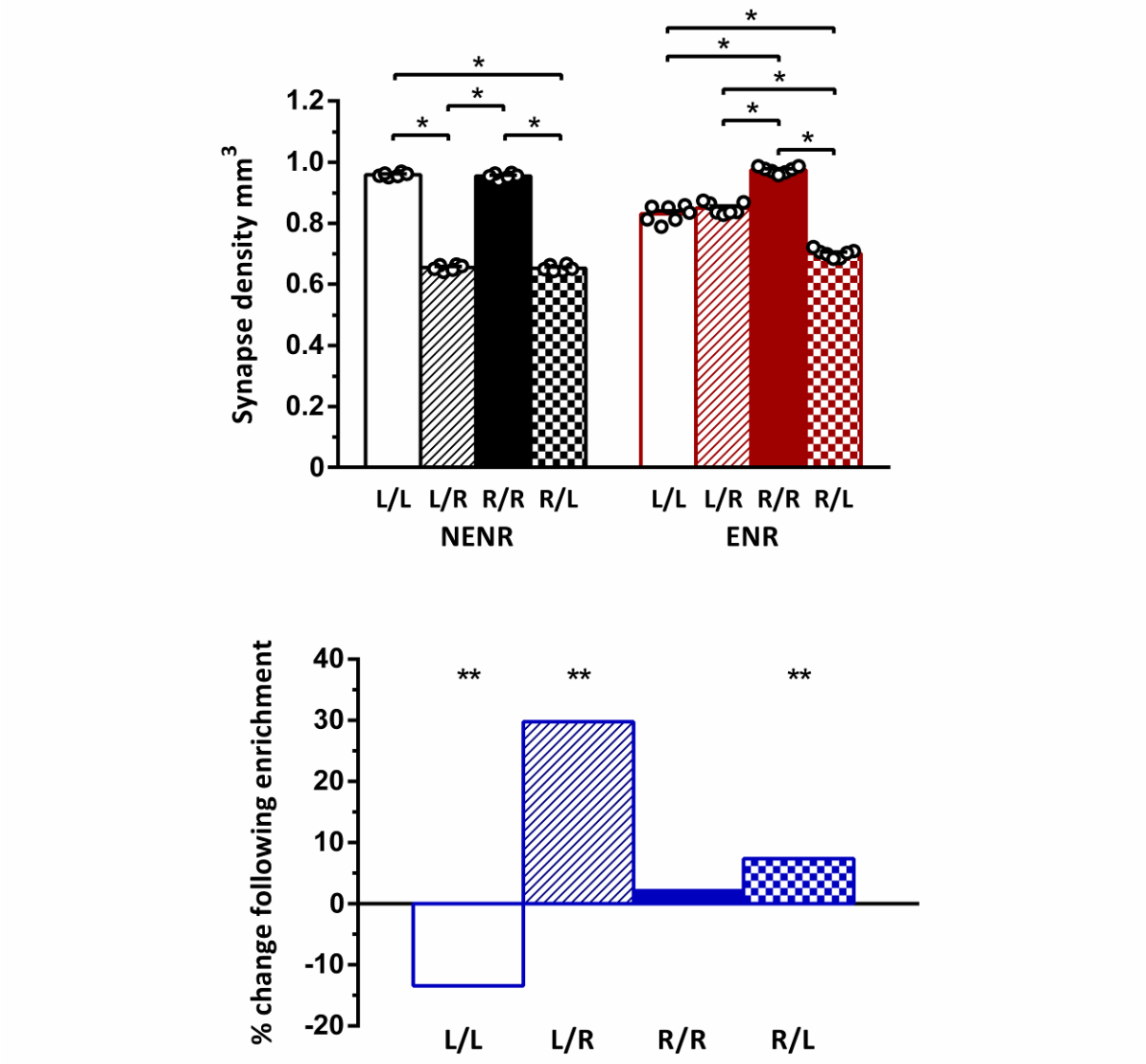

Estimated change in CA1 synapse density for ipsilateral and contralateral projections from each hemisphere

Upper chart shows estimated synapse density contributions for ipsilateral and contralateral CA3 - CA1 projections from each hemisphere in NENR and ENR. L/L (empty bars) = ipsilateral projections from left CA3, L/R (striped bars) = contralateral projections from left CA3, R/R (filled bars) = ipsilateral projections from right CA3, R/L (chequered bars) = contralateral projections from right CA3. Left injected NENR (L/L and L/R) n = 6, right injected NENR (R/R and R/L) n = 6, left injected ENR (L/L and L/R) n = 7, right injected ENR (R/R and R/L) n = 7. For upper chart, Wilcoxon matched-pairs signed rank test used for statistical analysis, with * for $p < 0.05$. Lower chart shows the percentage change following enrichment. This was calculated by taking the average values for the different projections in enriched animals and comparing them to the corresponding values from non-enriched animals. Mann Whitney test was used for statistical analysis with ** for $p < 0.01$

To determine the exact contribution to synaptic density values in each hemisphere, I used the algebra formulas laid out in figure 43. Because I used unilateral injections to determine the ratio of ipsilateral and contralateral projections from a single CA3 region in a single mouse, I did not know the exact ratio for the non-injected side. Therefore I made the assumption that the non-injected side would behave similarly to the average values I obtained from mice with the alternate hemispheric CA3 injection. As the ratio values I obtained in experiment 7 appear similar to the literature values, I can safely assume that the injection itself doesn't affect the ratio of ipsilateral and contralateral projections, therefore I felt confident in using the average values as a substitute for those from the non-injected hemisphere.

As expected, for both hemispheres, I calculated there to be around 1 synapse per μm^3 which originated from the ipsilateral-, and around 0.6 synapses per μm^3 from the contralateral hemisphere in non-enriched mice (figure 45). These values conform nicely with values obtained previously (Wu 2005). In the enriched mice, I found similar values, to those from non-enriched mice, in the projections from the right hemisphere. However, although I couldn't find any difference in the ipsilateral projections to the right-CA1 s.r (right to right), there appeared to be a significant increase in the contralateral projections (left to right). When I compared the values between enriched and non-enriched mice, I calculated that enrichment was responsible for a 30% increase in synapses formed from left-CA3-originating contralateral projections (bottom chart figure 45). Both the ipsilateral (left to left) and contralateral projections (left to right) to the left CA1 s.r. appeared significant, however the reduction in the ipsilateral contributions to the CA1 s.r. heavily outweighed the increase from the contralateral projections. It appears that the left CA3 is entirely responsible for the witnessed experience-driven changes in synaptic density detected in the both hemispheres.

Experience-driven changes to the morphology of synapses originating from each CA3 region

2:10

The finding that the left CA3 might be entirely responsible for synaptic density changes following environmental enrichment, led me to again question if any changes to synaptic morphology were occurring. Previously, in experiment 3, I had determined that experience-

driven laterality changes would be combined with changes to the size of the PSD area, as well as the percentage of synapses with a perforated PSD, in the right-CA1 s.r.. These values, however, did not take into account from which hemisphere the synapses originated. I therefore decided that it would be important to investigate this specifically, using viral injections (similar to those I performed in experiments 7 and 8), then measuring only labelled terminals.

As it appeared that the left-CA3 was entirely responsible for the changes we detected in the right-CA1 s.r., I believed it likely that the decrease in PSD area and perforation, previously detected in the right-hemisphere, would be evident in only labelled terminals from left-hemispheric injections.

Methods and results

Methods used: Unilateral injections into the CA3 (method 1), transcardial perfusion (method 2), pre-embedding labelling of mouse brain for analysis under TEM (method 7), dissector analysis (method 4).

Mice were housed in groups of 5 in enriched mouse cages (figure 28) for 6 weeks (see timelines next ENR). Cages were changed once a week, and food and water were supplied ad libitum.

3 week old C57bl/6J mice were used in this experiment.

Using unilateral CA3 injections and measuring only labelled terminals (figure 5), I was able to selectively measure the PSD area from the CA3 in each hemisphere (figure 6). Although I did not measure the synapse density, I used the dissector method instead to ensure an unbiased detection of labelled terminals. This meant that I would image a sequential series and only measure the length of newly appearing synapses. This helped to minimize size bias, as otherwise larger synapses were more likely to appear in images (as smaller synapses would be present in fewer serial images). I also ensured to only measure intact PSDs, as if the PSD was still visible in the first, or last, image of the series, I could not be sure that my measurements were complete for that synapse.

Measurements of TEM images were conducted using the Reconstruct software (Fiala 2005)

Figure 46

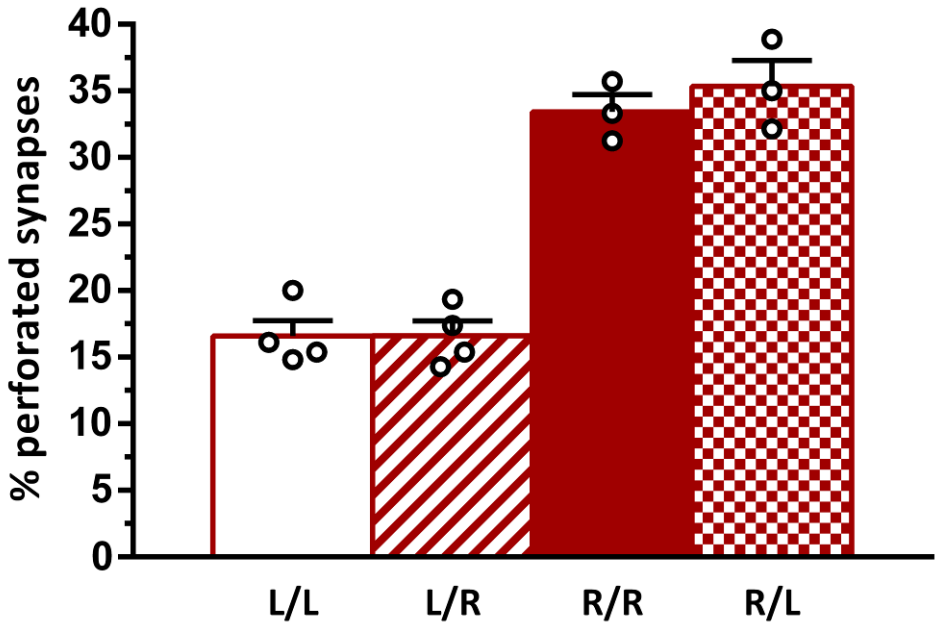

Effect of environmental enrichment on synapse perforation from ipsilateral and contralateral CA3-CA1 projections

Average percentage of labelled terminals in the CA1 s.r. with perforated PSD areas, from unilaterally CA3 injected C57bl6J mice. Only synapses where the total PSD area could be visualised were measured. Error bars display SEM and empty circles show average values for individual mice. Left injection (L/L + L/R) n = 4, right injection (R/R + R/L) n = 3. Students T-test used for statistical analysis with no significance noted.

Figure 47

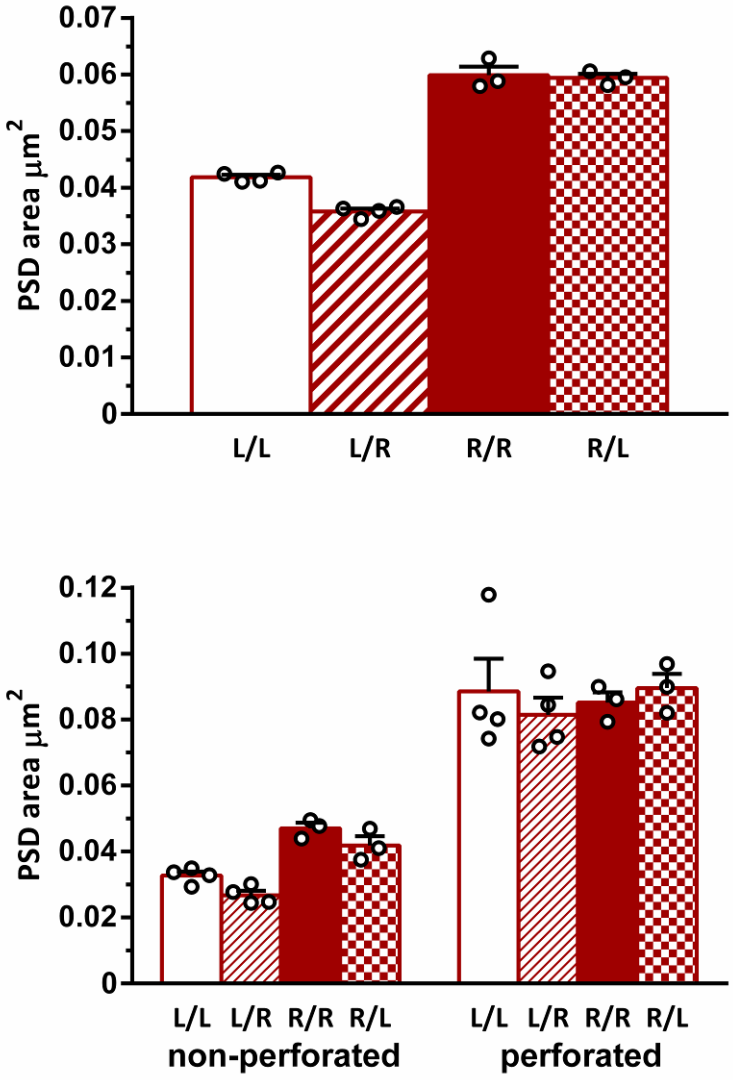

Effect of environmental enrichment on PSD area size from ipsilateral and contralateral CA3-CA1 projections

Upper chart shows average PSD area from labelled terminals in the CA1 s.r. from unilaterally injected enriched C57bl6J mice. Lower chart shows average PSD area from perforated (non-perf.) and perforated (perf.) synapses. Upper chart is made from the data contained in the lower chart. Only synapses where the total PSD area could be visualised were measured. For all charts, error bars display SEM and empty circles show average values for individual mice. Left injection (L/L + L/R) n = 4, right injection (R/R + R/L) n = 3. Both Wilcoxon matched-pairs signed rank and Mann Whitney tests used for statistical anaylsis, with no significance detectable. If normality assumed, Students T-test shows a $p < 0.05$ for non-perforated L/L vs L/R, as well as for L/R vs R/L, and $p < 0.01$ for non-perforated L/L vs R/R.

Following 6 weeks of environmental enrichment, as long as I assumed normality, it was possible to isolate a significant difference between the PSD areas of ipsilateral and contralateral projections from the left-CA3 (figure 47). However, there appeared to be no difference in synaptic perforation between left-originating projections after environmental enrichment (figure 46). When I divided the synapses into either those which had perforated, or non-perforated, PSDs, I can identify a significant difference in the PSD area measurements between non-perforated synapses originating from ipsilateral and contralateral projections only from the left CA3. There was no significance in the PSD area measurements from perforated synapses. Suggesting that the newly appearing synapses in the right CA1, from the left CA3, tend to be smaller than the ipsilateral projections from the same CA3. The values I obtained for synaptic perforation, for all projections, as well as for PSD area, from ipsilateral-left and all right projections, correlate nicely with the previous literature values (Shinohara 2008, Shinohara 2009). These results further highlight the importance of the left-CA3 for inducing experience-driven alterations to the right-CA1 s.r., increasing the density and decreasing the PSD area for left-originating projections, though they do not speak for the behavioural significance of these modifications.

Testing C57bl/6J mice for behavioural performance on the novel object location task

2:11

To investigate whether my enrichment protocol could induce any behavioural changes in wild-type mice, I decided to test mice that had undergone my particular environmental enrichment conditions on the novel object location task (NOL) task. This is a hippocampal dependent memory behavioural paradigm (Ennaceur 1997). However, before I performed the NOL paradigm on enriched mice, it was important to confirm that non-enriched mice would perform the task as expected. If this turned out not to be the case, I would have to examine whether it was down to some environmental disturbance in their housing, some issue with the behaviour room, or possibly, an observer-induced effect upon the mice.

Methods and results

Methods used: Novel object location task (method 8).

Mice were housed in groups of 5 in non-enriched mouse cages (figure 28) for 6 weeks (see timeline next to NENR). Cages were changed once a week, and food and water were supplied ad libitum.

3 week old C57bl/6J mice were used in this experiment.

Cages were kept in a environmentally controlled cabinet with a 12 hour shift in the light-dark cycle. Mice are nocturnal animals, so shifting the light-dark cycle by 12 hours means that their 'day' time equates to our 'night' time. This is a commonly used procedure in behavioural experimentations, enabling a researcher to investigate the behaviour of animals, without their internal clocks having an effect on the performance during testing, training, or habituation.

Mice were moved into a room adjoined to the experimental behavioural room at 8 am (1 hour after the cabinet light turned off), then were left alone for 1 hour, before any experimentations were conducted. This room was illuminated only via red light, so as not to disturb the animals.

Figure 48

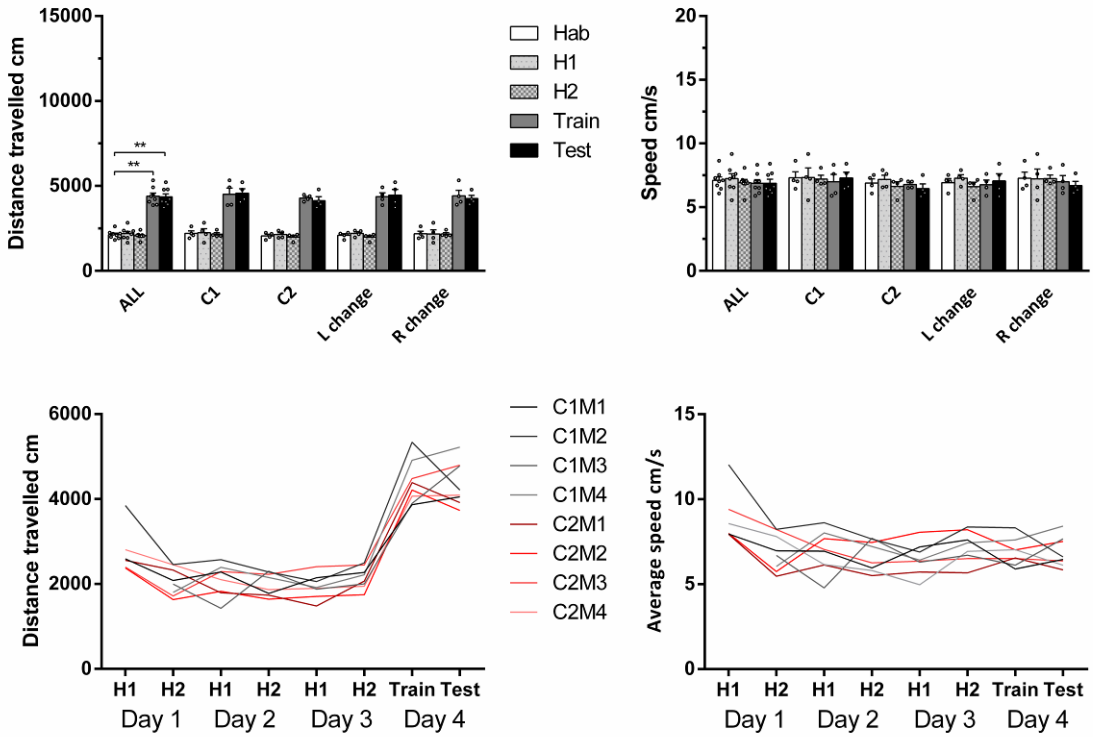

Locomotive activity of NENR mice during NOL

Top charts show the average distance travelled (top left) and average speed (top right) during the habituation (Hab, H1 and H2), as well as the training and testing, phases of the novel object location task (NOL) paradigm. Bottom charts show the total distance travelled (bottom left) and the average speed (bottom right) for individual mice. C# denotes the cage of the individual, M# denotes the individual's identification number. H1 denotes the first habituation phase of the day, H2 denotes the second habituation phase of the day. C1 and C2 show 2 different ENR cages. L/R change denotes whether the left or the right object was moved during the testing phase. Wilcoxon matched-pairs signed rank test used for statistical analysis with ** denoting p value < 0.01.

Figure 49

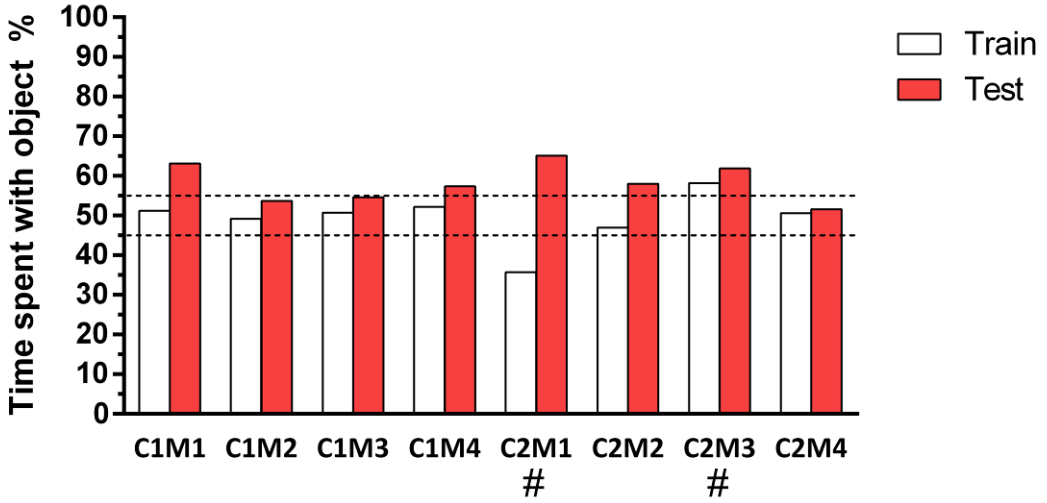

Time spent with moved object during training and testing phases for NENR mice

Chart of percentage time spent with the moved object, for individual NENR mice. Empty bar denotes training phase, filled bar denotes testing phase. Dotted lines show 45% and 55%. # denotes mice who showed preference for one object during the training phase, those whose % time with object was outside of the dotted region. These mice were excluded from analysis. C# denotes the cage of the individual, M# denotes the individual's identification number

Figure 50

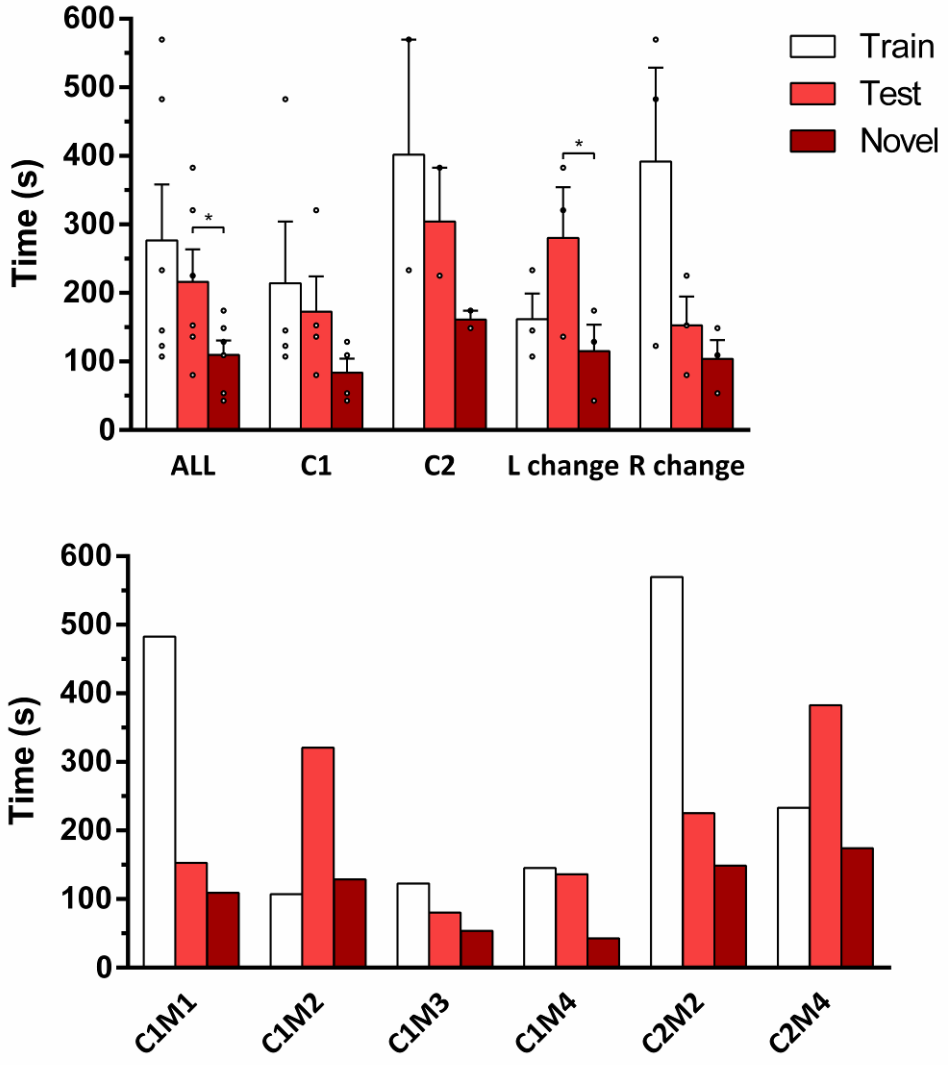

Time to complete the training and testing phases for NENR mice

Top chart shows the average data for NENR mice to complete the training and testing phases, as well as to explore the moved object (Novel) for 10 seconds. ALL is an average from all mice, C# denotes an average from cage #. L/R change denotes an average from mice where the left/right object was moved. Error bars show SEM. Circles show individual values. Lower chart shows the data for individual mice. C# denotes the cage the individual was from, M# denotes the individual's identification number. Wilcoxon matched-pairs signed rank test used for statistical analysis with * denoting p value < 0.05.

Figure 51

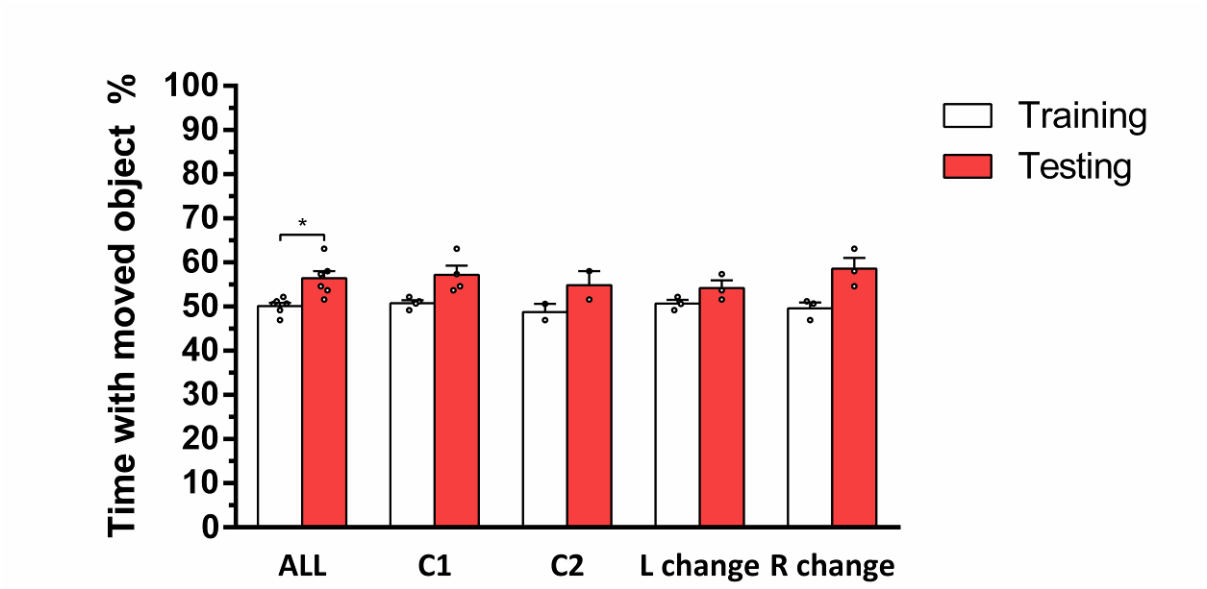

% time spent with the moved object for NENR mice

Chart of the percentage of time NENR mice spent with the moved object, in reference to time spent with both objects. ALL is an average from all mice, C# denotes an average from cage #. L/R change denotes an average from mice where the left/right object was moved. Error bars show SEM. Circles show individual values. Lower chart shows the data for individual mice. C# denotes the cage the individual was from, M# denotes the individual's identification number. Wilcoxon matched-pairs signed rank test used for statistical analysis with * denoting p value < 0.05

When performing any behavioural task, it is important to ensure that there are no extraneous variables which could affect the outcome of the experiment. One of the most common causes for misleading results is mouse health. Although I checked the condition of my mice through visual inspection, I also investigated the speed and distance-travelled for the mice throughout the whole behavioural paradigm (figure 48), as animals that are overly-stressed will often display changes in their locomotor activity (García-Díaz 2007, Tzanoulinou 2014). None of the mice investigated appeared to show any outwards signs of stress (freezing, jumping, excess grooming) during any of the habituation, training, or testing, phases. I could also detect no differences between mice from different cages (groups C1 and C2 figure 48).

The novel object location task is a behavioural paradigm which uses a rodent's natural curiosity for novelty as a tool to investigate their memory formation and retrieval (Vogel-Ciernia 2015). Following 6 habituation sessions (2 per day), mice were allowed to freely explore two identical objects (training phase). During this phase, I measured the time the animals spent with both objects. As the objects are identical, it is expected that the mice should show no preference for either object. Therefore, I placed an arbitrary limit of +/- 5% for each object. This means that, should an animal show a preference for one object (spending more than 55% of its time with that object, when compared with the other object), I would exclude the animal from all future experiments. With this restriction, I had to remove two mice from my experiment (denoted by # in figure 49) during the training phase. Once the mice had either explored both objects for 10 seconds (each), or spent over 10 minutes within the training chamber, the mice were returned to their home cage. Animal excrement was removed and the whole chamber was cleaned with ethanol, to remove any scent cues. Following this, one of the objects was moved (see method 8) and the mouse was immediately returned to the chamber, for the testing phase.

When I recorded the time it took for the mice to explore both objects, during the testing phase, I found that it would take mice a greater time to spend over the required (by the paradigm) 10 seconds with the non-moved object, than the moved one ('Novel' figure 50). The mice tended to immediately go to investigate the moved object, before going back to the one which had remained where it was from the previous training phase. This was shown when I compared the percentage of time the mice spent with both objects, with them spending significantly longer with the moved object (figure 51). This shows that mice were

performing the task as expected. I could not detect any significant difference in object preference between mice tested when the left or right object was moved. There was also no significance detectable in object preference when comparing both cages.

The effect of environmental enrichment on mouse behaviour during the NOL paradigm

2:12

Environmental enrichment has been well documented to improve the performance of animals undergoing numerous behavioural tests (Aujnarain 2018, Bhagya 2017, Nilsson 1999, Pang 2013, Simpson 2011, Yamaguchi 2017). However, in the majority of studies, environmental enrichment is used as a tool to improve performance in elderly or sick, rather than healthy and young, animals. Having already noticed subjective changes in the behaviour of my ENR animals, such as their decreased fear of me when I change their cages, I predicted that it should be possible to detect some behavioural changes via more objective analysis. From the previous results obtained from experiment 10, showing that non-enriched mice appear to adequately perform the novel object location task, I determined that I could now investigate the behavioural consequences of my environmental enrichment paradigm.

Methods and results

Methods used: Novel object location task (method 8).

Mice were housed in groups of 5 in enriched mouse cages (figure 28) for 6 weeks (see timeline next to ENR). Cages were changed once a week, and food and water were supplied ad libitum.

3 week old C57bl/6J mice were used in this experiment.

Cages were kept in a environmentally controlled cabinet with a 12 hour shift in the light-dark cycle. Mice are nocturnal animals, so shifting the light-dark cycle by 12 hours means that their 'day' time equates to our 'night' time. This is a commonly used procedure in behavioural experimentations, enabling a researcher to investigate the behaviour of animals, without their internal clocks having an effect on the performance during testing, training, or habituation.

Mice were moved into a room adjoined to the experimental behavioural room at 8 am (1 hour after the cabinet light turned off), then were left alone for 1 hour, before any experimentations were conducted. This room was illuminated only via red light, so as not to disturb the animals.

Figure 52

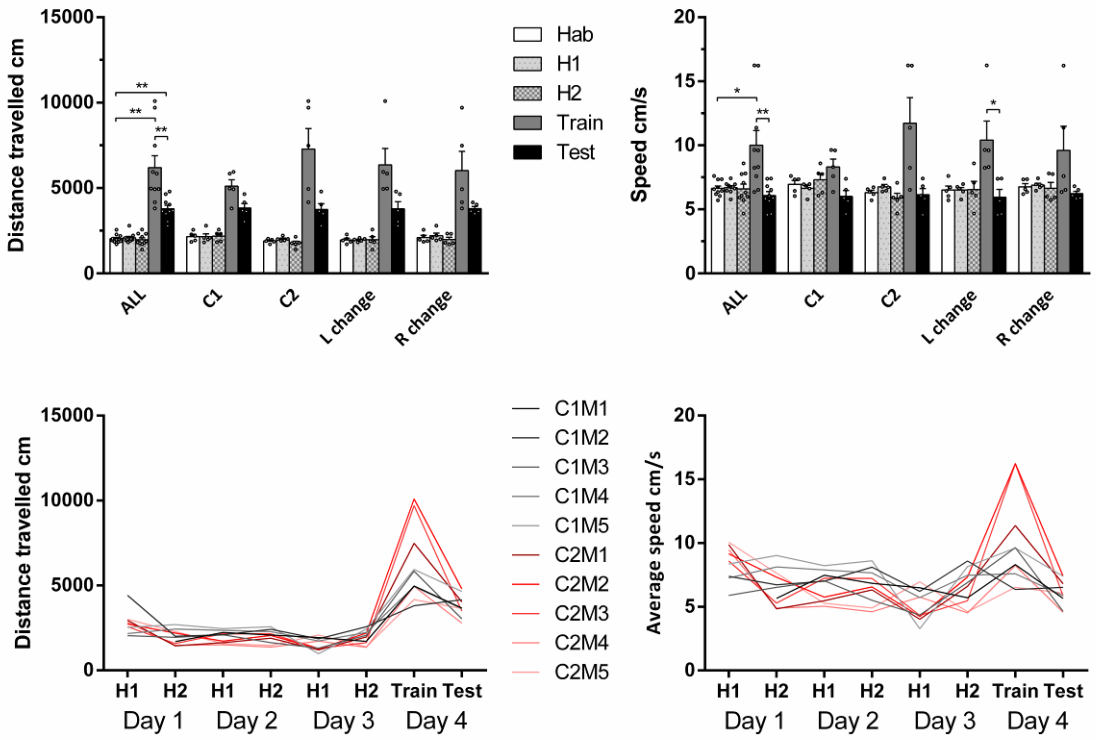

Locomotive activity of ENR mice during NOL

Top charts show the average distance travelled (top left) and average speed (top right) during the habituation (Hab, H1 and H2), as well as the training and testing, phases of the novel object location task (NOL) paradigm. Bottom charts show the total distance travelled (bottom left) and the average speed (bottom right) for individual mice. C# denotes the cage of the individual, M# denotes the individual's identification number. H1 denotes the first habituation phase of the day, H2 denotes the second habituation phase of the day. C1 and C2 show 2 different ENR cages. L/R change denotes whether the left or the right object was moved during the testing phase. Wilcoxon matched-pairs signed rank test used for statistical analysis with * denoting $p < 0.05$ and ** denoting p value < 0.01.

Figure 53

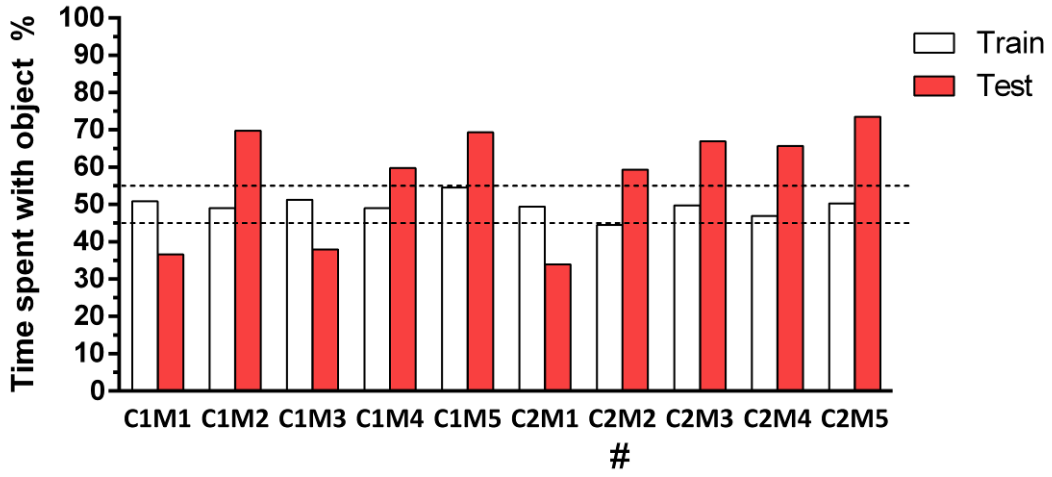

Time spent with moved object during training and testing phases for ENR mice

Chart of percentage time spent with the moved object, for individual ENR mice. Empty bar denotes training phase, filled bar denotes testing phase. Dotted lines show 45% and 55%. # denotes mice who showed preference for one object during the training phase, those whose % time with object was outside of the dotted region. These mice were excluded from analysis. C# denotes the cage of the individual, M# denotes the individual's identification number

Figure 54

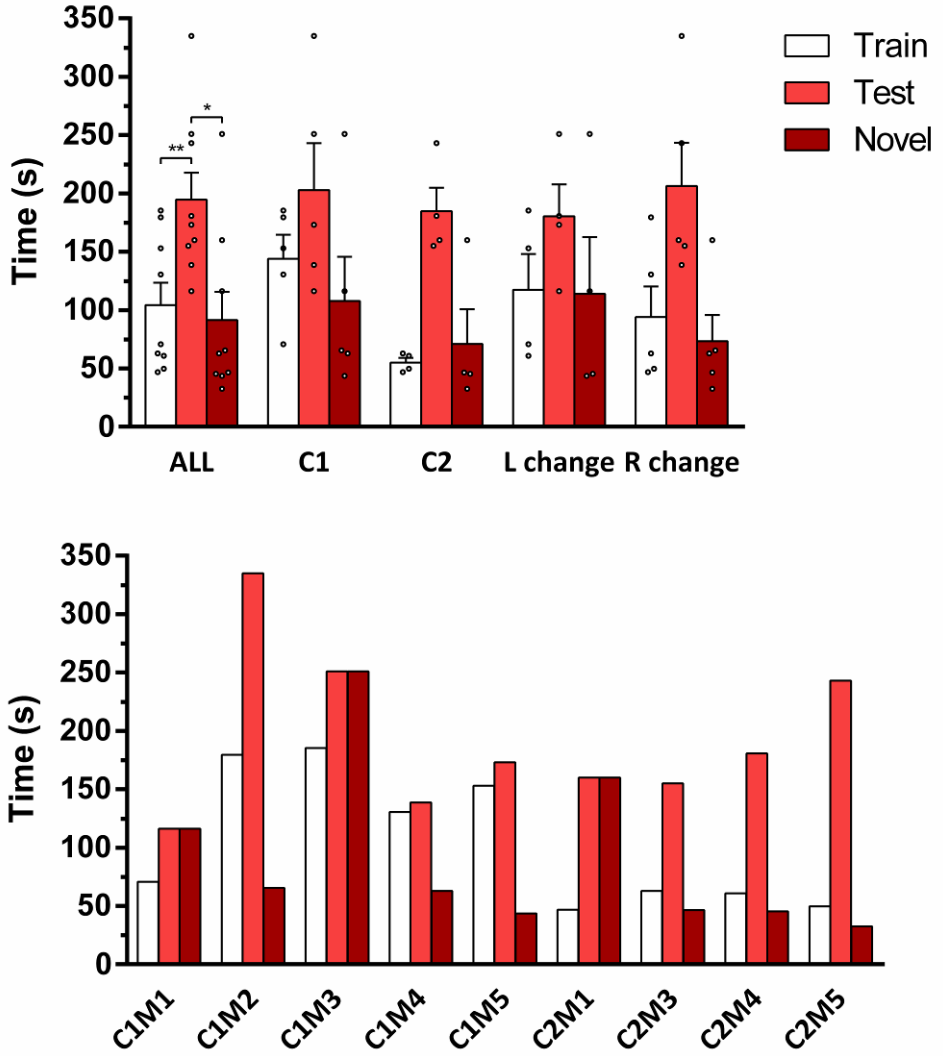

Time to complete the training and testing phases for ENR mice

Top chart shows the average data for ENR mice to complete the training and testing phases, as well as to explore the moved object (Novel) for 10 seconds. ALL is an average from all mice, C# denotes an average from cage #. L/R change denotes an average from mice where the left/right object was moved. Error bars show SEM. Circles show individual values. Lower chart shows the data for individual mice. C# denotes the cage the individual was from, M# denotes the individual's identification number. Wilcoxon matched-pairs signed rank test used for statistical analysis with * denoting p value < 0.05 and ** denoting p value < 0.01

Figure 55

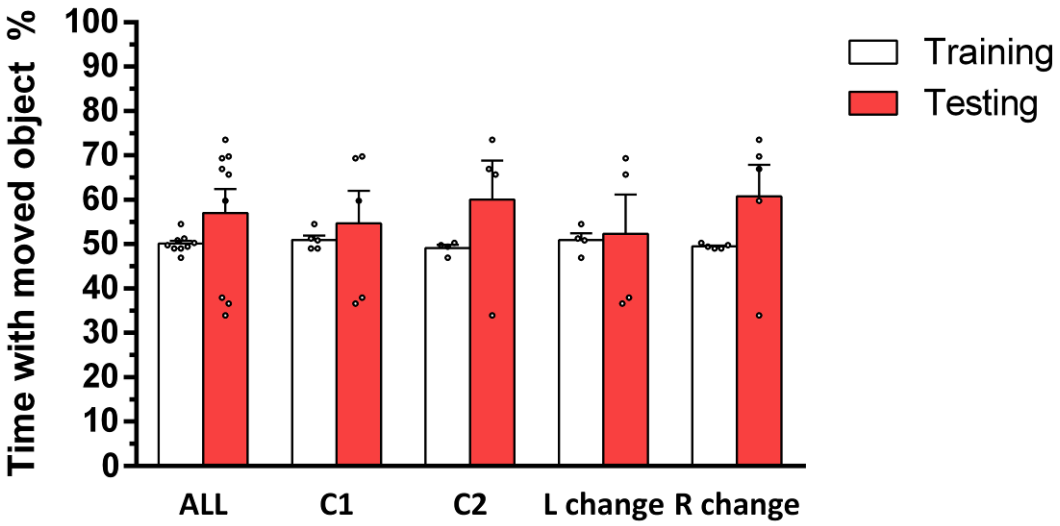

% time spent with the moved object for ENR mice

Chart of the percentage of time ENR mice spent with the moved object, in reference to time spent with both objects. ALL is an average from all mice, C# denotes an average from cage #. L/R change denotes an average from mice where the left/right object was moved. Error bars show SEM. Circles show individual values. Lower chart shows the data for individual mice. C# denotes the cage the individual was from, M# denotes the individual's identification number. Students T-test used for statistical analysis with no significance detectable

Like with the non-enriched animals, I investigated the speed and distance-travelled for the mice throughout the whole behavioural paradigm (figure 52) and was not able to detect any significant locomotive deficits amongst any of the individuals from either cage. I did notice that two of the mice from cage 2 (mice C2M2 and C2M3) covered more distance, at a faster average speed, than any of the non-enriched mice. Although C2M2 was later removed from the experiment, it was not due to any locomotive deficits, but rather due to the mouse showing object preference in the training phase (figure 53). Contrary to expectations, enriched mice didn't always show preference for the moved object, during the testing phase (figure 53). This is seen in the time it took for the mice to complete each phase (figure 54), with three mice completing their required 10 seconds of exploration with the non-moved object long before they did for the moved one. There appeared to be a significant difference between both enrichment cages, in the time it took for them to complete the training phase. This could be due to the order in which I trained the mice, completing all mice from cage 1 first, before testing those in cage 2, but is more likely an artefact of the low individual numbers used in this experiment. When I examined the percentage of time they explored the moved object, I found no significant difference between the training and testing phases (figure 55). This was due to some mice showing preference for the non-moved object rather than the moved one, as I had previously expected them to do.

Taking into account preference for non-moved objects during the NOL paradigm

2:13

Contrary to what I had previously expected, mice which had undergone environmental enrichment, using my enrichment paradigm, did not always show preference for the moved object, during examination under the novel object location task. I had noticed from the video footage that these mice would often explore the non-moved object then would take a quick trip to either the moved object, or the place where it had previously been, before returning to the non-moved object again. Therefore I decided to recalculate my results using a discrimination index, with 0.5 being equal time with both objects and 1 being the mouse spending all its time with one object (and not exploring the other object at all).

Figure 56

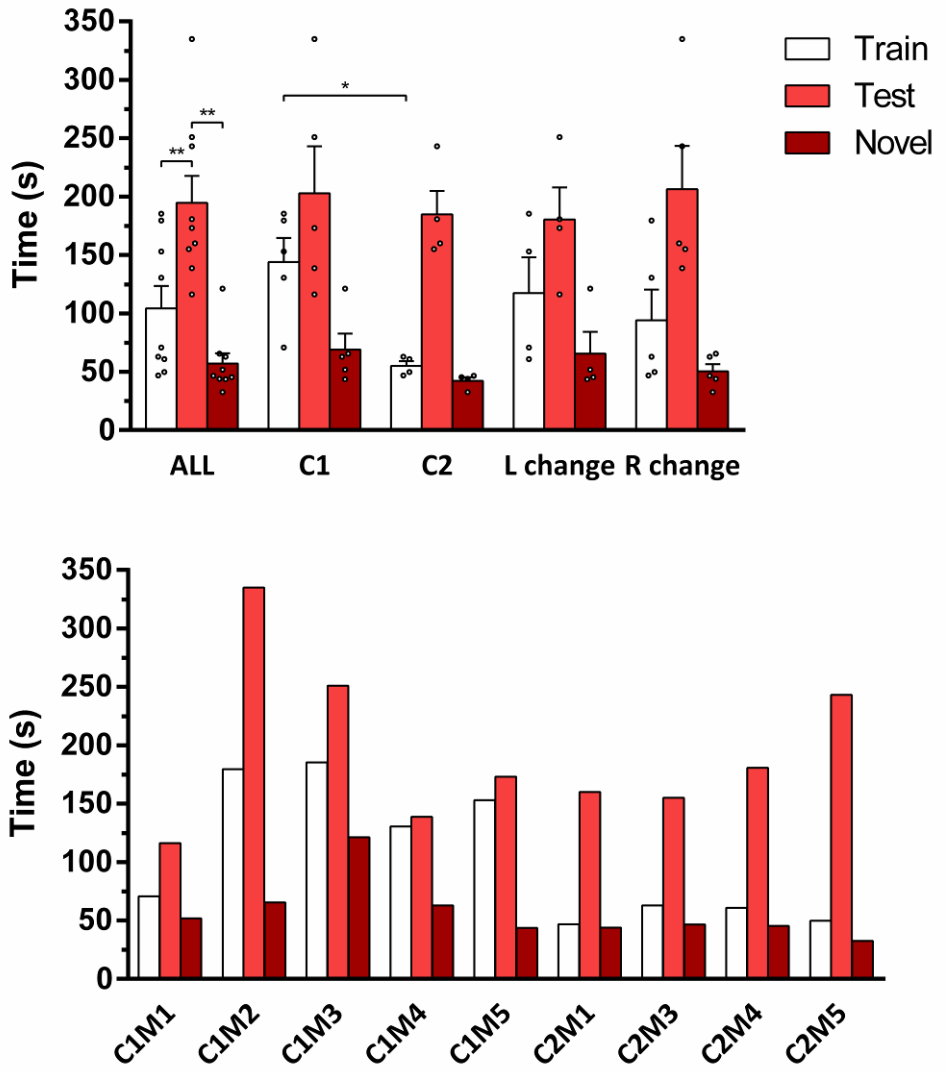

Time to complete the training and testing phases for ENR mice (2)

Top chart shows the average data for ENR mice to complete the training and testing phases, as well as for the first object explored for 10 seconds (Novel). ALL is an average from all mice, C# denotes an average from cage #. L/R change denotes an average from mice where the left/right object was moved. Error bars show SEM. Circles show individual values. Lower chart shows the data for individual mice. C# denotes the cage the individual was from, M# denotes the individual's identification number. Wilcoxon matched-pairs signed rank and Mann Whitney tests used for statistical analysis with * denoting p value < 0.05 and ** denoting p value < 0.01.

Figure 57

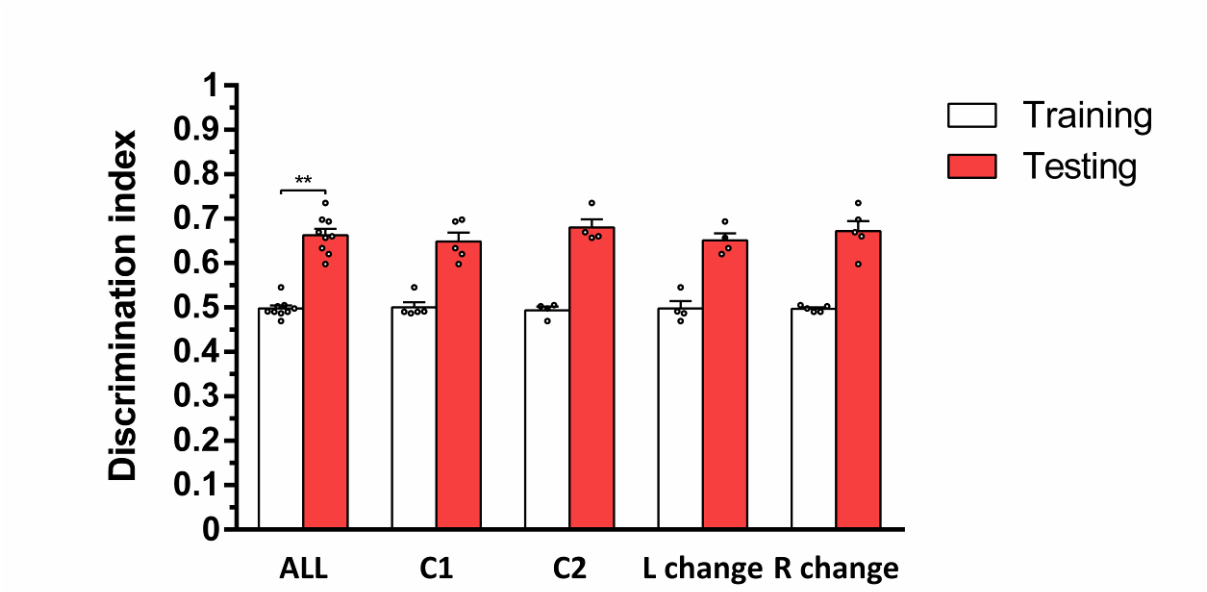

Discrimination index for ENR mice during training and testing phases

Chart of the discrimination index for ENR mice, during the NOL task. Discrimination index is calculated from the time the mouse spent with its preferred object (the object it spent the most time with during the testing phase), divided by the total time the mouse spent with both objects. A value of 0.5 denotes the mouse spent equal time with both objects and a value of 1 denotes that the mouse did not visit one object at all. ALL is an average from all mice, C# denotes an average from cage #. L/R change denotes an average from mice where the left/right object was moved. Error bars show SEM. Circles show individual values. Lower chart shows the data for individual mice. C# denotes the cage the individual was from, M# denotes the individual's identification number. Wilcoxon matched-pairs signed rank test used for statistical analysis with ** denoting a p value < 0.01.

Figure 58

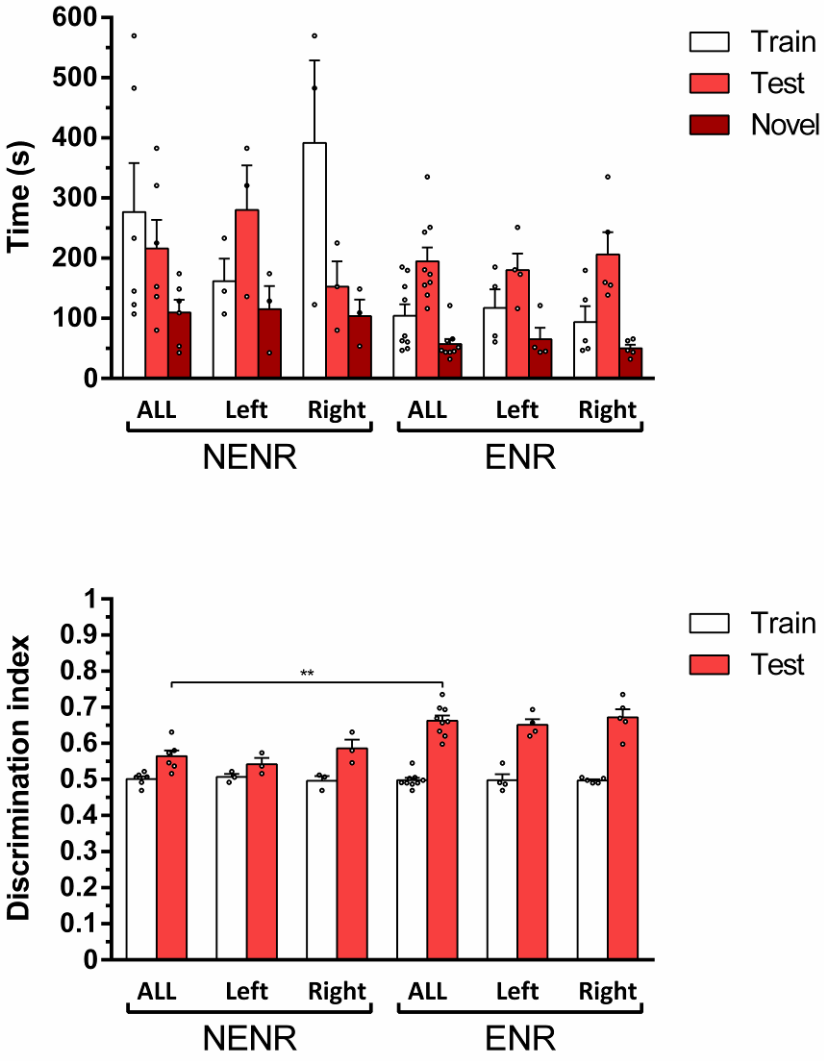

Discrimination index for NENR and ENR mice during NOL paradigm

Upper chart shows the average time taken for mice to complete the training and testing phases, as well as exploring their preferred object (the object they spent the most time with during the testing phase) for 10 seconds (Novel). Lower chart displays the discrimination index for NENR and ENR mice, during the NOL task. Discrimination index is calculated from the time the mouse spent with its preferred object divided by the total time the mouse spent with both objects. A value of 0.5 denotes the mouse spent equal time with both objects and a value of 1 denotes that the mouse did not visit one object at all. ALL is an average from all mice, L/R change denotes an average from mice where the left/right object was moved. Error bars show SEM. Circles show individual values. Mann Whitney test used for statistical analysis with ** denoting a p value < 0.01.

It is possible that the reduced interest in the moved object could be in response to the animals displaying neophobia (Vogel-Ciernia 2015). This is when an organism displays a fear of new or unfamiliar things, such as the moved object, in this particular example. However, not only did all the mice explore the moved object for the required amount of time (10 seconds each object), but they did so in a comparable time to the enriched mice which showed preference for the moved object (figure 54), as well as to the non-enriched mice that didn't display this preference (figure 50). There is conflicting evidence about the effect of enrichment on neophobia in rodents, with some papers suggesting a reduction in neophobia (Holson 1986) and others suggesting a possible increase (Leger 2013). It would therefore be important to investigate this further, to see if this could explain the results I found after enrichment. Unsurprisingly, it has been found that, when given the choice, mice which are more prone to neophobia are less willing to visit enriched environments (Walker 2011).

Allowing for individuals to have specific preference to either object, I could detect a significant difference in the time it took for the enriched mice to explore one object for 10 seconds during the testing phase. I could detect a significant difference in time taken between both enrichment cages (figure 56), but not between moved object side. When I investigated the discrimination index, I could now find a significant difference between the training and testing phases, but not between individual cages or moved object side (figure 57). This was what I had originally expected to see. Finally, when I compare non-enriched and enriched groups, using the discrimination index as a measure for object preference, I can detect a significant increase in performance for enriched individuals (figure 58), with enrichment improving the ability of a mouse to discriminate between two objects by around 17.5%.

Unfortunately, although I could detect a potential improvement in hippocampal working memory, caused via my environmental enrichment paradigm, I can not currently directly link this back to the morphological changes I have previously described. Further experiments are obviously required to overcome this deficit.

Chapter 2 experimental flowchart

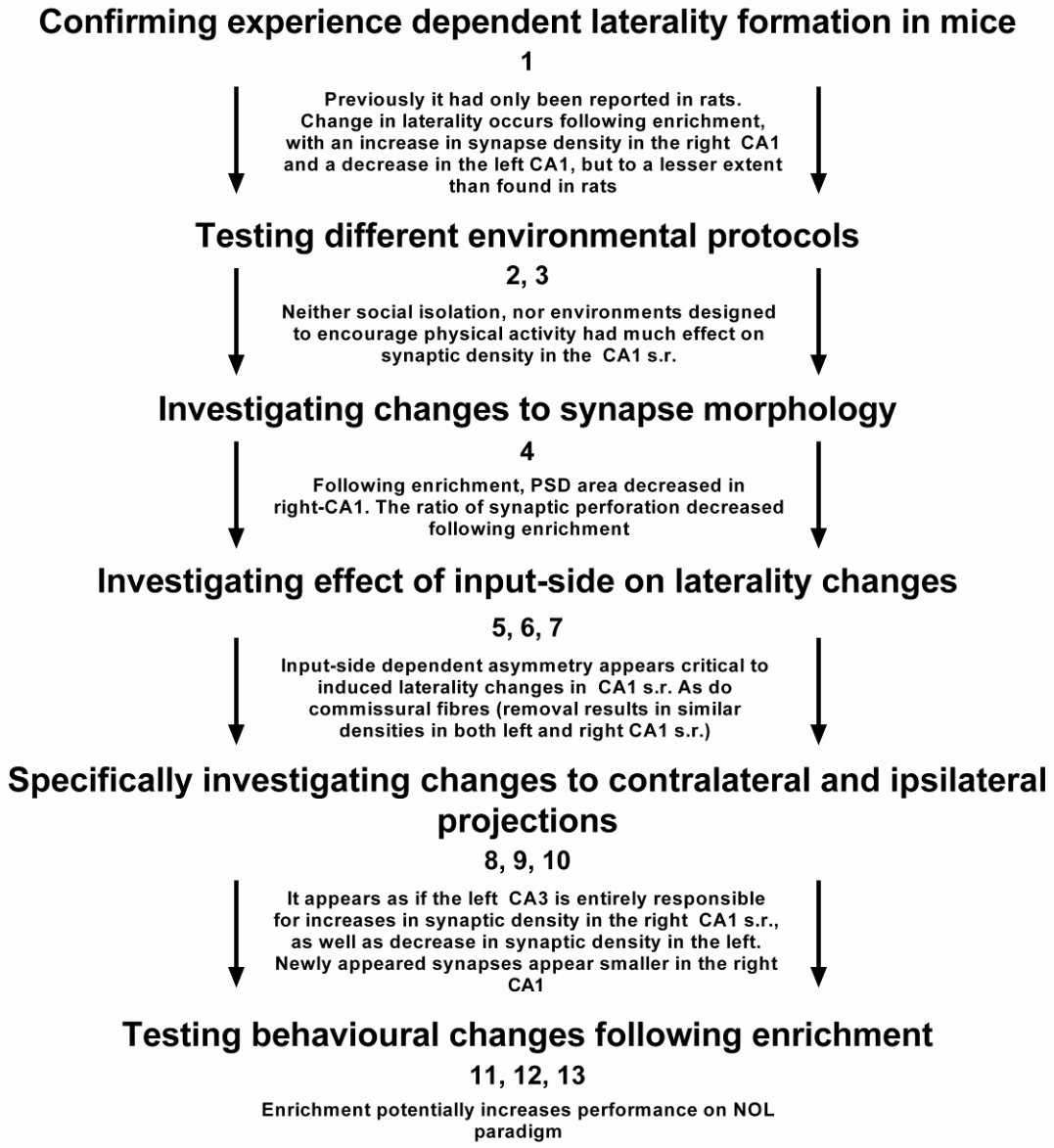

Chapter Summary

This chapter dealt with how using only the environmental enrichment paradigm, it was possible to induce changes in the CA1 stratum radiatum of mice. Like in the rat, I found a highly-reproducible experience driven change in CA1 pyramidal cell synapses, resulting in the synaptic density of the right CA1 being 19.12% higher than the left following environmental enrichment. This is far lower than the almost 100% difference detected by Shinohara et al. (Shinohara 2013) and could suggest that either the enrichment paradigm wasn't long or intense enough for the mice, or it could indicate a more fundamental difference between how rats and mice respond to environmental enrichment. It has been noted that, mice have far worse visual acuity than rats and rely more strongly on olfactory cues than visual ones in behavioural paradigms and that they tend to form place-cell maps based more on olfactory than visual cues (Hok 2016). Therefore, it is possible that an enriched environment based more on olfactory, rather than physical exercise, stimulation might have a greater influence on the mice than the current environmental protocol. Interestingly, I could also detect a significant decrease in the synapse density of the left CA1 following enrichment, a 5.19% decrease in the density of synapses from non-enriched mice. This decrease was unreported in the previous experiments with rats, its importance has yet to be determined and it is certainly worthy of further investigation.

In the mammalian brain, there is a high degree of interplay between both hemispheres, facilitated through the numerous commissural fibres connecting both sides. By selectively labelling CA3-CA1 projections in non-enriched mice, using unilateral injections of an adeno associated virus, I discovered that around 30% of the connections in the stratum radiatum originated from the contralateral side. This result is in agreement with other reports from rodents (Shinohara 2012a, Shinohara 2012b, Wu 2005), and speaks to the validity of my measurement protocol. Destroying the commissural fibres after enrichment through VHCT operation removed the asymmetry we found in non-VHCT animals, suggesting that the increase in density relied heavily on these connections. This is highly interesting as it has previously been shown that the commissural fibres themselves can mask asymmetries in hippocampal dominance during spatial learning paradigms, with the right-hemispheric dominance only becoming evident through the destruction of the commissural fibres (Corballis 2002, Shinohara 2012b). However, the asymmetry described here appears to rely on a completely unrelated mechanism, as it is only in the presence of the connections, rather than their absence, where this phenotype can be examined. This result highlights yet another

asymmetry in the hippocampus, to add to the ever growing list within this region. Judging from the ratios of ipsilateral and contralateral projections into the CA1, one might expect that the right-side specific increase in experience-driven synapse density would rely heavily on the right CA3, but it appears that this isn't the case. It is known that CA3 and CA1 gamma oscillation synchrony within and between hemispheres is associated with accurate reactivation of stored hippocampal memories (Carr 2012). Therefore, our results could highlight the importance of interhemispheric coordination experience-driven memory formation.

It is evident that the commissural fibres are important for modulating the synaptic densities in the CA1 s.r.. Although other regions in the hippocampus may have inputs from numerous different parts of the brain, the vast majority of inputs onto CA1 pyramidal cells in the CA1 s.r. originate from the CA3 (Shinohara 2012a). One of the most interesting features of CA3 – CA1 projections is the mechanism of input-side dependent asymmetry. This process describes an asymmetry based upon input-origin, rather than termination-site. It explains that, in the CA1 s.r., inputs from the left CA3 tend to be smaller, more prone to LTP, with a higher NR2B-receptor density, than those form the right (Wu 2005). When I examined the effect of enrichment on *iv* mice, which lack input-side dependent asymmetry (Kawakami 2008), no effect of enrichment on synapse density modulation could be detected. This meant that synaptic densities in both the non-enriched and enriched groups were similar, with neither differing from the densities recorded in the non-enriched wild-type. This highlights the potential importance of input-side dependent asymmetry in the experience dependent laterality of the brain, suggesting that its role extends past the previously reported effect on working memory formation (Goto 2010, Goto 2017). As the majority of the projections from the CA3 region appear to pass ipsilaterally, it is safe to assume that any input-side specific asymmetry should preferentially affect the ipsilateral side. Although this would explain the lack of laterality formation seen in the enriched *i.v.* mouse mutant, it fails to account for the absence of asymmetry seen in wild-type mice following VHCT operation. It also fails to explain why no significant difference was seen between the absolute synaptic densities between left- and right-isomerism *i.v.* mutants as, if the hypothesis that input-side solely determines density in the CA1 s.r. is to be believed, the right-isomerism mutant should've had a higher synaptic density than the left-isomerism. These results suggested that some other factor was involved in experience-dependent laterality formation. Through the process of unilateral CA3 tracer injections, I was able to specifically investigate the ipsilateral and

contralateral projections from each CA3 individually. Through this targeted approach, I was able to determine a startling difference between both hemispheres, with projections from the right CA3 remaining relatively unchanged and projections from the left being solely affected through enrichment.

Following enrichment, there was a 30% increase in the number of contralateral projections from the left CA3, causing it to project equally to both hemispheres. These newly appearing contralateral projections terminated in synapses with a PSD area that was around 16% smaller than those terminating in the ipsilateral CA1 (figure 59). As left-originating projections tend to be more plastic than those from the right (Wu 2005), it is possible to suggest that the increase we find is important for the mouse to accurately and continuously reorganize its connections to deal with the ever-changing environment. When I subdivided the PSD measurements into those with a perforated, or non-perforated, area, I was able to detect a significant difference between both hemispheres only in non-perforated synapses. It has previously been reported that enrichment would lead to an increase in non-perforated, but not perforated, synapses in the CA1 of healthy mice (Rampon 2000). As NR2B receptor number doesn't change based upon hemispheric origin of the projecting CA3, with the changes in density only occurring as a result of changes in synaptic area of the terminals (Shinohara 2008), it is possible that the newly appearing synapses in the right CA1 s.r. are even more susceptible to LTP then those from the left CA3 to the left CA1. This could suggest that newly appearing non-perforated synapses in the right CA1 s.r. are kept small so that they are potentially more plastic and able to rapidly change in response to the ever changing environment.

Figure 59

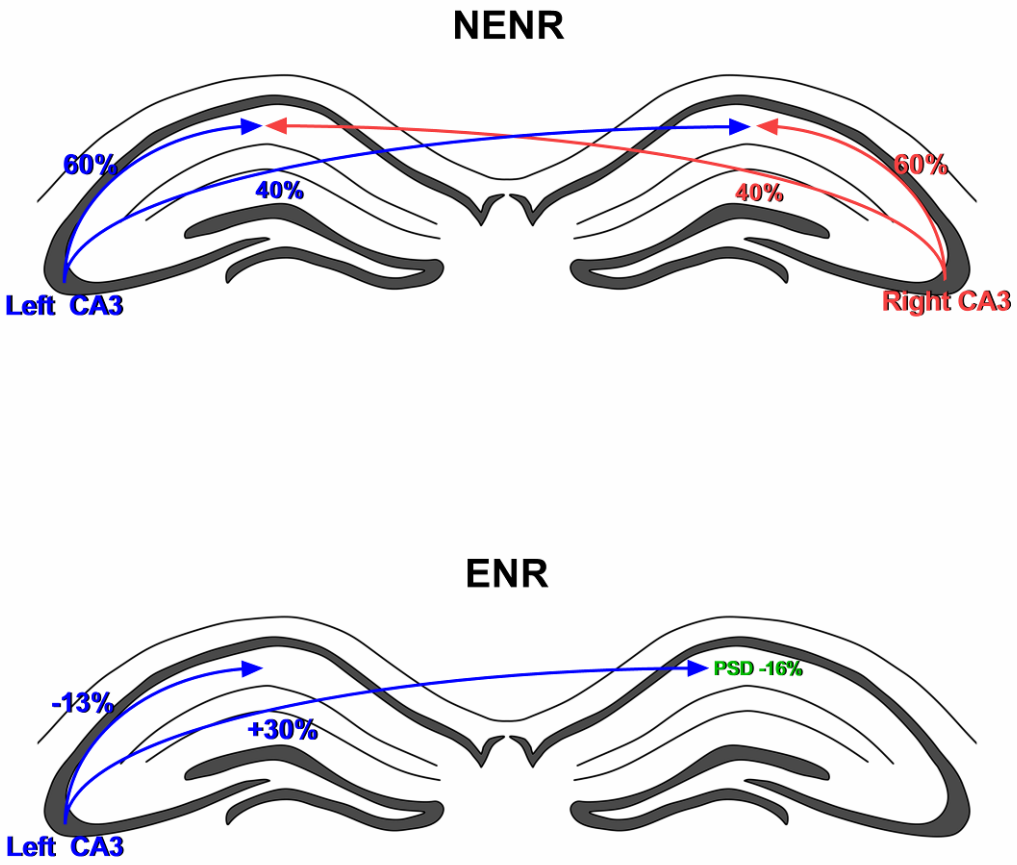

Changes to CA3 - CA1 projections caused by the environmental enrichment paradigm

NENR displays the percentage of projections from the CA3 to the CA1 s.r. in non-enriched mice
ENR displays the percentage change in projections from the left CA3 to the right CA1 s.r. (blue) as well as the change in PSD area of contralateral projections from the left CA3 (green).
In both figures, projections from the left CA3 are in blue and projections from the right CA3 are in red.

In spite of the significant changes detected in left-originating contralateral projections to the right-CA1 s.r., synapses formed via right-originating ipsilateral projections appeared to remain relatively unchanged, both in density and in morphology. There also appeared to be no change in the morphology of synapses forming from left-originating ipsilateral (left to left) projections. These results helps link together the previous reports of the importance of the left CA3 in supporting long-term memory formation (Shipton 2014a) with the well-studied importance of the right hippocampus in spatial memory and learning processes (Belcheva 2007, Klur 2009). Importantly, it may help explain the conflicting reports to do with the relative importance of the left or right hippocampus for memory formation and storage (Corballis 2002, Klur 2009, Maguire 1997, Maguire 2000, Shinohara 2012b, Shipton 2014a). One possible issue with this finding is that it relies heavily on my assumption that the fluorescence ratios between both hemispheres accurately reflect the synaptic densities within the CA1 s.r.. The AAV which I injected expressed VAMP2, a vesicle-associated membrane protein, and therefore should have been actively transported to the terminal. It is possible that a larger synapse might receive more Venus-VAMP2, and therefore fluoresce more strongly. This could bias my results, as it would mean that, although the ratio of 50% ipsilateral and 50% contralateral fluorescence, from the left CA3 in enriched mice, would still be correct, this would not correspond to the left-CA3 projecting equally to both hemispheres. As the PSD area measurements I obtained from left to right projections were smaller than those from left to left projections, it is possible that my results underestimate the number of contralateral projections from the left CA3. Although this wouldn't affect my final conclusions, it could highlight a stronger contralateral contribution from the left than I have assumed. It would also suggest that the number of ipsilateral left-CA3 originating projections might be fewer than I have predicted. One method by which I could attempt to tackle this question would be to perform ultra-thin (sub 40 nm) serial reconstructions of terminals in the CA1 s.r.. Following this, I could investigate whether vesicle number follows a linear relationship with PSD area. If so, I could use the reduced PSD area, which I detected in terminals from left to right projections, to normalize my calculations and, potentially, achieve a more accurate representation of the synaptic contributions of the CA3 in both hemispheres to each CA1 region.

One important aspect which is missing from these results is a satisfactory explanation for the behavioural importance of this phenomenon. Although I did begin to tackle this complicated question, and found some beneficial effects of my enrichment paradigm on

hippocampal working memory processing, the results are far from convincing. Firstly, although my results did show that enriched mice could discriminate between the moved and non-moved objects, in the novel object location task, I could not entirely remove the potential issue of neophobia being responsible for my results, rather than an improvement in hippocampal working memory. Further experiments, with different objects, might be required to tackle this issue. Another potential method to remove the possibility of neophobia could be to use objects from within the enrichment cage of the individuals, rather than completely new objects. The second critical issue is that, even if the enriched mice do have improved working memory function, with the experiments which I have performed so far, it isn't possible to directly link the morphological changes I have described with the behavioural changes, following enrichment. One method by which I could potentially address this issue would be to perform unilateral cre-injections into the CA3 of each hemisphere, in a PirB-floxed mouse mutant. Knockout of PirB has been shown to destroy input-side dependency in CA3 to CA1 projections (Ukai 2017). As I have shown that input-side dependency is critical to experience-driven laterality formation, it is possible that a difference in synaptic density might be generated in enriched mice, depending on the hemispheric site of CA3 injection. This procedure, combined with the novel object location task, could help shed light as to whether a difference in performance could be detectable based upon selective knockout of PirB in either CA3. A greater reduction in performance on the NOL task, combined with a reduction in the synaptic density of the right CA1 s.r., in left-CA3 injected enriched mice could prove to be a useful starting point to tie together the morphological changes with the behavioural consequences following environmental enrichment.

Although these results suggest a greater importance for the left CA3 in experience-dependent laterallity, these findings suggest that the change in density we observe relies on more than just input-side dependent asymmetry, but could also feature a hereto unreported target-cell-specific asymmetry in addition. Although this phenomenon is likely not restricted to the hippocampus, to my knowledge this is some of the first direct evidence of an asymmetry in the hippocampus which relies on both a genetic and environmental stimulus to form; with environmental factors modulating the inputs from the CA3 in an asymmetrical manner

Method 1

Unilateral injections into the CA3

1. Mice were deeply anaesthetized with Ketamine/Xylazine (80-100/10mg/kg BM, i.p.), with Metamizol (200mg/kg) being administered subcutaneously as painkiller

2. Mice were then fixed within a stereotaxic frame.

3. OleoVital was applied to the eyes, to stop drying out during surgery.

4. A small hole was drilled to expose the brain, so that a syringe could be lowered into the brain.
   - Injection coordinates (measuring from the bregma) were either:
     - - 1.82 mm caudally, 1.6 mm vertically, and 2.3 mm laterally, for injections into the right, or -2.3 mm laterally, for injections into the left CA3
     - -1.94 mm caudally, 1.72 mm vertically, and 2.33 mm laterally, for injections into the right, or -2.33 mm laterally, for injections into the left CA3

Although initially 1.82 mm caudally was used, I later switched to 1.94, due to more consistent injections

5. Any/all blood was removed and bleeding was allowed to stop before the experiment proceeded further.

6. A piece of parafilm was placed onto the mouse's head and a drop of water was formed onto the parafilm.
   - This water droplet was withdrawn using a 0.5 µl Hamilton syringe, to check that the glass capillary (attached via a dual RN, glass coupler) wasn't clogged.

7. The water was then ejected and the tracer/virus was taken up into the Hamilton.

8. Immediately afterwards, the capillary was slowly lowered into the brain and 0.2 µl tracer/virus was injected.
   - This was done over 10 minutes (0.02 µl/minute).

9. The apparatus was left for a further 10 minutes before the capillary was slowly retracted.

10. Following this, the skin was sutured back together.
    - To avoid infection, 0.1% gentamicin sulfate cream (Gentacin) was applied topically. Xylocain was used as a local anaesthetic.

11. The mouse was then placed on a heating pad to warm up, before being returned to its home cage.

12. The following day, Metamizol was re-administered subcutaneously.

13. 2 weeks later, the mice were perfused for analysis.

Method 2

Transcardial perfusion

1. Mice were deeply anaesthetized with Ketamine/Xylazine (80-100/10mg/kg BM, i.p.)

2. Once fully anaesthetized (tested via foot/tail pinch, as well as through rolling animal onto its back and testing if it tries to right itself), mice were fixed onto a polystyrene board via syringe needles through the hands and feet.

3. The ribcage was exposed and removed.

4. Following this a 27 gauge needle (connected to a perfusion pump) was inserted into the left ventricle.

5. The right atrium was immediately cut and the perfusion pump is switched on, with a speed of 7.2 ml/minute.

6. The mouse was perfused with PBS until the right atrium was completely clear of blood

7. The PBS was then switched with 4% Paraformaldehyde (PFA) + 0.05% glutaraldehyde solution.

8. Perfusion was continued for 12 minutes before the pump was stopped.

9. The brain was then carefully extracted and stored in ice-cold 0.1M PB solution.

4% PFA + 0.05% glutaraldehyde solution
per 100 ml

PFA – 4g
NaOH – 0.1g
dH2O – 28 ml
0.2M PB – 50 ml
Picric acid – 15 ml
Glutaraldehyde – 200 µl

1. Heat dH20 to approximately 60 °C – this should be done in a fume hood, in a glass beaker, with a magnetic stirrer.

2. Once the water reaches temperature, add the PFA and NaOH and leave until the PFA completely devolves and the solution clears. It is important not to let the temperature exceed 65 °C.

3. When completely clear, remove from the heater and cool to room temperature (on ice).

4. Then add the 0.2M PB and picric acid solutions.

5. Check the pH, and adjust it using HCl to between 7.3-7.4.

6. Filter the solution into another glass beaker and store at 4 °C.

Immediately before perfusing a mouse, add the glutaraldehyde solution.

Transcardial perfusion schematic

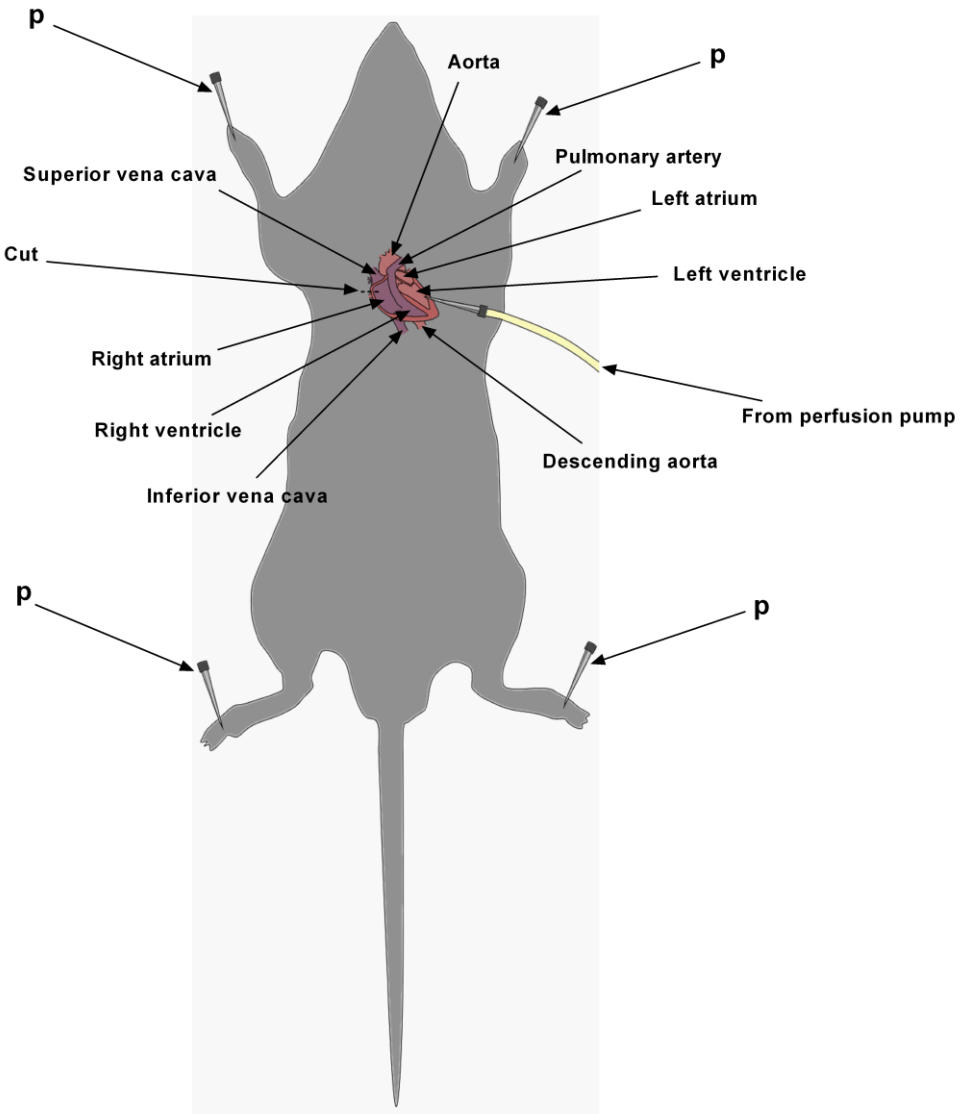

Diagram of transcardial perfusion method

Diagram depicting needle insertion into left ventricle. Dotted line represents cut to right atrium. Needles for pinning mouse to polystyrene board are marked with a 'p'. Left and right body axis reversed as image depicts mouse lying on its back.

Method 3

Preparation of mouse brain for analysis under TEM

1. Perfused brains were trimmed using a razor, so that they could be glued to a vibrotome (Leica VT1000S) stage. 50 µm coronal sections were then cut and transferred to a 0.1M PB solution

2. Slices were washed with:
    1. TBS twice (20 minutes each)
    2. PBS twice (10 minutes each)

3. Slices were then incubated in ABC solution (made 30 minutes beforehand) for 2 hours at room temperature.

4. Slices were washed with:
    1. PBS twice (10 minutes each)
    2. 50mM Tris/HCL buffer (for 10 minutes)

5. Slices were incubated in DAB solution (0.02% solution in 50mM Tris buffer) for 5 minutes, then were visualized using a 0.3% H_2O_2 solution (10 µl per 1 ml).

6. The reaction was stopped, through an excess of 0.1M PB.

7. Slices were washed twice in 0.1M PB (10 minutes each wash).

8. Slices were immersed in 1% OsO_4 (in 0.1M PB solution) for 25 minutes.

9. Slices were washed twice in dH_2O (10 minutes each wash).

10. Slices were immersed in 1% Uranyl Acetate (in dH_2O) for 35 minutes.

11. A gradual ethanol dehydration was performed (10 minutes per wash, series ranging from 50% to 95%), terminating in 2 washes of 100% ethanol (10 minutes per wash). The final wash being done in glass capsules.

12. Slices were immersed in propylene oxide twice (10 minutes each wash).

13. Slices were left overnight in freshly made Durcupan resin (1:1:0.03:0.033 A:B:C:D), to allow slow infiltration of the resin into the tissue.

14. The following day, slices were mounted on siliconised glass slides, with Aclar film as a cover, and polymerised in the oven overnight at 60 °C.

15. The region of interest (the inner 1/3rd of the CA1 s.r.) was then trimmed out and remounted in a Durcupan filled capsule (polymerised overnight at 60 °C).

16. Samples were cut into 70nm serial sections using an ultramicrotone (Leica EM UC7).

Method 4

TEM measuring techniques

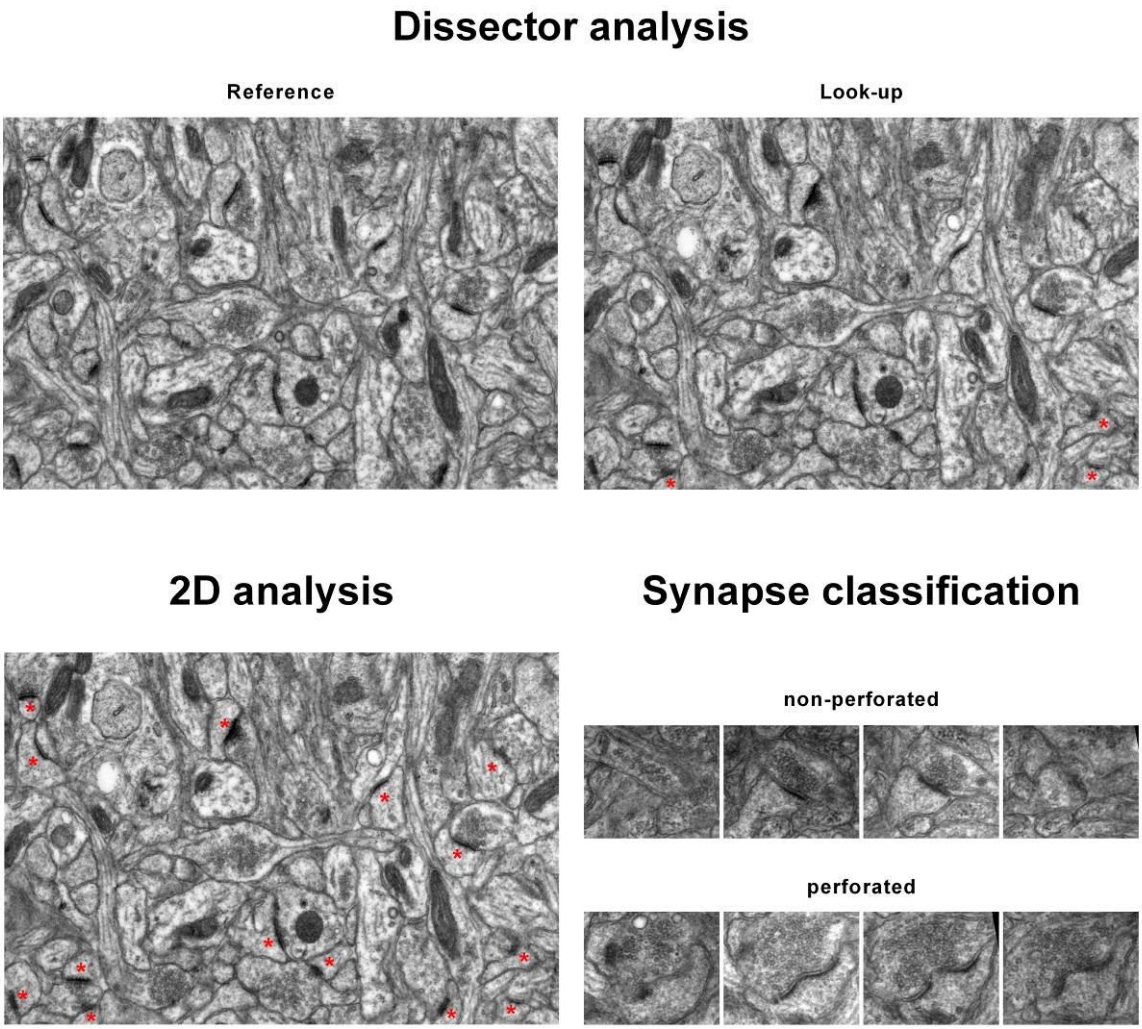

Measuring techniques

Dissector analysis
Left image shows reference image, right image shows look-up image. Only newly appeared synapses (marked with a *) are counted/measured. Density is calculated by dividing the total number of newly appearing synapses by the volumetric area analysed

2D analysis
All synapses are counted (marked with a *). Density is measured by dividing the total number of recorded synapses by the flat-area analysed

Synapse classification
Here are representative images of a non-perforated and a perforated synapse (in series). The non-perforated synapse has a uniform PSD throughout all images, whereas the PSD of the perforated synapse bifurcates then rejoins in latter images

Method 5

PCR and gel electrophoresis examination of interesting mutations

1. DNA concentration was calculated using the NanoDrop Microvolume Spectrophotometer

2. PCR was performed using Phusion High-Fidelity DNA polymerase (Thermo Scientific)

recipe for 50 µl polymerase solution for PCR

- 5x Phusion HF buffer – 10 µl
- Forward primer – 1 µl
- Reverse primer – 1 µl
- 10 mM dNTPs – 1 µl
- DMSO – 1.5 µl
- DNA - ≤ 250 ng concentration in final solution
- Phusion DNA polymerase – 0.5 µl
- H_2O – make up to 50 µl

PCR reaction times and temperatures using Physion High-Fidelity DNA polymerase solution

1. Initial denaturation 98 °C
2. 35 cycles
   - 98 °C (10 seconds)
   - 45-72 °C [depending on primers used] (30 seconds)
   - 72 °C (30 seconds per kb)
3. Final extension 72 °C (10 minutes)
4. Hold 4 °C (indefinitely)

3. PCR product mixed 6:1 with Gel Loading Dye purple (#B70245: New England BioLabs), loaded into a 1% agarose gel, containing 1:10000 SYBR Safe DNA gel stain (Invitrogen), and run at 115 V for 35 minutes

4. Bands of interest are trimmed out, put into sterile 1.5 ml tubes and weighed

5. PCR product purified using the Wizard SV Gel and PCR Clean-Up System (Promega) [protocol available online: https://www.promega.com/-/media/files/resources/protcards/wizard-sv-gel-and-pcr-clean-up-system-quick-protocol.pdf]

6. DNA concentration checked with NanoDrop Microvolume Spectrophotometer

7. DNA sent for sequencing by LGC genomics (https://shop.lgcgenomics.com/)

8. Sequences analysed with the SnapGene software (http://www.snapgene.com/)

Method 6

Ventral hippocampal commissure and corpus callosum transection (VHCCT)
For only ventral hippocampal commissure transection (VHCT) ignore step 11

1. Mice were deeply anaesthetized with Ketamine/Xylazine (80-100/10mg/kg BM, i.p.), with Metamizol (200mg/kg) being administered subcutaneously as painkiller.

2. Mice were then fixed within a stereotaxic frame.

3. OleoVital was applied to the eyes, to stop drying out during surgery.

4. The skull was exposed and a small window (3 mm wide and 4 mm long, including the bregma) was cut using a drill (the removed skull plate is kept on parafilm).

5. Removal of the underlying dura was confirmed. If it remained, it was carefully cut with a 27 gauge needle.

6. Any/all blood was removed and bleeding was allowed to stop before the experiment proceeded further.

7. A piece of razor (2.5mm wide), which had been glued to a rod and attached to a micro-manipulator, was aligned to the midline of the brain above the bregma.

8. The razor was shifted 0.5 mm laterally, lowered 0.5 mm, then returned to the midline. This will push the superior sagittal sinus out of the way, without damaging it.

9. The razor was lowered a further 4 mm into the brain, totally transecting the ventral hippocampal commissure.

10. The razor was left in place for 10 minutes.

11. The razor was raised 2 mm, then moved caudally 0.5 mm to cut the corpus callosum.

12. The razor is slowly retracted from the brain.

13. The piece of skull (previously removed) is then returned to the hole and the skin is sutured back together.

14. To avoid infection, 0.1% gentamicin sulfate cream (Gentacin) was applied topically. Xylocain was used as a local anaesthetic.

15. The mouse was then placed on a heating pad to warm up, before being returned to its home cage.

16. The following day, Metamizol was re-administered subcutaneously.

17. 5 days later, the mice were perfused for analysis.

Timeline for experiment 2:4, confirmation of total transection of the ventral hippocampal commissure, and example for analysing intact projections from individual CA3 regions

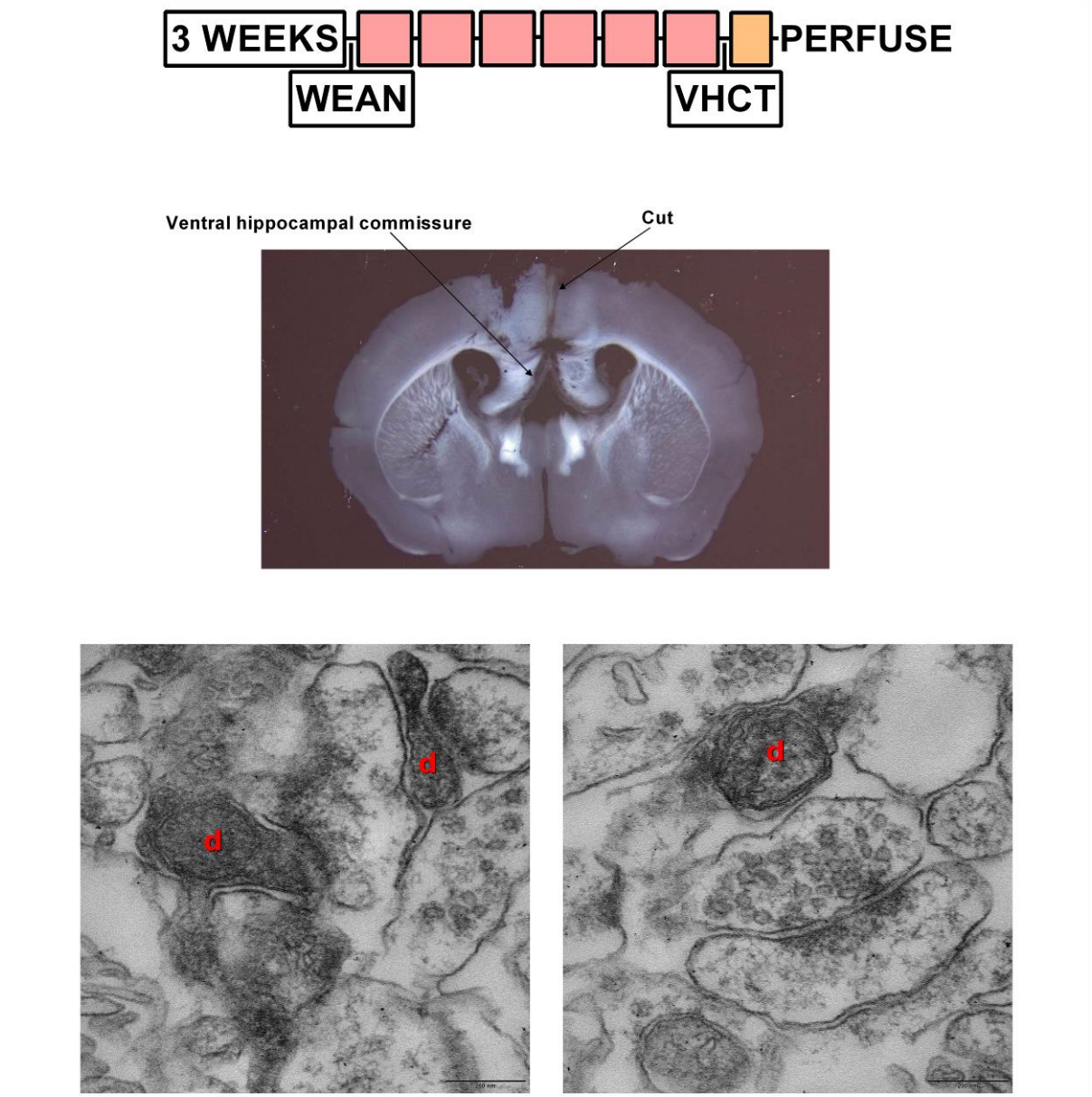

VHCT following environmental enrichment to investigate ipsilateral contribution to synaptic density in either hemisphere

Top scheme represents timeline of experiment. Red boxes represent 1 week of ENR, orange box represents 5 days of ENR. Middle image shows example of successful VHCT operation. The path the blade took when entering the brain is labelled 'cut'. Lower image shows example TEM image. Degenerating cells are labelled 'd'. Scale bar = 2 μm

Method 7

Pre-embedding labelling of mouse brain for analysis under TEM

1. Perfused brains were trimmed using a razor, so that they could be glued to a vibrotome (Leica VT1000S) stage. 50 µm coronal sections were then cut and transferred to a 0.1M PB solution

2. Slices were washed with:
    1. TBS twice (20 minutes each)
    2. PBS (for 20 minutes)
    3. PBS-Tx (0.05%) (for 20 minutes)
    4. TBS (20 minutes)

3. Slices were blocked with 20% NGS/TBS solution (for 1 hour)

4. Slices were washed in incubation buffer twice (10 minutes each)

5. Slices stored in incubation buffer containing primary antibody (1:3000 mouse anti-GFP monoclonal (Wako mFX73)) for 2 overnights

6. Slices washed three times in TBS (for 20 minutes each)

7. Slices stored in incubation buffer containing secondary antibody (1:10000 biotinylated Goat anti-Mouse IgG2a (Life Technologies M32315)) for one overnight

8. Slices were washed with:
    1. Incubation buffer four times (10 minutes each)
    2. PBS twice (10 minutes each)

9. Slices were then incubated in ABC solution (made 30 minutes beforehand) for 2 hours at room temperature.

10. Slices were washed with:
    1. PBS twice (10 minutes each)
    2. 50mM Tris/HCL buffer (for 10 minutes)

11. Slices were incubated in DAB solution (0.02% solution in 50mM Tris buffer) for 5 minutes, then were visualized using a 0.3% H2O2 solution (10 µl per 1 ml).

12. The reaction was stopped, through an excess of 0.1M PB.

13. Slices were washed twice in 0.1M PB (10 minutes each wash).

14. Slices were immersed in 1% OsO4 (in 0.1M PB solution) for 25 minutes.

15. Slices were washed twice in dH2O (10 minutes each wash).

16. Slices were immersed in 1% Uranyl Acetate (in dH2O) for 35 minutes.

17. A gradual ethanol dehydration was performed (10 minutes per wash, series ranging

from 50% to 95%), terminating in 2 washes of 100% ethanol (10 minutes per wash). The final wash being done in glass capsules.

18. Slices were immersed in propylene oxide twice (10 minutes each wash).

19. Slices were left overnight in freshly made Durcupan resin (1:1:0.03:0.033 A:B:C:D), to allow slow infiltration of the resin into the tissue.

20. The following day, slices were mounted on siliconised glass slides, with Aclar film as a cover, and polymerised in the oven overnight at 60 °C.

21. The region of interest (the inner 1/3rd of the CA1 s.r.) was then trimmed out and remounted in a Durcupan filled capsule (polymerised overnight at 60 °C).

22. Samples were cut into 70nm serial sections using an ultramicrotone (Leica EM UC7).

Method 8

Novel Object Location task (NOL)

1. Mice were kept in a cabinet with a 12 hour reversed day-night cycle for 6 weeks prior to the experiment.

2. On the day of testing, mice were moved down to a dark room adjoining the NOL stage at least 1 hour prior to start of the experiment.

3. The NOL stage was cleaned with ethanol, to remove any lingering scent cues. The room was illuminated at 45 lux, from above. This reading was checked each day via a digital Lux Meter.

4. A single mouse was carefully transported to the NOL stage, to cause minimal stress.

5. The mouse was placed in the centre of the stage and the timer was started. Whilst the mouse was being tested, the observer remained in an adjoining room, watching via an above-stage camera to ensure that the mouse was fine throughout the experiment.

6. Following the pre-defined time for the experiment, the timer was stopped and the mouse was returned to its home-cage.

7. The chamber was then thoroughly cleaned with 70% ethanol, removing any animal waste and scent marks, then another mouse was tested.
    - On day 4, the objects were also cleaned with ethanol, before being returned to the cage in a different layout (see Test:Left and Test:Right). The mouse was then returned to the stage following the training period, for the testing phase. This was followed by another cleaning step (7) before the next mouse could be investigated.

For habituation, the mouse was left alone in the chamber for 5 minutes, before being removed. This was done twice a day, for 3 days sequentially. For both the testing and training periods, the mouse was left alone in the chamber until it had explored both objects for 10 seconds each. Following that it would be removed from the stage. If it took longer than 10 minutes to complete the experiment, it would also be removed from the stage.

Habituation conditions for NOL

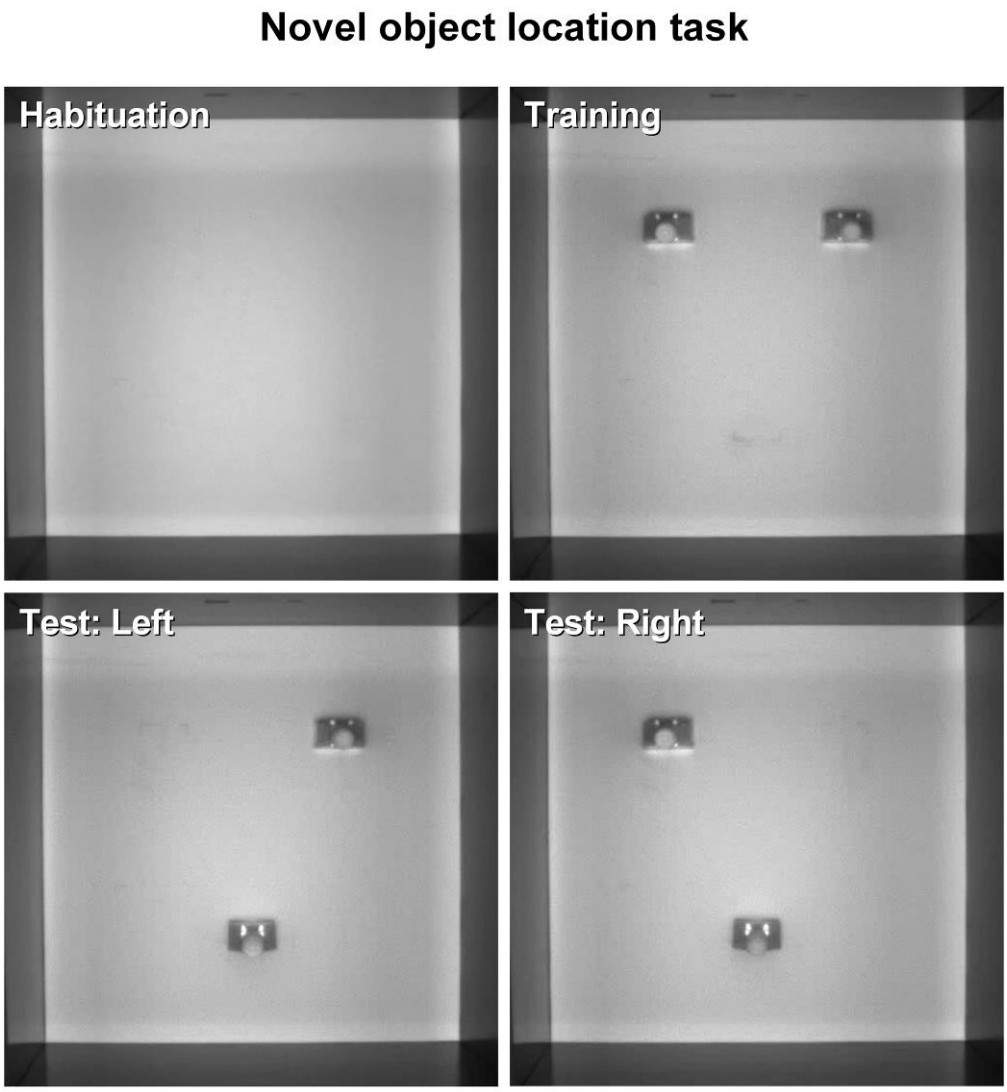

Different conditions in NOL task

Habituation
Empty chamber

Training
Two identical objects each spaced an equal distance from the top and closest wall

Test: Left
Left object moved to center of bottom wall. Distance from bottom wall equal to distance right object is from top wall

Test: Right
Right object moved to center of bottom wall. Distance from bottom wall equal to distance left object is from top wall

Timeline for NOL

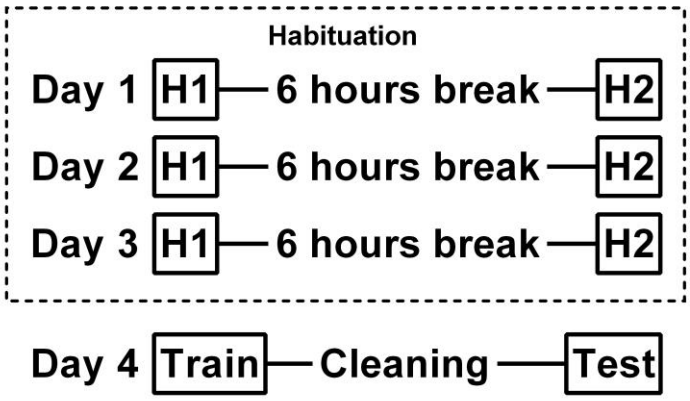

Upper picture shows objects used for training and testing. Flasks are filled with clean bedding material.

Timeline for NOL task

Days 1 - 3 are used for habituating the mice to the chamber. There are 2 habituation periods, H1 and H2. Habituation periods are 5 minutes long each.

Day 4 is the training and testing period. Both training and testing periods last until the mouse has either explored both objects for 10 seconds each, or the mouse has been in the chamber for 10 minutes. Following training, one object is moved and the chamber is quickly cleaned with ethanol (time < 5 minutes) to remove sent cues and remove any faeces/urine, then the mouse is immediately returned for the testing period.

Final conclusions

This work highlights two important, and related, processes in hippocampal development. It aims to further our understanding about the development of input-side dependent asymmetry formation in the hippocampus, suggesting Evl as a candidate gene which could play a role in the establishment of this phenomenon. Significantly, it also highlights how vital the phenomenon of input-side dependency is in the hippocampus, specifically in its relation to experience-driven alterations in synaptic morphology and neuroneal projection dynamics. This work helps to tie together the conflicting evidence of the relative importance of the left or right hippocampus, in memory formation and processing, suggesting a vital combinatory role for both the left and right hemisphere, rather than a specific importance of one side or the other. It also demonstrates a potentially unreported, yet significant, commissural fibre-specific pathway for hippocampal laterality development in the mouse. Potentially explaining one important method by which an animal can capably deal with an ever-changing environment.

References

- Andersen, P. et al. The Hippocampus Book. *Oxford University Press (US)*. Ch3 pp 37 – 114 (2007)

- Arakawa, H. Ethological approach to social isolation effects in behavioral studies of laboratory rodents. *Behav. Brain Res.* **341,** 98–108 (2018)

- Archer, G. S. & Mench, J. A. Natural incubation patterns and the effects of exposing eggs to light at various times during incubation on post-hatch fear and stress responses in broiler (meat) chickens. *Appl. Anim. Behav. Sci.* **152,** 44–51 (2014)

- Arjmand, H. A., Hohagen, J., Paton, B. & Rickard, N. S. Emotional responses to music: Shifts in frontal brain asymmetry mark periods of musical change. *Front. Psychol*. **8,** 1–13 (2017)

- Aujnarain, A. B., Luo, O. D., Taylor, N., Lai, J. K. Y. & Foster, J. A. *Effects of exercise and enrichment on behaviour in CD-1 mice. Behavioural Brain Research* **342,** 43-50 (2018)

- Barker, G. R. I. & Warburton, E. C. When Is the Hippocampus Involved in Recognition Memory? *J. Neurosci.* **31,** 10721–10731 (2011)

- Bartoloni, L. et al. Mutations in the DNAH11 (axonemal heavy chain dynein type 11) gene cause one form of situs inversus totalis and most likely primary ciliary dyskinesia. *Proc. Natl. Acad. Sci. U. S. A.* **99,** 10282–10286 (2002)

- Bayne, K. Potential for Unintended Consequences of environmental enrichment for laboratory animals and research results. *ILAR J.* **46,** 129-139 (2005)

- Belcheva, I., Tashev, R. & Belcheva, S. Hippocampal asymmetry in serotonergic modulation of learning and memory in rats. *Laterality*. **12,** 475-486 (2007)

- Bettio, L. E. B., Rajendran, L. & Gil-Mohapel, J. The effects of aging in the hippocampus and cognitive decline. *Neurosci. Biobehav. Rev.* **79,** 66–86 (2017)

- Bhagya, V. R., Srikumar, B. N., Veena, J. & Shankaranarayana Rao, B. S. Short-term exposure to enriched environment rescues chronic stress-induced impaired hippocampal synaptic plasticity, anxiety, and memory deficits. *J. Neurosci. Res.* **95,** 1602–1610 (2017)

- Bijlmakers, M. J. & Ploegh, H. L. Putting Together an MHC Class-I Molecule. *Curr. Opin. Immunol.* **5,** 21–26 (1993)

- Birch, A. M., Mcgarry, N. B. & Kelly, Á. M. Short-term environmental enrichment, in the absence of exercise, improves memory, and increases NGF concentration, early neuroneal survival, and synaptogenesis in the dentate gyrus in a time-dependent manner. *Hippocampus* **23,** 437–450 (2013)

- Bird, C. M. The role of the hippocampus in recognition memory. *Cortex* **93,** 155–165 (2017)

- Bochner, D. N. *et al.* Blocking PirB up-regulates spines and functional synapses to unlock visual cortical plasticity and facilitate recovery from amblyopia. *Sci. Transl. Med.* **6,** 258ra140 (2014)

- Bogen, J. E. & Bogen, G. M. Wernicke's Region - Where is it? *Ann N Y Acad Sci* **280,** 834–843 (1976)

- Bouchard-Cannon, P., Lowden, C., Trinh, D. & Cheng, H. M. Dexras1 is a homeostatic regulator of exercise-dependent proliferation and cell survival in the hippocampal neurogenic niche. *Sci. Rep.* 1–16 (2018). doi:10.1038/s41598-018-23673-z

- Brandler, W. M. & Paracchini, S. The genetic relationship between handedness and neurodevelopmental disorders. *Trends Mol. Med.* **20,** 84–89 (2014)

- Brenes, J. C. *et al.* Differential effects of social and physical environmental enrichment on brain plasticity, cognition, and ultrasonic communication in rats. *J. Comp. Neurol.* **524,** 1586–1607 (2016)

- Brueckner, M., D'Eustachio, P. & Horwich, a L. Linkage mapping of a mouse gene, iv, that controls left-right asymmetry of the heart and viscera. *Proc. Natl. Acad. Sci. U. S. A.* **86**, 5035–5038 (1989)

- Buschmann, J. U. F., Manns, M. & Güntürkün, O. 'Let There be Light!' pigeon eggs are regularly exposed to light during breeding. *Behav. Processes* **73,** 62–67 (2006)

- Carr, M. F., Karlsson, M. P. & Frank, L. M. Transient slow gamma synchrony underlies hippocampal memory replay. *Neurone* **75,** 700–713 (2012)

- Chaddock, L. *et al.* A neurogenic investigation of the association between aerobic fitness, hippocampal volume, and memory performance in preadolescent children. *Brain Res.* **1358,** 172–183 (2010)

- Chevaleyre, V. & Piskorowski, R. A. Hippocampal Area CA2: An Overlooked but Promising Therapeutic Target. *Trends Mol. Med.* **22,** 645–655 (2016)

- Clemenson, G. D., Deng, W. & Gage, F. H. Environmental enrichment and neurogenesis: From mice to humans. *Curr. Opin. Behav. Sci.* **4**, 56–62 (2015)

- Concha, M. L., Signore, I. A. & Colombo, A. Mechanisms of directional asymmetry in the zebrafish epithalamus. *Semin. Cell Dev. Biol.* **20,** 498–509 (2009)

- Concha, M. L., Bianco, I. H. & Wilson, S. W. Encoding asymmetry within neural circuits. *Nat. Rev. Neurosci.* **13,** 832–843 (2012)

- Corballis, P. M., Funnell, M. G. & Gazzaniga, M. S. Hemispheric asymmetries for simple visual judgments in the split brain. *Neuropsychologia* **40,** 401–410 (2002)

- Corballis, M. C. Left Brain, Right Brain: Facts and Fantasies. *PLoS Biol.* **12,** (2014)

- Cortese, G. P., Olin, A., O'Riordan, K., Hullinger, R. & Burger, C. Environmental enrichment improves hippocampal function in aged rats by enhancing learning and memory, LTP, and mGluR5-Homer1c activity. *Neurobiol. Aging* **63**, 1–11 (2018)

- Dadda, M., Domenichini, A., Piffer, L., Argenton, F. & Bisazza, A. Early differences in epithalamic left-right asymmetry influence lateralization and personality of adult zebrafish. *Behav. Brain Res.* **206,** 208–215 (2010)

- Dimsdale-Zucker, H. R., Ritchey, M., Ekstrom, A. D., Yonelinas, A. P. & Ranganath, C. CA1 and CA3 differentially support spontaneous retrieval of episodic contexts within human hippocampal subfields. *Nat. Commun.* **9,** 294 (2018)

- Dong, J. et al. Exercise improves recognition memory and synaptic plasticity in the prefrontal cortex for rats modelling vascular dementia. *Neurol.Res.* **40**, 68-77 (2018)

- Dougherty, C. C., Evans, D. W., Katuwal, G. J. & Michael, A. M. Asymmetry of fusiform structure in autism spectrum disorder: Trajectory and association with symptom severity. *Mol. Autism* **7,** 1–11 (2016)

- Drees, F. & Gertler, F. B. Ena/VASP: proteins at the tip of the nervous system. *Curr. Opin. Neurobiol.* **18,** 53–59 (2008)

- Dreosti, E., Vendrell Llopis, N., Carl, M., Yaksi, E. & Wilson, S. W. Left-right asymmetry is required for the habenulae to respond to both visual and olfactory stimuli. *Curr. Biol.* **24,** 440–445 (2014)

- Dronkers, N. F., Plaisant, O., Iba-Zizen, M. T. & Cabanis, E. A. Paul Broca's historic cases: High resolution MR imaging of the brains of Leborgne and Lelong. *Brain* **130,** 1432–1441 (2007)

- El-Gaby, M., Shipton, O. A. & Paulsen, O. Synaptic Plasticity and Memory: New insights from Hippocampal Asymmetries. *Neurosci.* **21,** 490–502 (2015)

- Elias, L. J., Saucier, D. M. & Guylee, M. J. Handedness and depression in university students: A sex by handedness interaction. *Brain Cogn.* **46,** 125–129 (2001)

- Ennaceur, A., Neave, N. & Aggleton, J. P. Spontaneous object recognition and object location memory in rats: The effects of lesions in the cingulate cortices, the medial prefrontal cortex, the cingulum bundle and the fornix. *Exp. Brain Res.* **113,** 509–519 (1997)

- Fabel, K. et al. Additive effects of physical exercise and environmental enrichment on adult hippocampal neurogenesis in mice. *Front. Neurosci.* **3**, 1–7 (2009)

- Facchin, L., Duboué, E. R. & Halpern, M. E. Disruption of Epithalamic Left-Right Asymmetry Increases Anxiety in Zebrafish. *J. Neurosci*. **35,** 15847–15859 (2015)

- Farovik, A., Dupont, L. M. & Eichenbaum, H. Distinct roles for dorsal CA3 and CA1 in memory for sequential nonspatial events. *Learn. Mem.* **17,** 12–17 (2010)

- Francks, C. et al. LRRTM1 on chromosome 2p12 is a maternally suppressed gene that is associated paternally with handedness and schizophrenia. *Mol. Psychiatry* **12,** 1129–1139 (2007)

- Franco, D. L., Rezával, C., Cáceres, A., Schinder, A. F. & Ceriani, M. F. ENA/VASP downregulation triggers cell death by impairing axonal maintenance in hippocampal neurones. *Mol. Cell. Neurosci.* **44,** 154–164 (2010)

- Fratiglioni, L., Paillard-Borg, S. & Winblad, B. An active and socially integrated

lifestyle in late life might protect against dementia. *Lancet Neurol.* **3,** 343–353 (2004)

- Freund, N. *et al.* Asymmetric top-down modulation of ascending visual pathways in pigeons. *Neuropsychologia* **83,** 37–47 (2016)

- Fridriksson, J., Fillmore, P., Guo, D. & Rorden, C. Chronic Broca's aphasia is caused by damage to Broca's and wernicke's areas. *Cereb. Cortex* **25,** 4689–4696 (2015)

- Fiala, J. C. Reconstruct: A free editor for serial section microscopy. *J. Microsc.* **218,** 52–61 (2005)

- Fischer, G. *et al.* Ro 25-6981, a highly potent and selective blocker of N-methyl-D-aspartate receptors containing the NR2B subunit. Characterization in vitro. *J. Pharmacol. Exp. Ther.* **283,** 1285–92 (1997)

- Fitzjohn, S., Bashir, Z. & Farrow, P. Group I mGluR induced LTD of NMDAR-synaptic transmission at the schaffer collateral but not temperoammonic input to CA1. *Curr. Neuropharmacol.* **14,** 435–440 (2016)

- Fu, Q. L. *et al.* Brain interleukin asymmetries and paw preference in mice. *Neuroscience* **116,** 639–647 (2003)

- García-Díaz, D. F. *et al.* Chronic mild stress induces variations in locomotive behavior and metabolic rates in high fat fed rats. *J. Physiol. Biochem.* **63,** 337–346 (2007)

- Gaudier-Diaz, M. M. *et al.* Social interaction modulates the neuroinflammatory response to global cerebral ischemia in male mice. *Brain Res.* **1673,** 86–94 (2017)

- Gerlai, R. T., McNamara, A., Williams, S. & Phillips, H. S. Hippocampal dysfunction and behavioral deficit in the water maze in mice: An unresolved issue? *Brain Res. Bull.* **57,** 3–9 (2002)

- Giljov, A., Karenina, K., Ingram, J. & Malashichev, Y. Parallel Emergence of True Handedness in the Evolution of Marsupials and Placentals. *Curr. Biol.* **25,** 1878–1884 (2015)

- Goes, T. C., Antunes, F. D. & Teixeira-Silva, F. Environmental enrichment for adult rats: Effects on trait and state anxiety. *Neurosci. Lett.* **584,** 93–96 (2015)

- Goto, K. *et al.* Left–right asymmetry defect in the hippocampal circuitry impairs spatial learning and working memory in IV mice. *PLoS One* **5,** 1–7 (2010)

- Goto, K. & Ito, I. The asymmetry defect of hippocampal circuitry impairs working memory in β2-microglobulin deficient mice. *Neurobiol. Learn. Mem.* **139,** 50–55 (2017)

- Govind, C. K. Claw asymmetry in lobsters: Case study in developmental neuroethology. *J. Neurobiol.* **23,** 1423–1445 (1992)

- Haettig, J., Sun, Y., Wood, M. a & Xu, X. Cell-type specific inactivation of hippocampal CA1 disrupts location-dependent object recognition in the mouse. *Learn. Mem.* **20,** 139–46 (2013)

- Hall, T. *et al.* The relationship between Hippocampal asymmetry and working memory processing in combat-related PTSD – a monozygotic twin study. *Biol. Mood Anxiety Disord.* **2,** 21 (2012)

- Harburger, L. L., Lambert, T. J. & Frick, K. M. Age-dependent effects of environmental enrichment on spatial reference memory in male mice. *Behav. Brain Res.* **185,** 43–48 (2007)

- Hayashi, Y. Driving AMPA Receptors into Synapses by LTP and CaMKII : Requirement for GluR1 and PDZ Domain Interaction. **2262,** 2262–2267 (2011)

- Heinla, I., Leidmaa, E., Visnapuu, T., Philips, M. A. & Vasar, E. Enrichment and individual housing reinforce the differences in aggressiveness and amphetamine response in 129S6/SvEv and C57BL/6 strains. *Behav. Brain Res.* **267,** 66–73 (2014)

- Hell, J. W. CaMKII: Claiming Center Stage in Postsynaptic Function and Organization. *Neurone* **81,** 249–265 (2014)

- Hendershott, T. R., Cronin, M. E., Langella, S., McGuinness, P. S. & Basu, A. C. Effects of environmental enrichment on anxiety-like behavior, sociability, sensory gating, and spatial learning in male and female C57BL/6J mice. *Behav. Brain Res.* **314,** 215–225 (2016)

- Herbert, M. R. et al. Brain asymmetries in autism and developmental language disorder: A nested whole-brain analysis. *Brain* **128,** 213–226 (2005)

- Hitti, F. L. & Siegelbaum, S. A. The hippocampal CA2 region is essential for social memory. *Nature* **508,** 88–92 (2014)

- Hok, V., Poucet, B., Duvelle, É., Save, É. & Sargolini, F. Spatial cognition in mice and rats: similarities and differences in brain and behavior. Wiley Interdiscip. Rev. Cogn. Sci. 7, 406–421 (2016)

- Holson, R. R. Feeding neophobia: A possible explanation for the differential maze performance of rats reared in enriched or isolated environments. *Physiol. Behav.* **38,** 191–201 (1986)

- Hopkins, W. D. *et al.* Hand Preferences for Coordinated Bimanual Actions in 777 Great Apes: Implications for the Evolution of Handedness in Hominins. *J Hum Evol.* **60,** 605–611 (2011)

- Huang, Q., Zhou, Y. & Liu, L. Y. Effect of post-weaning isolation on anxiety- and depressive-like behaviors of C57BL/6J mice. *Exp. Brain Res.* **235,** 2893–2899 (2017)

- Hullinger, R., O'Riordan, K. & Burger, C. Environmental enrichment improves learning and memory and long-term potentiation in young adult rats through a mechanism requiring mGluR5 signaling and sustained activation of p70s6k. *Neurobiol. Learn. Mem.* **125**, 126–134 (2015)

- Hunsaker, M. R., Rosenberg, J. S. & Kesner, R. P. The role of the dentate gyrus, CA3a,b, and CA3c for detecting spatial and environmental novelty. *Hippocampus* **18,** 1064–1073 (2008)

- Hutchinson, E., Avery, A. & VandeWoude, S. Environmental Enrichment for Laboratory Rodents. *ILAR J.* **46,** 148–161 (2005)

- Hüttenrauch, M., Salinas, G. & Wirths, O. Effects of Long-Term Environmental Enrichment on Anxiety, Memory, Hippocampal Plasticity and Overall Brain Gene Expression in C57BL6 Mice. *Front. Mol. Neurosci*. **9**, 1–11 (2016)

- Ivanova, M., Ternianov, A., Tashev, R., Belcheva, S. & Belcheva, I. Lateralized learning and memory effects of vasoactive intestinal peptide infused into the rat hippocampal CA1 area. *Regul. Pept.* **156,** 42–46 (2009)

- Jahanshad, N. et al. Genetic influences of brain asymmetry: A DTI study of 374 Twins and Siblings. *Neuroimage* **52,** 455–469 (2010)

- Jeong, S. K. & Xu, Y. The impact of top-down spatial attention on laterality and hemispheric asymmetry in the human parietal cortex. *J. Vis*. **16,** 1-21 (2016)

- Ji, J. & Maren, S. Differential roles for hippocampal areas CA1 and CA3 in the contextual encoding and retrieval of extinguished fear. *Learn. Mem.* **15,** 244–251 (2008)

- Jones, B. C. *et al.* Facial symmetry and judgements of apparent health: Support for a 'good genes' explanation of the attractiveness-symmetry relationship. *Evol. Hum. Behav.* **22,** 417–429 (2001)

- Jones, M. W. & Mchugh, T. J. Updating hippocampal representations: CA2 joins the circuit. *Trends Neurosci.* **34,** 526–535 (2011)

- Kawahara, A. *et al.* Neuroneal major histocompatibility complex class I molecules are implicated in the generation of asymmetries in hippocampal circuitry. *J. Physiol.* **591,** 4777–4791 (2013)

- Kawakami, R. et al. Asymmetrical allocation of NMDA receptor ε2 subunits in hippocampal circuitry. *Science* **300**, 990–994 (2003)

- Kawakami, R., Dobi, A., Shigemoto, R. & Ito, I. Right isomerism of the brain in inversus viscerum mutant mice. *PLoS One* **3**, 1–6 (2008)

- Kempermann, G., Kuhn, H. G. & Gage, F. H. More hippocampal neurones in adult mice living in an enriched environment. *Nature* **386,** 493–495 (1997)

- Kempermann, G., Kuhn, H. G. & Gage, F. H. Experience-induced neurogenesis in the senescent dentate gyrus. *J Neurosci* **18,** 3206–3212 (1998a)

- Kempermann, G., Brandon, E. P. & Gage, F. H. Environmental stimulation of 129/SvJ mice causes increased cell proliferation and neurogenesis in the adult dentate gyrus. *Curr. Biol.* **8,** 939–42 (1998b)

- Kesner, R. P. Behavioral functions of the CA3 subregion of the hippocampus. *Learn. Mem.* **14,** 771–781 (2007)

- Kesner, R. P. A process analysis of the CA3 subregion of the hippocampus. *Front. Cell. Neurosci.* **7,** 1–17 (2013)

- Kim, J. W. *et al.* Comparison of Adult Hippocampal Neurogenesis and Susceptibility to Treadmill Exercise in Nine Mouse Strains. *Neural Plast.* **2017,** 1–13 (2017)

- Klur, S. et al. Hippocampal-dependent spatial memory functions might be lateralized in rats: An approach combining gene expression profiling and reversible inactivation. *Hippocampus* **19,** 800–816 (2009)

- Koboldt, D. C. *et al.* VarScan: Variant detection in massively parallel sequencing of individual and pooled samples. *Bioinformatics* **25,** 2283–2285 (2009)

- Koboldt, D. C. *et al.* VarScan 2 : Somatic mutation and copy number alteration discovery in cancer by exome sequencing. *Genome Res.* **22,** 568–576 (2012)

- Kohl, M. M. et al. Hemisphere-specific optogenetic stimulation reveals left-right asymmetry of hippocampal plasticity. Nat. Neurosci. 14, 1413–1415 (2011)

- Kopec, C. D., Real, E., Kessels, H. W. & Malinow, R. GluR1 Links Structural and Functional Plasticity at Excitatory Synapses. *J. Neurosci.* **27,** 13706–13718 (2007)

- Kozareva, D. A., O'Leary, O. F., Cryan, J. F. & Nolan, Y. M. Deletion of TLX and social isolation impairs exercise-induced neurogenesis in the adolescent hippocampus. *Hippocampus* **28,** 3–11 (2018)

- Kuhn, H. G., Dickinson-Anson, H. & Gage, F. H. Neurogenesis in the dentate gyrus of the adult rat: age-related decrease of neuroneal progenitor proliferation. *J Neurosci* **16,** 2027–2033 (1996)

- Kwiatkowski, A. V. *et al.* Ena/VASP Is Required for Neuritogenesis in the Developing Cortex. *Neurone* **56,** 441–455 (2007)

- Langmead B, Salzberg S. Fast gapped-read alignment with Bowtie 2. *Nature Methods* **9**, 357-359 (2012)

- Latuske, P., Kornienko, O., Kohler, L. & Allen, K. Hippocampal Remapping and Its Entorhinal Origin. *Front. Behav. Neurosci.* **11,** 1–13 (2018)

- Lee, I., Rao, G. & Knierim, J. J. A double dissociation between hippocampal subfields: Differential time course of CA3 and CA1 place cells for processing changed environments. *Neurone* **42,** 803–815 (2004)

- Leger, M. *et al.* Object recognition test in mice. *Nat. Protoc.* **8,** 2531–2537 (2013)

- Leggio, M. G. et al. Environmental enrichment promotes improved spatial abilities and enhanced dendritic growth in the rat. *Behav. Brain Res.* **163**, 78–90 (2005)

- Lein, E. S., Callaway, E. M., Albright, T. D. & Gage, F. H. Redefining the boundaries of the hippocampal CA2 subfield in the mouse using gene expression and 3-dimensional reconstruction. *J. Comp. Neurol.* **485,** 1–10 (2005)

- Li, H. *et al.* The Sequence Alignment/Map format and SAMtools. *Bioinformatics* **25,** 2078–2079 (2009)

- Li, H. A statistical framework for SNP calling, mutation discovery, association mapping and population genetical parameter estimation from sequencing data. *Bioinformatics* **27,** 2987–2993 (2011)

- Loftis, J. M. & Janowsky, A. The N-methyl-d-aspartate receptor subunit NR2B: localization, functional properties, regulation, and clinical implications. *Pharmacol. Ther.* **97,** 55–85 (2003)

- Lopez-Rojas, J. & Kreutz, M. R. Mature granule cells of the dentate gyrus-Passive bystanders or principal performers in hippocampal function? *Neurosci. Biobehav. Rev.* **64,** 167–174 (2016)

- Martin, M. Cutadapt removes adapter sequences from high-throughput sequencing reads. *EMBnet.journal* **17**, 10-12 (2011)

- Maguire, E. A, Frackowiak, R. S. & Frith, C. D. Recalling routes around London: activation of the right hippocampus in taxi drivers. *J. Neurosci.* **17**, 7103–7110 (1997)

- Maguire, E. A. et al. Navigation-related structural change in the hippocampi of taxi drivers. *Proc. Natl. Acad. Sci*. **97,** 4398–4403 (2000)

- Majima, T. *et al.* Involvement of afadin in the formation and remodeling of synapses in the hippocampus. *Biochem. Biophys. Res. Commun.* **385,** 539–544 (2009)

- Malenka, R. C. & Bear, M. F. LTP and LTD: An embarrassment of riches. *Neurone* **44,** 5–21 (2004)

- Markou, P., Ahtam, B. & Papadatou-Pastou, M. Elevated Levels of Atypical Handedness in Autism: Meta-Analyses. *Neuropsychol. Rev.* **27,** 258–283 (2017)

- Mankin, E. A., Diehl, G. W., Sparks, F. T., Leutgeb, S. & Leutgeb, J. K. Hippocampal CA2 Activity Patterns Change over Time to a Larger Extent than between Spatial Contexts. *Neurone* **85,** 190–202 (2015)

- Manning, J. T., Scutt, D. & Lewis-Jones, D. I. Developmental stability, ejaculate size, and sperm quality in men. *Evol. Hum. Behav.* **19,** 273–282 (1998)

- Manns, M. & Ströckens, F. Functional and structural comparison of visual lateralization in birds - Similar but still different. *Front. Psychol.* **5,** 1–10 (2014)

- McGrath, J., Somlo, S., Makova, S., Tian, X. & Brueckner, M. Two populations of node monocilia initiate left-right asymmetry in the mouse. *Cell* **114,** 61–73 (2003)

- Mercer, A., Trigg, H. L. & Thomson, A. M. Characterization of Neurones in the CA2 Subfield of the Adult Rat Hippocampus. *J. Neurosci.* **27,** 7329–7338 (2007)

- Mesa-Gresa, P., Pérez-Martinez, A. & Redolat, R. Environmental enrichment improves novel object recognition and enhances agonistic behavior in male mice. *Aggress. Behav.* **39,** 269–279 (2013)

- Miller, B. *et al.* Handedness and the risk of glioma. *J. Neurooncol.* **0,** 1–6 (2018)

- Monteiro, B. M. M., Moreira, F. A., Massensini, A. R., Moraes, M. F. D. & Pereira, G. S. Enriched environment increases neurogenesis and improves social memory persistence in socially isolated adult mice. *Hippocampus* **24,** 239–248 (2014)

- Montgomery, S. M. & Buzsaki, G. Gamma oscillations dynamically couple hippocampal CA3 and CA1 regions during memory task performance. *Proc. Natl. Acad. Sci.* **104,** 14495–14500 (2007)

- Moskal, J. R. et al. Distinct patterns of gene expression in the left and right hippocampal formation of developing rats. *Hippocampus* **16,** 629–34 (2006)

- Moser, M. B., Trommald, M. & Andersen, P. An increase in dendritic spine density on hippocampal CA1 pyramidal cells following spatial learning in adult rats suggests the formation of new synapses. *Proc. Natl. Acad. Sci. U. S. A.* **91,** 12673–5 (1994)

- Moser, M. B., Trommald, M., Egeland, T. & Andersen, P. Spatial training in a complex enviroment and isolation alter the spine destribution differently in rat CA1 pyramidal cells. *J. Comp. Neurol.* **380,** 373–381 (1997)

- National Research Council (US) Committee on Recognition and Alleviation of Distress in Laboratory Animals. Recognition and Alleviation of Distress in Laboratory Animals. *Washington (DC): National Academies Press (US)*. ch4 pp 66 - 67 (2008)

- Nakamura, A., Kobayashi, E. & Takai, T. Exacerbated graft-versus-host disease in Pirb−/− mice. *Nat. Immunol.* **5,** 623–629 (2004)

- Neidl, R. *et al.* Late-Life Environmental Enrichment Induces Acetylation Events and Nuclear Factor B-Dependent Regulations in the Hippocampus of Aged Rats Showing Improved Plasticity and Learning. *J. Neurosci.* **36,** 4351–4361 (2016)

- Neuhoff, H., Roeper, J. & Schweizer, M. Activity-dependent formation of perforated synapses in cultured hippocampal neurones. *Eur. J. Neurosci.* **11,** 4241–4250 (1999)

- Normann, M. C. *et al. The Influence of Environmental Enrichment on Cardiovascular and Behavioral Responses to Social Stress*. *Psychosomatic Medicine* (2018). doi:10.1097/PSY.0000000000000558

- Nilsson, M., Perfilieva, E., Johansson, U., Orwar, O. & Eriksson, P. S. Enriched environment increases neurogenesis in the adult rat dentate gyrus and improves spatial memory. *J. Neurobiol.* **39,** 569–578 (1999)

- Ocklenburg, S. *et al.* Visual experience affects handedness. *Behav. Brain Res.* **207,** 447–451 (2010)

- Oviedo, H. V. Connectivity motifs of inhibitory neurones in the mouse Auditory Cortex. *Sci. Rep.* **7,** 1–9 (2017)

- Pang, T. Y. C. & Hannan, A. J. Enhancement of cognitive function in models of brain disease through environmental enrichment and physical activity. *Neuropharmacology* **64,** 515–528 (2013)

- Pedraza, O., Bowers, D. & Gilmore, R. Asymmetry of the hippocampus and amygdala in MRI volumetric measurements of normal adults. *J. Int. Neuropsychol. Soc.* **10,** 664–678 (2004)

- Pernía-Andrade, A. J. & Jonas, P. Theta-Gamma-Modulated Synaptic Currents in Hippocampal Granule Cells InVivo Define a Mechanism for Network Oscillations. *Neurone* **81,** 140–152 (2014)

- Perrett, D. I. *et al.* Symmetry and Human Facial Attractiveness. *Evol. Hum. Behav.* **20,** 295–307 (1999)

- Pham, T. M., Söderström, S., Winblad, B. & Mohammed, A. H. Effects of environmental enrichment on cognitive function and hippocampal NGF in the non-handled rats. *Behav. Brain Res.* **103,** 63–70 (1999)

- Pi, H. J. *et al.* CaMKII control of spine size and synaptic strength: Role of phosphorylation states and nonenzymatic action. *Proc. Natl. Acad. Sci.* **107,** 14437–14442 (2010)

- Piazza, E. A. & Silver, M. A. Persistent hemispheric differences in the perceptual selection of spatial frequencies. *J Cogn Neurosci* **26,** 2021–2027 (2014)

- Poremba, A., Bigelow, J. & Rossi, B. Processing of communication sounds: Contributions of learning, memory, and experience. *Hear. Res.* **305,** 31–44 (2013)

- Prakash, R., Snook, E., Moti, R. & Kraemer, A. Aerobic Fitness is Associated with Gray Matter Volume and White Matter Integrity in Multiple Sclerosis. *Brain Res* 41–51 (2010). doi:10.1016/j.brainres.2009.06.063.Aerobic

- Propper, R. E. *et al.* A combined fMRI and DTI examination of functional language lateralization and arcuate fasciculus structure: Effects of degree versus direction of hand preference. *Brain Cogn.* **73,** 85–92 (2010)

- Raiker, S. J. *et al.* Oligodendrocyte-Myelin Glycoprotein and Nogo Negatively Regulate Activity-Dependent Synaptic Plasticity. *J. Neurosci.* **30,** 12432–12445 (2010)

- Rampon, C. *et al.* Enrichment induces structural changes and recovery from nonspatial memory deficits in CA1 NMDAR1-knockout mice. *Nat. Neurosci.* **3,** 238–244 (2000)

- Razafimandimby, A., Tzourio-Mazoyer, N., Mazoyer, B., Maïza, O. & Dollfus, S. Language lateralization in left-handed patients with schizophrenia. *Neuropsychologia* **49,** 313–319 (2011)

- Restivo, L. et al. Enriched environment promotes behavioral and morphological recovery in a mouse model for the fragile X syndrome. *Proc. Natl. Acad. Sci. U. S. A.* **102**, 11557–11562 (2005)

- Rhodes, G., Proffitt, F., Grady, J. M. & Sumich, A. Facial symmetry and the perception of beauty. *Psychon. Bull. Rev.* **5,** 659–669 (1998)

- Ribeiro, A. S., Eales, B. A. & Biddle, F. G. Learning of paw preference in mice is strain dependent, gradual and based on short-term memory of previous reaches. *Anim. Behav.* **81,** 249–257 (2011)

- Ribeiro, A. S., Eales, B. A., Lloyd-Price, J. & Biddle, F. G. Predictability and randomness of paw choices are critical elements in the behavioural plasticity of mouse paw preference. *Anim. Behav.* **98,** 167–176 (2014)

- Ribeiro-Carvalho, A., Abreu-Villaça, Y., Paes-Branco, D., Filgueiras, C. C. & Manhães, A. C. Novelty affects paw preference performance in adult mice. *Anim. Behav.* **80,** 51–57 (2010)

- Robinson, J. T. *et al.* Integrative Genomics Viewer. *Nature Biotechnology* **29,** 24–26 (2011)

- Rogers, L. J. & Deng, C. Light experience and lateralization of the two visual pathways in the chick. *Behav. Brain Res.* **98,** 277–287 (1999)

- Rogers, L. J. Development and function of lateralization in the avian brain. *Brain Res. Bull*. **76,** 235–244 (2008)

- Rolls, E. T. The storage and recall of memories in the hippocampo-cortical system. *Cell Tissue Res.* 1–28 (2017). doi:10.1007/s00441-017-2744-3

- Roussigné, M., Bianco, I. H., Wilson, S. W. & Blader, P. Nodal signalling imposes left-right asymmetry upon neurogenesis in the habenular nuclei. *Development* **136,** 1549–1557 (2009)

- Roussigné, M., Blader, P. & Wilson, S. W. Breaking symmetry: The zebrafish as a model for understanding left-right asymmetry in the developing brain. *Dev. Neurobiol.* **72,** 269–281 (2012)

- Rugani, R., Rosa Salva, O., Regolin, L. & Vallortigara, G. Brain asymmetry modulates perception of biological motion in newborn chicks (Gallus gallus). *Behav. Brain Res.* **290,** 1–7 (2015)

- Saenger, V. M., Barrios, F. A., Martínez-Gudiño, M. L. & Alcauter, S. Hemispheric asymmetries of functional connectivity and grey matter volume in the default mode network. *Neuropsychologia* **50,** 1308–1315 (2012)

- Sakalem, M. E. et al. Environmental enrichment and physical exercise revert behavioral and electrophysiological impairments caused by reduced adult neurogenesis. *Hippocampus* **27,** 36–51 (2017)

- Sauer, S. & Klar, A. J. S. Left-right symmetry breaking in mice by left-right dynein may occur via a biased chromatid segregation mechanism, without directly involving the Nodal gene. *Front. Oncol.* **2,** 1–10 (2012)

- Scharfman, H. E. The CA3 ‘Backprojection’ to the Dentate Gyrus. *Prog. Brain Res.* **163,** 627–637 (2007)

- Schindelin, J. *et al.* Fiji: An open-source platform for biological-image analysis. *Nat. Methods* **9,** 676–682 (2012)

- Schmitz, J., Lor, S., Klose, R., Güntürkün, O. & Ocklenburg, S. The functional genetics of handedness and language lateralization: Insights from gene ontology, pathway and disease association analyses. *Front. Psychol.* **8,** 1–12 (2017)

- Shatz, C. J. MHC Class I: An Unexpected Role in Neuroneal Plasticity. *Neurone* **64,** 40–45 (2009)

- Shi, F., Liu, B., Zhou, Y., Yu, C. & Jiang, T. Hippocampal volume and asymmetry in mild cognitive impairment and Alzheimer's disease: Meta-analyses of MRI studies. *Hippocampus* **19,** 1055–1064 (2009)

- Shimbo, A., Kosaki, Y., Ito, I. & Watanabe, S. Mice lacking hippocampal left-right asymmetry show non-spatial learning deficits. *Behav. Brain Res*. **336,** 156–165 (2018)

- Shinohara et al., Left-right asymmetry of the hippocampal synapses with differential subunit allocation of glutamate receptors. *Proc. Natl. Acad. Sci.* **105,** 19498–19503 (2008)

- Shinohara, Y, Hirase, H. Size and receptor density of glutamatergic synapses: a viewpoint from left-right asymmetry of CA3-CA1 connections. *Front. Neuroanat.* **3,** 1–6 (2009)

- Shinohara, Y. *et al.* Hippocampal CA3 and CA2 have distinct bilateral innervation patterns to CA1 in rodents. *Eur. J. Neurosci.* **35,** 702–710 (2012a)

- Shinohara, Y. et al. Right-hemispheric dominance of spatial memory in split-brain mice. Hippocampus 22, 117–121 (2012b)

- Shinohara, Y., Hosoya, A. & Hirase, H. Experience enhances gamma oscillations and interhemispheric asymmetry in the hippocampus. *Nat. Commun.* **4**, 1652–1659 (2013)

- Shipton, O. A. et al. Left–right dissociation of hippocampal memory processes in mice. *Proc. Natl. Acad. Sci*. **111,** 15238–15243 (2014a)

- Shipton, O. A & Paulsen, O. NMDA receptors in hippocampal plasticity. (2014b)

- Simpson, J. & Kelly, J. P. The impact of environmental enrichment in laboratory rats-Behavioural and neurochemical aspects. *Behav. Brain Res.* **222,** 246–264 (2011)

- Skillings, E. A., Wood, N. I. & Morton, A. J. Beneficial effects of environmental enrichment and food entrainment in the R6/2 mouse model of Huntington's disease. *Brain Behav.* **4,** 675–686 (2014)

- Sobczyk, A., Scheuss, V. & Svoboda, K. NMDA Receptor Subunit-Dependent [Ca2+] Signaling in Individual Hippocampal Dendritic Spines. *J. Neurosci.* **25,** 6037–6046 (2005)

- Somers, M., Sommer, I. E. C. & Kahn, R. S. Hand-preference and population schizotypy: A meta-analysis. *Lang. Lateralization Psychos.* **108,** 121–132 (2009)

- Sorra, K. E., Fiala, J. C. & Harris, K. M. Critical assessment of the involvement of perforations, spinules, and spine branching in hippocampal synapse formation. *J. Comp. Neurol.* **398,** 225–240 (1998)

- Soyman, E., Tunckol, E., Lacin, E. & Canbeyli, R. Right-but not left-paw use in female rats provides advantage in forced swim tests. *Behav. Brain Res.* **293,** 162–165 (2015)

- Starkey, H. D. V. *et al.* Neuroglial expression of the mhci pathway and pirb receptor is upregulated in the hippocampus with advanced aging. *J. Mol. Neurosci.* **48,** 111–126 (2012)

- Stepan, J., Dine, J. & Eder, M. Functional optical probing of the hippocampal trisynaptic circuit in vitro: Network dynamics, filter properties, and polysynaptic induction of CA1 LTP. *Front. Neurosci.* **9,** 1–9 (2015)

- Sullivan, R. M., Chehab, S. L., Dufresne, M. M. & Laplante, F. Role of sex in the neurochemical and neuroendocrine correlates of paw preference in the rat. *Neuroscience* **202,** 192–201 (2012)

- Supp, D. M., Witte, D. P., Potter, S. S. & Brueckner, M. Mutation of an axonemal dynein affects left-right asymmetry in inversus viscerum mice. *Nature* **389,** 963–966 (1997)

- Taglialatela, J. P., Russell, J. L., Schaeffer, J. A. & Hopkins, W. D. Visualizing vocal perception in the chimpanzee brain. *Cereb. Cortex* **19,** 1151–1157 (2009)

- Takai, T. Paired immunoglobulin-like receptors and their MHC class I recognition. *Immunology* **115,** 433–440 (2005)

- Thorvaldsdóttir, H., Robinson, J. T. & Mesirov, J. P. Integrative Genomics Viewer (IGV): High-performance genomics data visualization and exploration. *Brief. Bioinform.* **14,** 178–192 (2013)

- Tzanoulinou, S., Riccio, O., De Boer, M. W. & Sandi, C. Peripubertal stress-induced behavioral changes are associated with altered expression of genes involved in excitation and inhibition in the amygdale. *Transl. Psychiatry* **4,** e410-9 (2014)

- Uezu, A. *et al.* Identification of an elaborate complex mediating postsynaptic inhibition. *Science* **353,** 960–962 (2016)

- van Praag, H., Christie, B. R., Sejnowski, T. J. & Gage, F. H. Running enhances neurogenesis, learning, and long-term potentiation in mice. *Proc. Natl. Acad. Sci.* **96**, 13427–13431 (1999)

- van Praag, H. Exercise Enhances Learning and Hippocampal Neurogenesis in Aged Mice. *J. Neurosci.* **25**, 8680–8685 (2005)

- Vogel-Ciernia, A. & Wood, M. A. Examining Object Location and Object Recognition Memory in Mice. *Curr Protoc Neurosci.* **69**, 1–22 (2015)

- Voss, J. L., Bridge, D. J., Cohen, N. J. & Walker, J. A. A Closer Look at the Hippocampus and Memory. *Trends Cogn. Sci.* **21,** 577–588 (2017)

- Waitt, C. & Little, A. C. Preferences for symmetry in conspecific facial shape among Macaca mulatta. *Int. J. Primatol.* **27,** 133–145 (2006)

- Walker, M. D. & Mason, G. Reprint of Female C57BL/6 mice show consistent individual differences in spontaneous interaction with environmental enrichment that are predicted by neophobia. *Behav. Brain Res.* **227,** 508–513 (2012)

- Watkins, K. E. et al. Structural asymmetries in the human brain: a voxel-based statistical analysis of 142 MRI scans. *Cereb Cortex* **11,** 868–877 (2001)

- Wintzer, M. E., Boehringer, R., Polygalov, D. & McHugh, T. J. The Hippocampal CA2 Ensemble Is Sensitive to Contextual Change. *J. Neurosci.* **34,** 3056–3066 (2014)

- Woolard, A. & Heckers, S. Anatomical and functional correlates of human hippocampal volume asymmetry. *Psychiatry Res.* **201,** 48–53 (2012)

- Wright, L., Hardie, S. M. & Wilson, K. Handedness and behavioural inhibition: Left-handed females show most inhibition as measured by BIS/BAS self-report. *Pers. Individ. Dif.* **46,** 20–24 (2009)

- Wu, Y. et al. Target-Cell-Specific Left-Right Asymmetry of NMDA Receptor Content in Schaffer Collateral Synapses in ε1/NR2A Knock-Out Mice. *J. Neurosci.* **25**, 9213–9226 (2005)

- Yamaguchi, H. *et al.* Environmental enrichment attenuates behavioral abnormalities in valproic acid-exposed autism model mice. *Behav. Brain Res.* **333,** 67–73 (2017)

- Yashiro, K. & Philpot, B. D. Regulation of NMDA receptor subunit expression and its implications for LTD, LTP, and metaplasticity. *Neuropharmacology* **55,** 1081–1094 (2008)

- Yue, X. *et al.* The First Call Note Plays a Crucial Role in Frog Vocal Communication. *Sci. Rep.* **7,** 1–11 (2017)

- Zeleznikow-Johnston, A., Burrows, E. L., Renoir, T. & Hannan, A. J. Environmental enrichment enhances cognitive flexibility in C57BL/6 mice on a touchscreen reversal learning task. *Neuropharmacology* **117,** 219–226 (2017)

- Zemla, R. & Basu, J. Hippocampal function in rodents. *Curr. Opin. Neurobiol*. **43,** 187–197 (2017)

- Zhang, F., Wen, Y. & Guo, X. CRISPR/Cas9 for genome editing: Progress, implications and challenges. *Hum. Mol. Genet.* **23,** 40–46 (2014)